Universidad de Navarra

Facultad de Medicina

On mechanisms underlying efficacy and safety in cancer immunotherapy

Luna Ridan Cordeiro Minute

2019

Universidad de Navarra

Facultad de Medicina

On mechanisms underlying efficacy and safety in cancer immunotherapy

Memoria presentada por Dª Luna Ridan Cordeiro Minute para aspirar al grado de Doctor por la Universidad de Navarra

El presente trabajo ha sido realizado bajo nuestra dirección en el Departamento de Inmunología e Inmunoterapia del Centro de Investigación Médica Aplicada (CIMA) y autorizo su presentación ante el Tribunal que lo ha de juzgar.

Pamplona, septiembre de 2019.

Dr. Ignacio Melero Bermejo

Dr. Pedro Berraondo López

Este trabajo se ha llevado a cabo con la ayuda de una Beca Predoctoral de la Asociación Española Contra el Cancer (AECC).

Antes de todos agradezco el CIMA y la Universidad de Navarra por la oportunidad de realizar esta tesis doctoral.

Gracias a Nacho y a Kepa por haber creído en mi preparación y capacidad y haberme dado la posibilidad de entrar en el mundo de la inmunoterapia, por haber supervisionado este trabajo, por haberme guiado en esta etapa y aconsejadome sobre mi futuro.

Gracias a la Asociación Española Contra el Cancer por la financiación que ha permitido la realización de este trabajo.

Gracias a mis queridos compañeros del 3.03 y 3.04.

Gracias a Celia, Nuria, Eli, Inma, Arantxa, Saray, Carmen, Itziar M, Doina, Sandra y Esther. Gracias por la ayuda y que sepáis que sois indispensables para el funcionamento de estos estupendos grupos de trabajo.

Gracias a Alfonso, Itziar O, Alvaro, Iñaki, Menchu, Alba, Maite, Maria G, Shirley, Myriam, Elizabeth P, Irene, Claudia y Susy por las discusiones científicas siempre estimulantes y los consejos.

Gracias a todos vosotros por los cafés, los cotilleos, las risas, el apoyo en momentos de frustración, los sanfermines, las comidas, los viajes, las navidades y las nochesviejas. Habeis sido una gran familia que nunca me ha dejado sola cuando realmente lo necesitaba.

Gracias a mis amigos en Pamplona que me han acompañado y apoyado en estos cuatro años.

Gracias a mis padres, Valerio y Lourdes, y a mi hermano Marcio, por haberme siempre apoyado e impulsado en mis decisiones de vida, haber sacrificado vuestras voluntades para que yo pudiera seguir mis objetivos, por haber estado siempre tan cerca estando tan lejos y haberme formado como persona.

Todo esto no habría sido posible sin todos vosotros. Gracias.

INDEX

ABBREVIATIONS

List of abbreviations

AICD	Activation-induced cell death
ANXA 1	Annexin 1
APC	Antigen-Presenting Cells
BATF-3	Basic Leucine Zipper ATF-Like Transcription Factor 3
CRT	Calreticulin
CTL	Cytotoxic T Lymphocyte
CTLA-4	Cytotoxic T-Lymphocyte Antigen 4
DAMPs	Damage-Associated Molecular Patterns
DCs	Dendritic Cells
DISC	Death-Inducing Signalling Complex
dMMR	MisMatch Repair deficient
DSS	Dextran sulfate sodium salt
Eomes	Eomesodermin
Epcam	Epithelial Cell Adhesion Molecule
FADD	Fas Associated via Death Domain
FDA	Food and Drug Administration
FLT3-L	FMS-like tyrosine kinase 3 ligand
FT	Frozen-Thawed
GFP	Green Fluorescent Protein
GM-CSF	Granulocyte-macrophage colony-stimulating factor
GPX4	Glutathione Peroxidase 4

GSH	Glutathione
HMGB1	High Mobility Group Box 1
HSPs	Heat Shock Proteins
ICB	Immune Checkpoint Blockade
ICD	Immunogenic Cell Death
IFNAR	Interferon-α/β receptor
IFNγ	Interferon-gamma
IL	Interleukin
MHC	Major Histocompatibility Complex
MLK	Mixed Lineage Kinase domain-Like protein
MOMP	Mitochondrial Outer Membrane Permeabilization
MSI-H	MicroSatellite Instability-High
NK	Natural Killer Cell
NSCLC	Non-Small Cell Lung Cancer
ORR	Overall Response Rate
OVA	Ovalbumin
PAMPs	Pathogen Associated Molecular Patterns
PBMCs	Peripheral Blood Mononuclear Cells
PD-1/PD-L1	Programmed cell Death protein 1/ Programmed cell Death-Ligand 1
PUFA	PolyUnsaturated Fatty Acids
RCD	Regulated Cell Death
STING	Stimulator of Interferon Genes
T-bet	T-box transcription factor
Tcf-1	T cell Factor 1

TCR	Antigen-specific T-Cell Receptor
Tim-3	T-cell Immunoglobulin Mucin 3
TLR4	Toll-Like Receptor 4
TNF	Tumor Necrosis Factor
TNFR	Tumor Necrosis Factor Receptor
TRADD	TNFRSF1A Associated via Death Domain
TRAF2	TNF receptor-associated factor 2

GENERAL INTRODUCTION

In the nineteenth century Rudolf Virchow observing "lymphoreticular infiltrates" in neoplastic tissues put unconsciously the basis of the revolutionary field of immunotherapy, which allowed to Dr. James Patrick Allison and Dr. Tasuku Honjo to be the winners of the 2018 Nobel Prize for Medicine for their studies about Cytotoxic T-Lymphocyte Antigen 4 (CTLA-4) and Programmed cell death protein 1 (PD-1) respectively. Since the first lymphocytes were observed in tumors, the field of immunotherapy has evolved to the development of drugs that had revolutionized the clinical oncology.

In 2011, the Food and Drug Administration (FDA) approved Ipilimumab, an anti-CTLA-4 fully-humanized monoclonal antibody for the treatment of metastatic melanoma since it led to better responses compared to standard chemotherapy. Ipilimumab works masking the CTLA-4 epitope that binds to B7 proteins, blocking the crucial interaction that normally suppresses T cell responses.

Moreover, in 2014, the FDA approved anti-PD-1 antibodies, Nivolumab (Bristol-Myers-Squibbs) and Pembrolizumab (Merck) for melanoma as 2nd-line treatment. Nivolumab reached an overall response rate (ORR) of 32%. In case of Pembrolizumab it achieved an ORR of 37%. Since then, Nivolumab as monotherapy has been approved by FDA as 2nd-line or 3rd-line treatment for seven different malignancies including non-small cell lung cancer (NSCLC), Hodgkin's lymphoma and head and neck cancer. Nivolumab in combination with Ipilimumab was also approved as 1st-line-treatment for melanoma in 2015 and for renal cell carcinoma in 2018. Pembrolizumab is now the 1st-line treatment as monotherapy for melanoma, urothelial bladder cancer, PD-L1+ non-small cell lung cancer, Merkel cell carcinoma. For head and neck cancer and non-small cell lung cancer, Pembrolizumab was approved as 1st-line treatment in combination with chemotherapy while for the treatment of renal cell carcinoma it has been approved also as 1st-line in

combination with Axitinib (tyrosine kinase inhibitor). Moreover, Pembrolizumab has been approved as 3rd or 2nd-line of treatment for other six types of malignancies including microsatellite instability-high (MSI-H) or mismatch repair deficient (dMMR) cancers. The bests results in terms of ORR obtained by anti-PD-1 therapies are 59% for Pembrolizumab plus Axitinib in renal cell carcinoma and of 57% for Nivolumab plus Ipilimumab in melanoma, thus revolutionizing in this way the clinical oncology for solid tumors.

Atezolizumab (Roche), another monoclonal antibody targeting the pathway of PD-1 and PD-L1 (PD-1 ligand is expressed by tumor cells and myeloid cells), has been approved in 2016 for urothelial bladder cancer and NSCLC despite an overall response rate of only 15% and 17% respectively, which nonetheless is higher than the 10% achieved by the classical therapies. By 2018, Atezolizumab passed to be recommended as 1st-line-treatment for NSCLC and urothelial bladder cancer. Besides Atezolizumab two more anti-PD-L1 monoclonal antibodies have been approved: Durvalumab (AstraZeneca) and Avelumab (Pfizer/Merck). Anti PD-1 and anti-PD-L1 therapies block the interaction between these proteins that in normal conditions, bring T cells to cell cycle arrest, suppression of T cell migration, and reduced cytolytic mediators [141] .

Evidence clearly suggests that inhibiting the CTLA-4/B7.1,B7.2 and PD-1/PD-L1 signaling pathways reinvigorates tumor-specific T cells at the tumor site, but T cell recognition of tumor cells antigens is only the final step of an extremely complex system that involves countless players [1].

The Cancer-Immunity Cycle

The Cancer-Immunity Cycle (Figure 1), described by Chen and Mellman in 2013, pinpoints all the steps believed necessary to achieve an efficient immune response against cancer and all the factors that stimulate and inhibit this complex stepwise process.

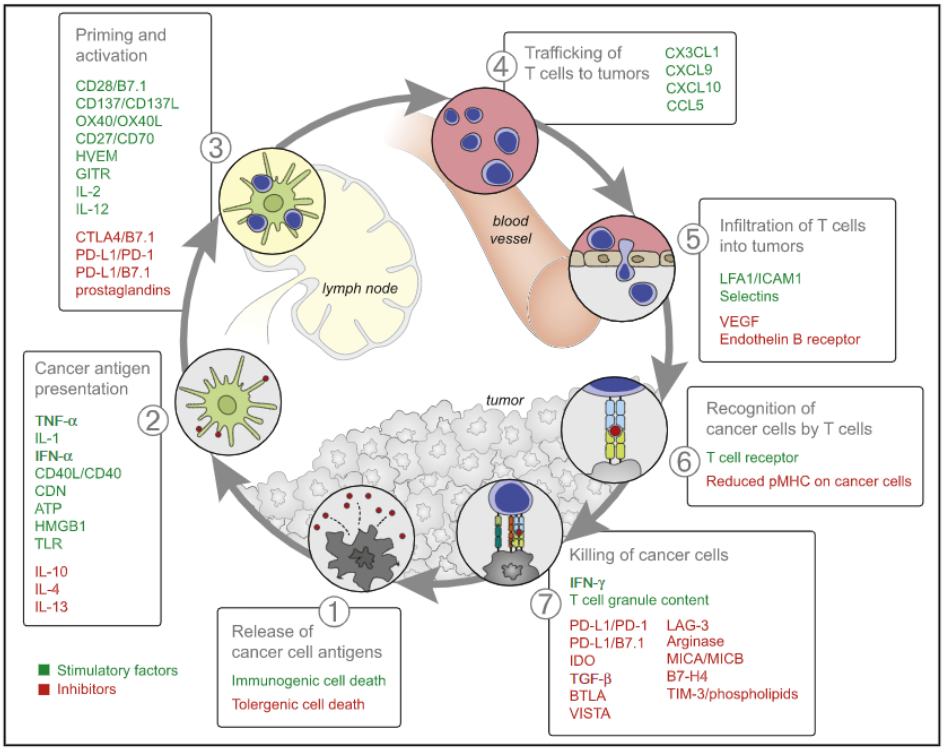

Figure 1: ***The Cancer-Immunity Cycle and the stimulatory and inhibitory factors involved [2].***

First of all, tissue cells following oncogenesis have to express and release abnormal proteins, that are the result of genetic alterations, known as neoantigens (Step 1). In order to promote DCs recruitment and an active adaptive response this step has to be accompanied by proinflammatory cytokines, signals released by dying cancer cell (i.e., HMGB1, ATP, cyclic dinucleotides) [3, 4] or by gut microbiome [5] that render the cancer cell death immunogenic rather than tolerogenic. Released antigens have to be captured and processed for antigen presentation by mature dendritic cells (DCs) (Step 2).

IL-10, TGF-β, IL-4, and IL-13 in the tumor microenvironment can prevent an adequate dendritic cell maturation and subsequent antigen processing while IFN-α is probably the most important stimulus of this step [6, 7]. Next, dendritic cells need to migrate to tumor-draining lymph nodes to prime and activate T cells. Here, T cells recognizing antigens presented by Major Histocompatibility Complex (MHC) class I and class II molecules may evolve as cytotoxic effectors against cancer cells (Step 3). The TCR-dependent antigen recognition is not sufficient to prime T cells. Signal 2 is indispensable in the priming phase. CD28-B7.1 (CD80) interaction, for example, represent an important stimulator of T-cell priming. B7.1 also binds to CTLA-4 with a higher affinity as compared to CD28, so the balance between activatory and inhibitory stimuli is considered critical in this step. Other important co-stimuli are mediated by CD137-CD137L, CD27-CD40 or OX40-OX40L [8]. In the next step, activated effector T cells are chemoattracted (i.e., CX3CL1, CXCL9, CXCL10, CCL5) to the tumor (Step 4), and infiltrate the tumor microenvironment (Step 5)[9]. There T cells recognize tumor antigens (Step 6) and attack cancer cells potentially until the complete clearance of the antigen (Step 7). However, it is well known that tumor antigens are often not presented because of intrinsic cancer cell mechanisms of immune escape, such as the dampening of MHC I expression [10]. Furthermore, in some cases, DCs and T cells do not recognize modified tumor proteins as dangerous entities, fostering T regulatory cell responses rather than effector responses. Moreover, the interaction of PDL-1 on cancer cells with PD-1 on T cells drives T cells towards an exhausted phenotype and an overall inefficient anti-cancer immune response [11].

The efficiency of effector cells in killing cancer cells is therefore controlled by the balance between the above mentioned inhibitory and activatory factors, that play a major role conceptualized in the Cancer-Immunity Cycle. The goal of immunotherapy is thus, acting

on such steps, initiate or reinitiate the cancer-immunity cycle, creating a self-sustaining immune response without causing autoimmune disorders.

Among the inhibitory and activatory factors involved in the first step of the cycle, some are linked to a process that is focusing the interest of many cancer immunologists: programmed cell death and its role in cancer immunotherapy.

Cell death and Immunity in cancer

The “Self /Non-self model”

Historically the immune system-driven tumor rejection has been explained with the “Self /Non-self model.” According to this model, the innate immune system activates against “microbial non-self” or “altered self” molecules, “missing self” states but keeps silent against “self” entities. Furthermore, the model proposed that autologous cells undergoing cell death do not elicit an immune response and are cleared in an “immunologically silent” manner, leading to immunological ignoprance or tolerance. Nonetheless, these views of the “Self/Non-self model” on immune response still hold true in some instances, it has been necessary switch to other models that could explain better the immune response [12, 13].

The Danger Model

The Danger Model was proposed to explain the immune-stimulation by self-cell death in sterile condition, that was not conceived by the “Self/Non-Self model". The Danger Model hypothesizes that the immune system responds preferentially to damage rather than to foreignness [12]. In other words, it hypothesizes that the immune system distinguishes between “safe” and “dangerous” entities. Endogenous danger signals linked to cell death have been subsequently identified as “damage-associated molecular patterns” (DAMPs) [14].

The phenomenon of Immunogenic Cell Death

The Danger Model inspired the hypothesis that cancer cells undergoing processes of cell death, including apoptosis, could be able to stimulate an effective immune response against neoplastic cells [15, 16]. Until recently most immunologists believed that only necrosis could be immunogenic because its morphological features that distinguish this type of cell death from other processes of programmed cell death.

An extensive number of studies published between 2005 and 2007 questioned the mechanisms that link cancer cell death by apoptosis and immunological response. This process is currently actually known as Immunogenic Cell Death (ICD) [17-19].

During this process cancer cells undergoing stress, mediated by several different stimulus (i.e., chemotherapy, radiotherapy, targeted anti-cancer drugs) release damage-associated molecular patterns (DAMPs) capable of alerting the immune system by binding to receptors on immune cells. Among these DAMPs (Figure 2) the most well known are:

- Extracellular High Mobility Group Box 1 (HMGB1) protein: A nuclear protein normally associated with histones that, when released, binds to toll-like receptor 4 (TLR4) and activates the Myd88 pathway in DCs facilitating tumor antigen processing [19-21].
- Surface exposed Calreticulin (CRT) and ecto Heat Shock Proteins (HSPs): Both act as “eat me” signals stimulating phagocytosis of cell corpses by antigen-presenting cells (APC), the release of pro-inflammatory cytokines (i.e. IL-6, TNF) from DCs as well as polarization to a Th1-like response [18, 22, 23].

- Extracellular ATP: “Find me” signal that mediates chemotactic and adjuvant-like effects binding to ionotropic and metabotropic purinergic receptors on APC and their precursors. By P_2X_7 receptor, ATP can also activate NLRP3 inflammasome, resulting in caspase-1 activation and production of IL-1β [24, 25].
- Extracellular Annexin 1 (ANXA1): ANXA1 belongs to a superfamily of proteins that bind acidic phospholipids in a Ca^{2+}-dependent manner, and it is expressed by myeloid, lymphoid cells as well as by many epithelial cell types. It attaches to formyl peptides receptors and APC lacking these receptors are not able to initiate an effective adaptive immune response [26, 27].
- Type I Interferons: Released by dying cancer cells, it acts on the same cells to induce CXCL10, which in turn recruits T cells to the tumor site [28, 29].

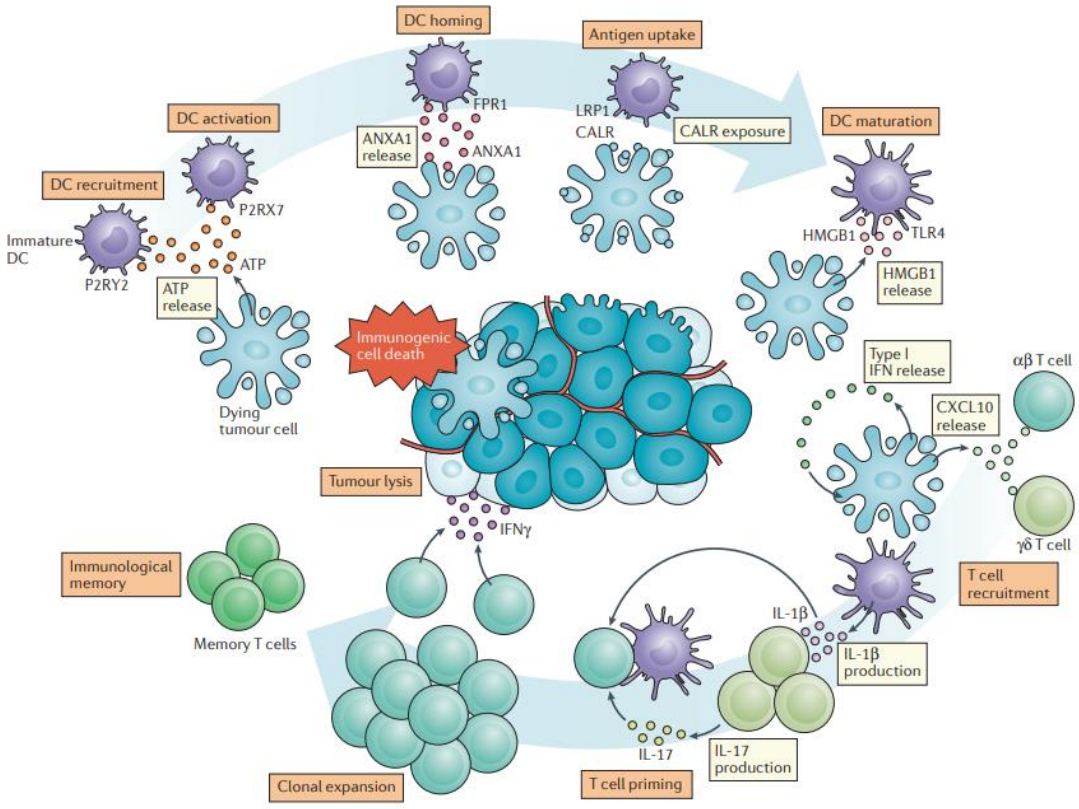

Figure 2: ***DAMPs and their role in Immunogenic Cell Death [4].***

Mechanisms of Regulated Cell Death

Several types of regulated cell death are relevant for cancer immunotherapy and potentially involved in immunogenic cell death. Here, in brief, are summarized the most studied:

- Apoptosis: It is initiated by perturbations of the extracellular environment or genetic stress that results in cells dying without early destruction of the plasma membrane and degradation of genomic DNA in nucleosome fragments. Two pathways named Extrinsic and Intrinsic pathway execute apoptosis [30].

  The Extrinsic Pathway is mediated by two types of membrane receptors:

  (1) death receptors (Fas, TRAILR1/2, TNFR1) whose activation depends on the binding of the cognate ligands [31].

  (2) dependency receptors that activate when the level of their ligands drops below a specific threshold [32].

  Fas-ligand and TRAIL binding to Fas or TRAILRs respectively causes receptor homotrimerization and a conformational change at the intracellular tails that permits the association of the adaptor FADD (Fas Associated via Death Domain). FADD, in turn, recruits the death-inducing signaling complex (DISC) which promotes the switch of the procaspase-8 to its active form [33].

  In contrast TNFR1 associated with TRADD (TNFRSF1A Associated via Death Domain) which works as an adaptor for the assembly of the caspase-8 activator complex I, encompassing among other proteins, the TNF receptor-associated factor 2 (TRAF2) and the receptor-interacting serine/threonine-protein kinase 1 (RIPK1)[34].

The activated caspase-8 triggers, thus the signaling cascade having as executioners mostly caspases 3 and 7 [34].

Viral infection, DNA damage, and growth factor deprivation are the major stimuli that trigger the intrinsic (or mitochondrial) pathway of apoptosis [35-37]. Cytotoxic cells induce this pathway during killing by granzyme-containing cytotoxic granules. The intrinsic pathway is initiated by mitochondrial outer membrane permeabilization (MOMP), controlled by pro-apoptotic or anti-apoptotic members of the BCL2 protein family [38]. Best characterized pro-apoptotic members involved in MOMP are BAK and BAX [39]. On the contrary, MOMP can be inhibited for example by BCL2 itself or BCL-X_L [39]. Subsequently, MOMP promotes the irreversible release of apoptogenic mitochondrial factors (i.e., APAF1, Cytochrome C) [38], formation of the apoptosome and autocatalytic activation of initiator caspase 9 [40]. In this process, caspase 3 and 7 are the major executioners due to their role in destroying the subcellular structures (Figure 3) [41].

It has also been described a caspase-independent pathway. It is mediated by the release of endonuclease G and apoptosis–induced factors from mitochondria that relocate in the nucleus and cleave the DNA in a caspase-independent manner. Morphologically, apoptosis is characterized by non-lytic cell shrinkage, DNA fragmentation, and apoptotic bodies [42].

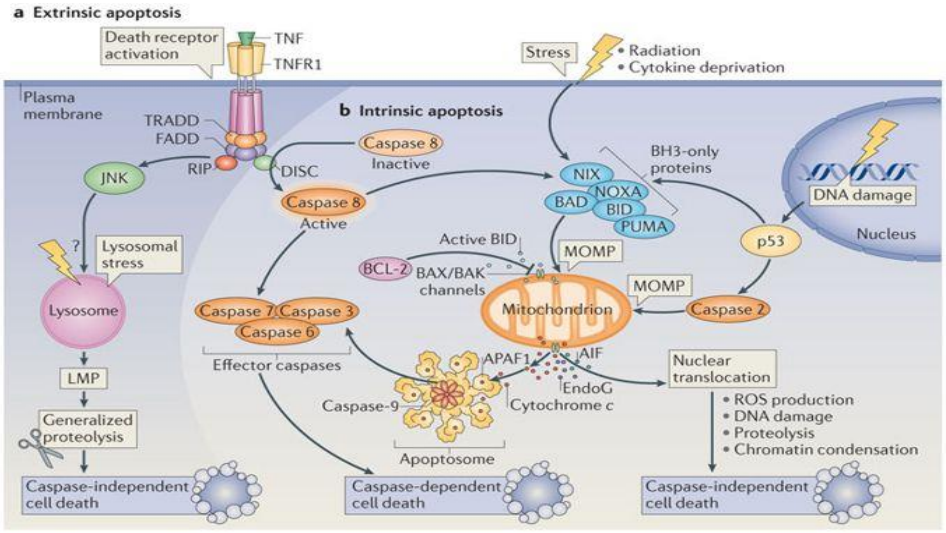

Figure 3*: Apoptosis Extrinsic and Intrinsic pathways* [43]

- Necroptosis: It is induced by death receptors (TNFR1) [44] or pathogen recognition receptors (i.e., TLR3, TLR4, ZBP1) [45] signaling and activation of the receptor-interacting protein (RIP) family [44]. This phenomenom is apparent when cells are stimulated by TNF under inhibition of caspase protease activity, Upon initiation, phosphorylated RIP kinase 1 (RIPK1) activates RIP kinase 3 (RIPK3), and together these proteins generate a complex called “necrosome” which triggers necroptosis [46]. RIPK3 catalyzes the phosphorylation of mixed lineage kinase domain-like protein (MLKL) facilitating its oligomerization. Oligomerized MLKL translocates into the plasma membrane resulting in formation of pores membrane permeabilization [47]. Inhibitors of RIPK1 such as necrostatin-1, inhibit TNFR1-driven necroptosis *in vivo* and *in vitro* [48]. Moreover, experimental inhibition of caspase-8, upon TNFR1 activation, redirects apoptosis to a necroptosis program[34]. Morphologically, necroptosis is

described as a non-lytic process characterized by loss of plasma membrane integrity and swollen cellular organelles [42].

- Pyroptosis: Initiated by pathogen-associated molecular patterns (i.e., LPS), this form of regulated cell death, in contrast to apoptosis, is mediated mostly by caspase-1 (both in mice and humans) which is triggered by the "inflammasome" complex [49]. Caspase-1 cleaves the proforms of IL-1β and IL-18 to their active forms and releases the autoinhibitory domain of the executioner Gasdermin-D leading to its insertion into the plasma membrane generating a large pore [49, 50]. Morphologically it is characterized by a peculiar form of chromatin condensation that differs from that one present during apoptosis, cellular swelling, and plasma membrane permeabilization [42].
- Ferroptosis: This form of regulated cell death occurs via an iron-catalyzed process of lipid peroxidation initiated through non-enzymatic (Fenton reactions) and enzymatic mechanisms (lipoxygenases) [51]. It is caspase and necrosome independent. Polyunsaturated fatty acids (PUFAs) are the targets of lipid peroxidation [51]. Glutathione peroxidase 4 (GPX4) has been demonstrated to be the major physiological inhibitor of ferroptosis because it limits lipids peroxidation producing glutathione (GSH) from intracellular cysteine [51]. Also vitamin E, liproxstatin-1, ferrostatin-1 can block de deleterious consequences of lipid peroxidation [52, 53] . Lipid peroxidation, as the final step of this process, causes membrane destabilization and pores formation [54]. The balance between iron accumulation-induced ROS production and antioxidants that avoid lipid peroxidation are critical for ferroptosis. Morphologically it appears similar to necrosis. It is characterized by mitochondrial alterations and shrinkage, reduced/disappeared cristae, and membrane permeabilization [42].

- Autophagy–dependent cell death: It is a caspase-independent form of regulated cell death that triggers lysosomal-proteinase regulated elimination of cellular organelles. It is initiated by nutrient deprivation, hypoxia or infectious pathogens. It is characterized by the formation of intracellular vacuoles and, in contrast to apoptosis, it does not present chromatin condensation. It has been demonstrated that dying cells lacking autophagy-related genes are not able to present "eat me" signals [55].

One of the consequences of the conceptual revolution of considering regulated cell death (RCD) such as apoptosis not to be tolerogenic, was the root of our experimental approach to this field. In fact, the gold standard to determine whether a compound leads to immunogenic cell death or not does not depend on the morphological features induced by the mode of cell death but rather relies on immunization of immunocompetent mice with the corresponding dying cells and observation of their immune response to a challenge with the corresponding vaccination-matched living cancer cells [56].

Cell death and cross-presentation

Antigen presentation on MHC molecules on antigen presenting cells may occur via two different pathways. In general, endogenous peptides, derived from intracellular proteins are exposed on the surface of presenting cells on MHC-I to be recognized by cytotoxic $CD8^+$ T-cells. Through this pathway infected cells are able to present peptides from intracellular pathogens such as viruses or bacteria and elicit the resolution of the infection and from endogenous transduced proteins. All nucleated cells can present endogenous peptides via this pathway albeit this is strongly increased by type I and II interferons [57].

Cross-presentation, exerted by special subpopulation of dendritic cells, is the particular process trough which exogenous internalized proteins are presented in the form of cognate peptides to cytotoxic T-cells on MHC-I molecules [57]. In general, is well accepted that cDC1s, in mouse, are the cells responsible for cross-presentation of dead cell-associated antigens, since cDC2s seem to do not present this capability. In humans this dichotomy is not so clear [58]. cDC1s depend on the transcription factors BATF3 and IRF8 for their development [59]. It has been demonstrated that Batf3 dependent cDC1 are necessary for the anti-tumoral activity of immunotherapies such PD-1/PD-L1 blockade or CD137 agonists [60, 61]. In mice cDC1 are characterized for the expression of XCR1, CD8α, CD103 and Clec9a [62]. In human they present XCR1, Clec9a and CD141 (BDCA-3) [62].

It is becoming increasingly clear that the presence of cells that efficiently cross-present tumor antigens to T-cells is extremely important to elicit an effective immune response against cancer. The T-cell expansion and activation that occur with cross-presentation is known as cross-priming [57]. Cross-priming mostly occurs in secondary lymphoid organs.

ICD, cross-priming and cross-presentation are strongly connected since some DAMPs, released by dying cells, attract cross-presenting DCs (cDC1), increase the uptake and the presentation of dead cell-related antigens, mature dendritic cells allowing to these cells to cross-prime. In absence of maturation, DCs will induce anergy or apoptosis of T-cells, by a mechanism known as cross-tolerance. Several studies [19, 63] have demonstrated that ICD agents such as conventional chemotherapy and radiotherapy require dendritic cells for their anti-tumoral effect and when these cells are absent these cancer treatments are inefficient.

cDC1 receptors mostly involved in dead cell-associated antigens capture are DEC205 and Clec9a, recognizing respectively keratin and filamentous actin [64, 65]. Other proteins that have been described to be involved in cross-presentation are Sec22b, a regulator of endoplasmic reticulum–phagosome traffic, and WDFY4 also involved in subcellular vesicular trafficking [66, 67].

Activation-induced cell death in T lymphocytes

As it is well known, lymphocytes when activated by the recognition of a specific antigen epitope experience clonal expansion phase followed by a subsequent contraction phase characterized by the apoptotic elimination of most such activated lymphocytes. Peripheral deletion is controlled at least in part by activation-induced cell death (AICD). In theory, this phenomenon occurs to compensate the immune system production of large numbers of T cells, so the balance between expanding and apoptotic T cells is necessary to prevent excessive immune reactions that can cause host pathology. AICD is triggered by repeated antigen receptor ligation and may occur in immature, transformed T cells, as well as mature and activated peripheral blood T lymphocytes. AICD can be elicited by engagement of TNFRs superfamily members on activated T lymphocytes by their activated neighbors resulting fratricide killing. Additionally, after activation, T lymphocytes express Fas L that mediates cell death of themselves or neighboring sister cells. Moreover, it has been demonstrated that activated T cells could mediate via TNF/TNFR1/NF-kB pathway the expression of FasL in nonlymphoid tissues (i.e., intestinal epithelial cells). Fas-bearing lymphocytes undergo peripheral deletion when binding to Fas L -expressing cells. Probably the "fratricide" killing is frequent in lymphoid organs while the induced Fas L acquires importance in nonlymphoid organs, where T cells work "solo" [68, 69].

HYPOTHESIS AND AIMS

HYPOTHESIS

The main hypothesis of this thesis is that cell death, involving cancer cells as well as effector cells, plays a major role in immune response and in the outcome of immunotherapy.

On one hand, based on the improvement of tumor control achieved by immunotherapies (i.e., immune checkpoint blockade) which lead to the augment of effector capabilities of cytotoxic cells, we hypothesized that cytotoxicity "per se" exerted by T cells and NK cells, is able to induce a cancer cell death characterized by immunogenic features, comparable to those resulting from immunogenic treatments such as chemotherapy, triggering an active adaptive immune response.

On the other hand, we hypothesize that Tumor Necrosis Factor (TNF), released upon lymphocytes activation during immune checkpoint blockade therapy with anti-PD1 and anti-CTLA-4 agents, is not essential for tumor control, being conversely a detrimental factor for the outcome of the treatment because its involvement in activation-induced cell death (AICD) of antigen-specific T cells and in immune-related adverse events.

OBJECTIVES

1. To analyze markers of immunogenic cell death following cytotoxicity by T cells or NK cells cytotoxicity *in culture.*
2. To study *in vivo*, with a model of vaccination/challenge, the immunogenicity of T and NK cell-mediated cytotoxicity and the indispensable immunological mechanistic requirements for this process.
3. To study the effects of TNF neutralization on ICB therapy-induced side effects using a mouse model of colitis.
4. To study the effects of TNF neutralization on the anti-tumoral activity of ICB therapy.
5. To study the role of TNF on effector T cells, in terms of AICD and exhaustion, upon ICB therapy.

RESULTS

Chapter 1

“CELLULAR CYTOTOXICITY IS A FORM OF IMMUNOGENIC CELL DEATH”

CELLULAR CYTOTOXICITY IS A FORM OF IMMUNOGENIC CELL DEATH

Authors: Luna Minute[1,2], Alvaro Teijeira[1,2,3], Alfonso Rodriguez Sanchez-Paulete[1,2], Maria Carmen Ochoa[1,2,3], Maite Alvarez[1,2], Itziar Otano[1,2], Iñaki Etxeberria[1,2], Elixabet Bolaños[1,2], Arantza Azpilikueta[1,2], Saray Garasa[1,2], Noelia Casares[1,2], José L. Perez-Gracia[2,4], Maria Esperanza Rodriguez-Ruiz[1,2,4], Pedro Berraondo[1,2,3], Ignacio Melero[1,2,3,4].

Affiliation: [1]Program of Immunology and Immunotherapy, Center for Applied Medical Research (CIMA), Pamplona, Spain.[2]Navarra Institute for Health Research (IDISNA), Pamplona, Spain.[3]Centro de Investigación Biomédica en Red de Cáncer (CIBERONC), Spain.[4]Department of Oncology, Clínica Universidad de Navarra, Pamplona, Spain.

KEYWORDS: Immunogenic cell death, cytotoxicity, $CD8^+$ T cells, NK cells, cross-priming.

ABSTRACT

Background: The immune response to cancer is often conceptualized with the Cancer Immunity Cycle. An essential step in this interpretation is that antigens released by dying tumors are presented by dendritic cells to naive or memory T cells in the tumor-draining lymph nodes. Whether tumor cell death resulting from cytotoxicity, as mediated by T cells or NK lymphocytes, is actually immunogenic currently remains unknown.

Methods: In this study, tumor cells were killed by antigen-specific T-cell receptor (TCR) transgenic CD8 T cells or activated natural killer cells. Immunogenic cell death was studied analyzing the membrane exposure of calreticulin and the release of high mobility group box 1 (HMGB1) by the dying tumor cells. Furthermore, the potential immunogenicity of the tumor cell debris was evaluated in immunocompetent mice challenged with an unrelated tumor sharing only one tumor-associated antigen and by class I MHC-multimer stainings. Mice deficient in BATF-3, IFNAR and STING were used to study mechanistic requirements.

Results: We observe in co-cultures of tumor cells and effector cytotoxic cells, the presence of markers of immunogenic cell death such as calreticulin exposure and soluble HMGB1 protein. OVA-transfected MC38 colon cancer cells, exogenously pulsed to present the gp100 epitope are killed in culture by mouse gp100 specific TCR transgenic CD8 T cells. Immunization of mice with the resulting destroyed cells induces epitope spreading as observed by detection of OVA-specific T cells by MHC multimer staining and rejection of OVA^+ EG7 lymphoma cells. Similar results were observed in mice immunized with cell debris generated by NK-cell mediated cytotoxicity. Mice deficient in BATF3-dependent dendritic cells (cDC1), fail to develop an anti-OVA response when immunized with tumor cells killed by cytotoxic lymphocytes. In line with this, cultured

cDC1 dendritic cells can readily cross-present antigen from cytotoxicity-killed tumor cells to cognate CD8 T lymphocytes.

Conclusion: Taken together, these results support that an ongoing cytotoxic antitumor immune response can lead to immunogenic tumor-cell death.

INTRODUCTION

Antitumor immunity largely relies on effector cytotoxic T or NK cells [70]. Tumor cells may succumb upon contact with activated cytotoxic lymphocytes as a result of pores formed by poly-perforin that permit the entrance of granzyme B to activate caspase-dependent apoptosis [70, 71]. Furthermore, activated cytotoxic cells exhibit TNF-family pro-apoptotic ligands such as Fas-L [72] and TRAIL [73] that may elicit processes of apoptosis in the tumor cells [70].

Under normal circumstances, apoptosis is considered a form of immunologically-silent programmed cell death. In tumor immunotherapy, it becomes important to know if cytotoxicity would be immunogenic or on the contrary tolerogenic to sustain and diversify the immune response. In fact, immunogenicity of tumor cell death coupled to release of intracellular tumor antigens has been postulated in the so-called cancer immunity cycle [2, 74].

Immunogenic versus non-immunogenic death of tumor cells has been extensively investigated by the groups of G. Kroemer, L. Zitvogel and L. Galluzzi [4, 75]. Following incisive experiments in mice [17] which correlated with clinical findings, immunogenic cell death was categorized as being able to enhance T- cell recognition of tumor antigens thereby delaying tumor growth in immunocompetent but not in immunodeficient mice [56]. Mechanistic and correlative experiments linked immunogenic cell death to the endoplasmic reticulum stress response, and to the release or exposure of eat-me signals and alarmins that act on dendritic cells to induce functional maturation into cells efficiently presenting tumor antigens [63]. Calreticulin exposure on the plasma membrane [76], ATP release [22, 77], HMGB1 release [78], mitochondrial and extracellular formyl peptides [26] are considered hallmarks of immunogenic cell death [56]. These findings

are reminiscent of the danger model as postulated by Dr. P Matzinger, which predicts that factors released upon tissue damage or cell stress are responsible for immunogenicity [12, 79]. These are termed damage-associated molecular patterns (DAMPs) [80].

The main inherent mechanism to turn on and sustain CD8 T-cell immunity is tumor-antigen cross-priming as mediated by BATF-3 dependent cDC1 dendritic cells [57, 81]. These cells are able to capture antigens from cell-death-associated debris and present such exogenous antigens via the major histocompatibility complex (MHC) Class I in the context of both costimulation and IL-12 production [57, 81]. Of note, these cDC1 cells closely cooperate with NK cells in the tumor microenvironment to elicit antitumor immunity [82, 83].

Our quest in this study was to ascertain if cytotoxicity as mediated by CD8 T cells or NK cells is a form of immunogenic cell death or not. Multiples lines of experimental evidence laid before us in mouse models unequivocally show that cytotoxicity is indeed a form of immunogenic cell death since the remains of killed cells efficaciously induce antitumor immunity.

MATERIALS AND METHODS

Mice and cell lines

Experiments involving mice were approved by the Ethics Committee of the University of Navarra. C57BL/6 mice (5-8 weeks old, female) were obtained from Envigo (Huntingdon, Cambridgeshire, UK) and maintained in the animal facility of Cima Universidad de Navarra. C57Bl/6 *Batf3*$^{tm1Kmm/J}$ (Batf3KO), *Tmem173*$^{gt/J}$ (STINGKO), *IFNα/bR*$^{o/o}$ (IFNARKO), *C.129S7(B6)Tag1tm1Mom/J* (RAG1), *B6.Cg-Thy1*^{a}*/CyTg(TcraTcrb)8Rest/J* (Pmel-1) [84], C57BL/6-*Tg(TcraTcrb)1100Mjb/J* (OT-I), C57Bl/6 *Tg14(act/EGFP)Osby* (OT-I-EGFP) mice were bred at CIMA Universidad de Navarra in specific pathogen-free conditions. Batf3KO [85], STINGKO [86], and IFNARKO [87] mice were kindly provided, respectively by Dr. Kenneth M. Murphy (Washington University, St. Louis, MO, USA), by Dr. Gloria González Aseguinolaza (Cima Universidad de Navarra, Pamplona, Spain), and by Dr. Matthew Albert (Institut Pasteur, Paris, France). The MC38hEGFR cell line was kindly provided by Dr. Pablo Umaña (Roche). This cell line was stably transfected with Lipofectamine 2000 (Thermo Fisher Scientific, San Jose, CA, USA) with pCI-neo plasmid expressing membrane-bound ovalbumin (OVA) (#25099, Addgene, Cambridge, MA, USA). MC38hEGFROVA clones were established by limiting dilution. OVA expression was confirmed by intracellular OVA staining (ab85584, Abcam, Cambridge, UK) and real-time PCR. The MC38hEGFROVA, EG7, MC38, B16OVA, CHO FLT3-L FLAG cell lines were maintained at 37ºC in 5% CO_2 and were grown in RPMI Medium 1640+Glutamax (Gibco, Invitrogen, Carlsbad, CA) containing 10% heat-inactivated FBS (Gibco, Invitrogen), 100 IU/mL penicillin and 100 µg/mL streptomycin

(Gibco) and 50 µM 2-Mercaptoethanol (Gibco). The MC38hEGFROVA cell line was grown with 6 µg/ml of Puromycin (Gibco) and 400 µg/ml of Geneticin (Gibco). To avoid loss of transgene expression, B16OVA and EG7 were maintained with 400 µg/ml of Geneticin.

The HT29 cell line was cultured as other cells but without 2-Mercaptoethanol supplementation in the culture medium.

X-63 GM-CSF was grown in Iscove's modified Dulbecco Medium (Sigma-Aldrich, St. Louis, MO, USA) supplemented with 1mg/ml of Geneticin with 5% FCS, 100 IU/mL penicillin and 100 µg/mL streptomycin.

Murine lymphocyte activation

Spleens from euthanized Pmel-1 mice were excised and splenocytes isolated mechanically and cultured at a concentration of $1{,}5x10^6$/ml for 48 hours with 100 ng/ml of human $gp100_{25\text{-}33}$ (KVPRNQDWL, RP20344, GenScript, Piscataway, NJ, USA). After 48 hours, we added fresh media and 30 UI/ml of IL-2 (Proleukin, Novartis) and kept the culture for 48 hours.

To generate murine activated NK cells, we injected at a high hydrostatic pressure into the tail vein of RAG1 mice 10 µg of Apo-Sushi-IL-15 expressing plasmid [88] in 2 ml of physiological saline solution. We harvested spleens after three days and isolated murine NK cells by negative selection following the manufacturer's instructions (NK Cell Isolation Kit II mouse, Miltenyi Biotec, Bergisch Gladbach, Germany).

In vitro killing

To obtain T cell-derived tumor debris, MC38hEGFROVA cells were incubated for 48 hours with 15 UI/ml of murine IFNγ (Miltenyi Biotec) to increase expression of MHC-I and 100 ng/ml of human gp100 peptide (KVPRNQDWL). Following activation during 48h, Pmel-1 splenocytes were mixed with MC38hEGFROVA at a ratio of 10:1 in the presence of 30 UI/ml of IL-2 and 100 ng/ml of human gp100 and cultured for 3 days.

To obtain NK cell-derived tumor debris, *in vivo* activated NK cells (following the protocol described above) were co-cultured with MC38hEGFROVA cells at a ratio of 3.5:1 with 200 UI/ml of IL-2 for 3 days.

Cell debris was washed twice in ice-cold PBS and pellets resuspended in ice-cold PBS to be used in the immunization experiments.

Immunogenic cell death markers

We set up co-cultures of tumor cells and murine T cells or murine NK cells as described above, and 24 hours later, supernatants were collected for HMGB1 detection by ELISA (IBL International, Hamburg, Germany) or stored at -80 C until use. Tumor cells were analyzed for calreticulin expression. Cells were washed with Staining Buffer (0.5% FBS, 0.5% EDTA 0.5 M, 1% Penicillin/Streptomycin) and stained for 30 minutes on ice with a mix containing: anti-mouse CD16/32 (S17011E, 1:100, Biolegend, San Diego, CA, USA), CD45BV510 (30-F11, 1: 200, Biolegend) and Calreticulin Alexa Fluor 647 (1:100, Abcam). Cells were then washed and stained with a mix of AnnexinV FITC (1:200, Biolegend) and 7-AAD (1:75, Biolegend) in Annexin Binding Buffer (Biolegend) for 15 minutes at RT.

Human peripheral blood mononuclear cells (PBMCs) were isolated by density gradient separation (Ficoll-Paque Plus, GE Healthcare, Chicago, IL, USA) from healthy donor whole blood. T and NK cells were separated using magnetic beads (human $CD8^+$ T cell isolation kit or human NK Cell Isolation Kit, Miltenyi Biotec).

$5x10^4$ human T cells were co-cultured with HT29 (1:1) in 96 U bottom plate in 200 µl of complete medium with or without 1 µg/ml Epcam-CD3 bi-antibody (Creative Biolabs, Shirley, NY, USA) for 48 hours [89].

Human NK cells immunomagnetically selected as $CD3^-CD56^+$ were pre-activated 48 hours with 100 UI/ml IL-2 and 10 ng/ml of IL-15 (Peprotech) in NK MACS medium (Miltenyi). 48 hours later, $8,5x10^4$ NKs were incubated with HT29 (1:1) for 48 hours in 1ml of complete medium in 12 well plates.

Supernatants were collected for HMGB1 detection by ELISA (IBL International), and tumor cells were analyzed for surface calreticulin expression as described above (Human IgG, 1:100 -CD45, 2D1, FITC, Biolegend, 1:500 - Calreticulin Alexa Fluor 647, Abcam, 1:100 - Annexin V PE, Biolegend, 1:100 - 7AAD, Biolegend, 1:75).

Immunization experiments

A total of $1.2x10^6$ tumor cells killed in different ways (10:1 for T cells, 3,5:1 for NK cells), Doxorubicin (Sigma Aldrich) or FT were resuspended in 200 µl of Phosphate Buffered Saline (Gibco) and injected subcutaneously above the tail. After 7 days, we subcutaneously challenged mice with $5x10^5$ EG7 in the right flank.

Positive control with Doxorubicin was performed treating cells with 2.5 µM of Doxorubicin for 24 hours [17]. For T cell-derived debris immunization experiments,

doxorubicin-treated cells were also pulsed with 100 ng/ml of human gp100 synthetic peptide.

Control FT was generated by killing cells by 3 cycles of dry-ice and immersion in a 37ºC bath. To prepare debris for immunization, all $4x10^5$ cells were incubated with 300 ng of human gp100 peptide for 1 hour at 37ºC before being killed by freeze / thawing.

Tumor growth was monitored twice a week with an electronic caliper. Mice were sacrificed when the tumor reached 18 mm.

Detection of antigen-specific T cells

At day seven post-immunization, whole blood was drawn from mice, and 100 µl of peripheral blood were stained with H-$2K^b$ OVA PE (iTag MHC Tetramer, 1:200, MBL International, Woburn, MA, USA), anti-mouse CD16/32 (S17011E, 1:100) for 15 minutes at 4ºC. Without washing, we added 5 µl of a mix of CD8 Alexa Fluor 647 (53-6.7, 1:200, Biolegend) and incubated samples for 15 minutes at 4ºC. Erythrocytes were eliminated by adding 1 ml of FACS Lysing Solution (BD, Franklin Lakes, NJ, USA) per sample for 5 minutes at RT [60, 90]. Samples were acquired at BD FACS Canto II system and analyzed with Flow Jo 10 software.

Subcutaneous in vivo killing

Splenocytes from OT-I mice were plated at $1.5x10^6$/ml and activated for 48 hours with SIINFEKL peptide ($OVA_{257-264}$, Invivogen, San Diego, CA, USA). Two days later, we added fresh new medium and 30 UI/ml of IL2. After 48 hours, $5x10^5$ MC38hEGFROVA were injected with 10^7 activated OT-I splenocytes (20:1) into the right flank of C57BL/6

mice. After seven days, we challenged mice by injecting $5x10^5$ MC38 cells into the left flank. Tumor growth was monitored twice a week with an electronic caliper. Mice were sacrificed when the tumor reached 18 mm.

Subcutaneous in vivo killing imaging

In vivo killing control was performed injecting subcutaneously into the ear of C57BL/6 mice, pre-activated splenocytes from OT-I EGFP mice, and DRAQ 5 (Thermo Scientific) stained MC38hEGFROVA cells (20:1).

Mice were anesthetized with Ketamin/Xylazine and subsequently, ears were depilated with Veet cream. After extensive rinsing, mice were placed on a custom made microscopy stage with the ears placed on top of a cover glass. Images were taken in a LSM880 inverted microscope (Zeiss) equipped with a 25x Objective LD LCI Plan APO N/A 0.8. DRAQ 5 was excited with an HeNE 633 laser, and OT-I GFP cells were excited with a 488 Argon laser. Images were then acquired and analyzed with the Zen software (Zeiss). Linear gamma correction was applied to both the DRAQ 5 and GFP channel to eliminate skin background in all images.

Bone marrow-derived CD103$^+$cDC1

Bone marrow cells were harvested from femurs and tibiae of C57BL/6 mice and $15x10^{\wedge 6}$ cells were cultured in a sterile Petri dish (Sarstedt, Nümbrecht, Germany) in 10 ml of medium (RPMI Medium 1640+Glutamax + containing 10% heat-inactivated FBS + 100 IU/mL penicillin and 100 µg/mL streptomycin + 50 µM 2-Mercaptoethanol) containing 45% and 1.25% of FLT3-L [91] and GM-CSF [92] enriched supernatants respectively produced by the CHO FLT3-L FLAG and X-63 GM-CSF cell lines. At day 5, complete

medium without enriched supernatants was added. At day 9, non-adherent cells were harvested, and $3x10^6$ cells were re-plated in 10 ml of complete medium with enriched supernatants as at day 0 [93].

In vitro cross-presentation

T cell- and NK cell-derived debris was obtained as described before. After 16 hours, we added $4x10^5$ BM-derived $CD103^+$ cDC1. After 3 hours, we stained (CD11c APC, N418, 1:200, Biolegend - CD103 PerCP-Cy5.5, 2E7, Biolegend, 1:100 - SYTOX green Nucleic Acid Stain, Thermo Fisher,1:200000) the samples for flow cytometry-based sorting (FACSAria III, BD) and isolated alive $CD11c^+CD103^+$ DCs. DCs were incubated at a ratio of 1:5 with OT-I mice-derived splenocytes previously labeled with Violet Cell Proliferation Dye 450 (BD Horizon) according to the kit protocol for assessing to antigen-specific proliferation. After 72 hours, we checked $CD8^+$ cell proliferation by flow cytometry [60, 90]. Samples were acquired using a BD FACSCanto™ system and analyzed with Flow Jo 10 software.

Statistical analysis

GraphPad Prism version 6.01 software (GraphPad Software, Inc.) was used for statistical analysis. We used the log-rank test to determine the significance of differences in tumor development curves. Mean differences were compared with t-tests for two group comparisons or one-way ANOVA followed by Dunnet multiple comparison tests for three or more group comparisons. P values <0.05 were considered to be statistically significant.

RESULTS

Cytotoxic T lymphocytes and natural killer cells induce features of immunogenic cell death on tumor cells.

Immunogenic cell death is characterized by the release or exposure on the cell surface of different DAMPs that can prime an antitumor immune response. We focused our characterization of immunogenic cell death on two of its most prominent hallmarks [56]. First, we analyzed the exposure on the cell membrane of calreticulin, which is localized in the endoplasmic reticulum in the steady state but becomes relocated to the cell surface as a result of reticulum stress responses. Furthermore, we studied the release from the nucleus of high mobility group box 1 (HMGB1) to the supernatant. To achieve a complete cytotoxic killing of the MC38hEGFROVA cell line, tumor cells were pretreated with IFNγ to upregulate surface MHC I expression and loaded with the immunodominant human gp100 peptide. Under these conditions, *in vitro* pre-activated TCR-transgenic Pmel-1-derived $CD8^+$ splenocytes were able to induce over 95% tumor cell death (Supp.Fig. 1).

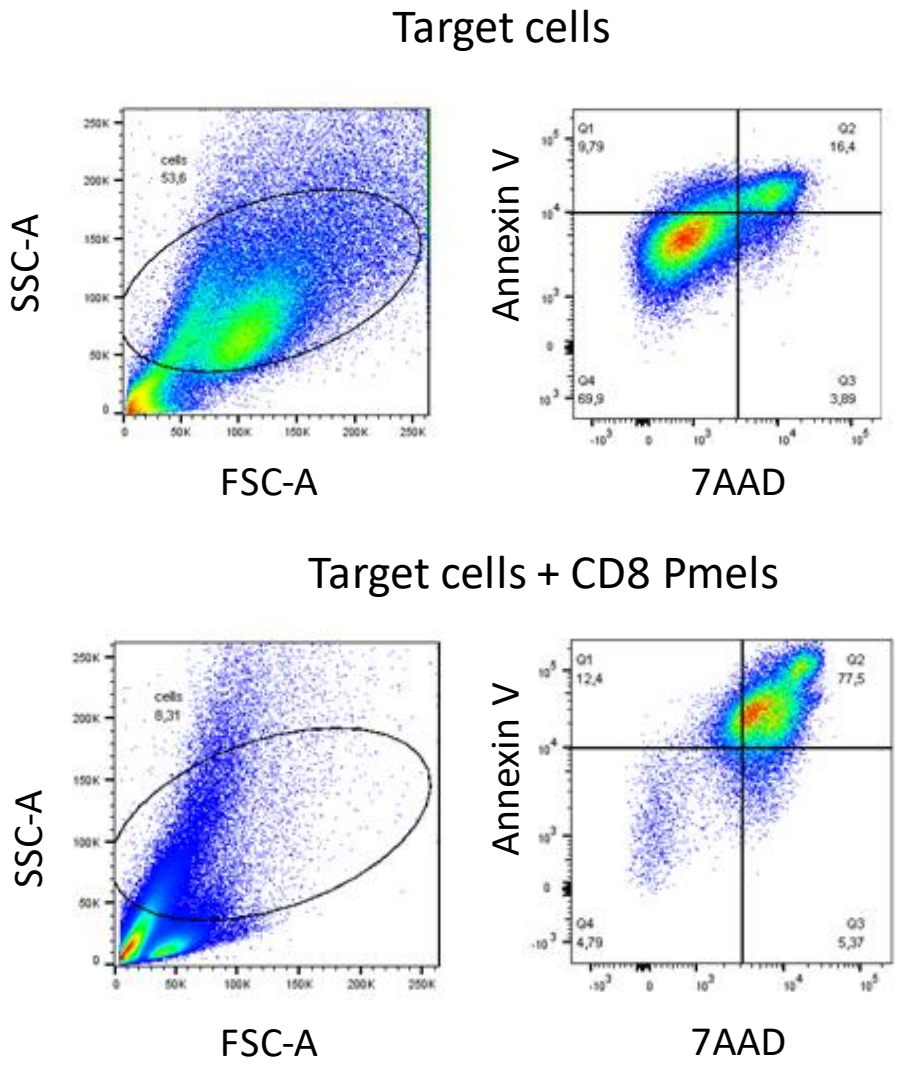

Supplemental Figure 1. Assessment of CTL-induced tumor cell death by flow cytometry. MC38hEGFROVA cells were incubated 48 hours with IFNγ (15UI/ml) and gp100 peptide (100ng/ml) and Pmel-1-derived splenocytes were activated for 48 hours with gp100 peptide (100ng/ml) and 48 hours with IL-2 (30 UI/ml). At day -3, tumor cells and Pme1-1 cells were co-cultured. At day 0, the result of the co-culture was analyzed by flow cytometry after staining with 7-AAD, and Annexin V. Dot plots represent the gating strategy and 7-AAD and Annexin V double staining in a representative co-culture.

The mean fluorescence intensity of calreticulin surface exposure on dying tumor cells defined as CD45$^-$7AAD$^-$Annexin V$^+$ was ten-fold higher than the calreticulin found on dying tumor cells from cell cultures in the absence of cytotoxic lymphocytes (Fig. 1A). Moreover, the supernatants of co-cultures of gp100 pre-loaded tumor cells with preactivated Pmel-1-derived CD8$^+$ splenocytes contained large amounts of HMGB1, a finding not observed in any of the control conditions (Fig. 1B).

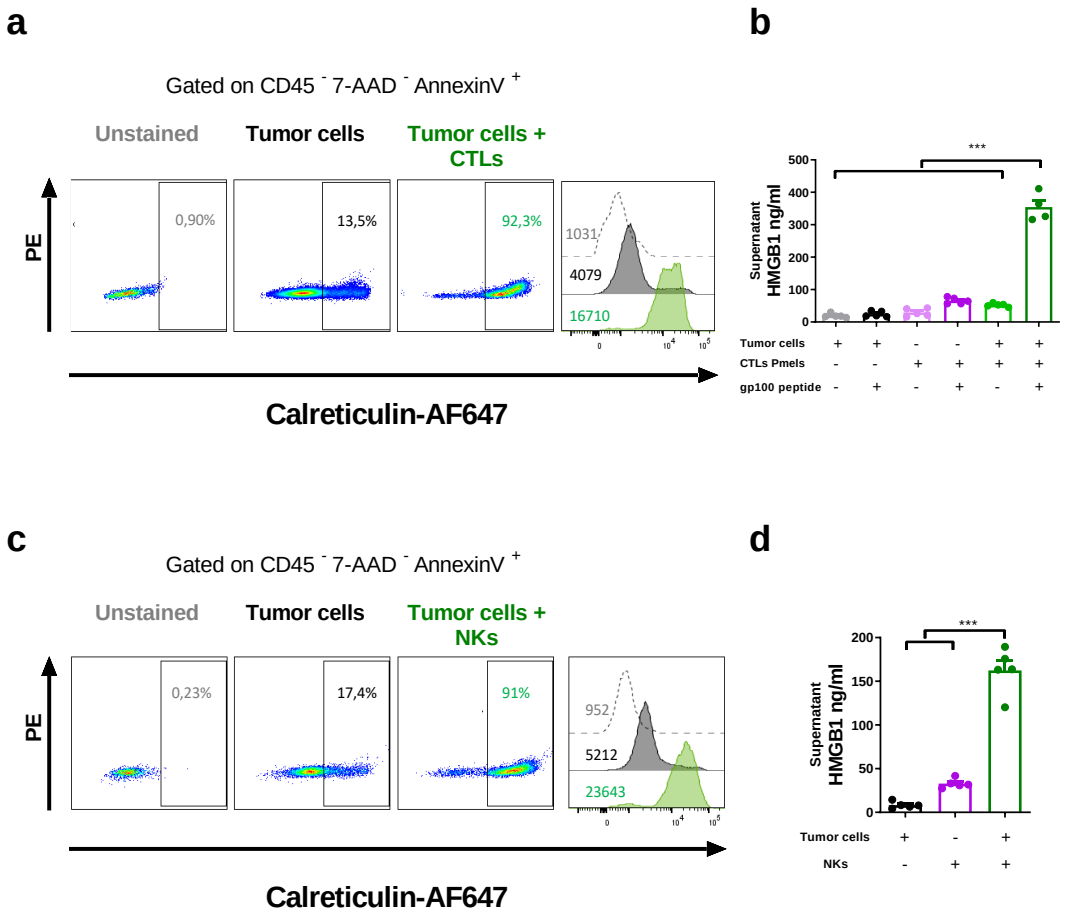

Figure 1. Cellular cytotoxicity induces the release of danger-associated molecular patterns by dying cancer cells in culture. A) MC38hEGFROVA cells were incubated for 48 hours with IFNγ (15UI/ml) and gp100 peptide (100ng/ml). Subsequently, *in vitro* pre-activated Pmel-1-derived splenocytes were added at a ratio of 10:1. Calreticulin surface expression on dying tumor cells (CD45$^-$7-AAD$^-$AnnexinV$^+$) was analyzed after 24 hours by flow cytometry. Representative experiments are presented in dot plots and histograms indicating MFI. B) Supernatants from the co-cultures were analyzed for the concentration of HMGB1 by ELISA. As controls, tumor cells, or T cells with or without pulsed peptide were used. Data are mean ± SEM. n=4 for co-culture with peptide and n=5 for other groups C) MC38hEGFROVA cells were incubated with *in vivo* activated NK

cells at a ratio of 3.5:1 for 24 hours. Subsequently, calreticulin surface expression on dying tumor cells ($CD45^{-}7\text{-}AAD^{-}AnnexinV^{+}$) was analyzed by flow cytometry. Representative experiments are presented in dot plots and histograms indicating FMI. D) HMGB1 concentrations in the supernatant were determined by ELISA. As controls, tumor cells or NK cells alone were used. Data are mean ± SEM. n=5 for all groups. One-way ANOVA test with Tukey's multiple comparisons tests, ***$p<0.001$. Results are representative of at least two experiments performed.

Thus, T lymphocyte-mediated cytotoxicity induces features considered hallmarks of immunogenic cell death [56]. We next addressed whether other cytotoxic immune cells, such as natural killer cells, induced the exposure of calreticulin and the release of HMGB1. In these experiments, the MC38hEGFROVA tumor cells were not preconditioned, but NK cells were activated and expanded *in vivo* by hydrodynamic gene-transfer to the liver of a plasmid encoding a fusion protein of IL-15 [88, 94]. The *in vivo* pre-activated NK cells were able to extensively lyse tumor cells (Supp. Fig. 2).

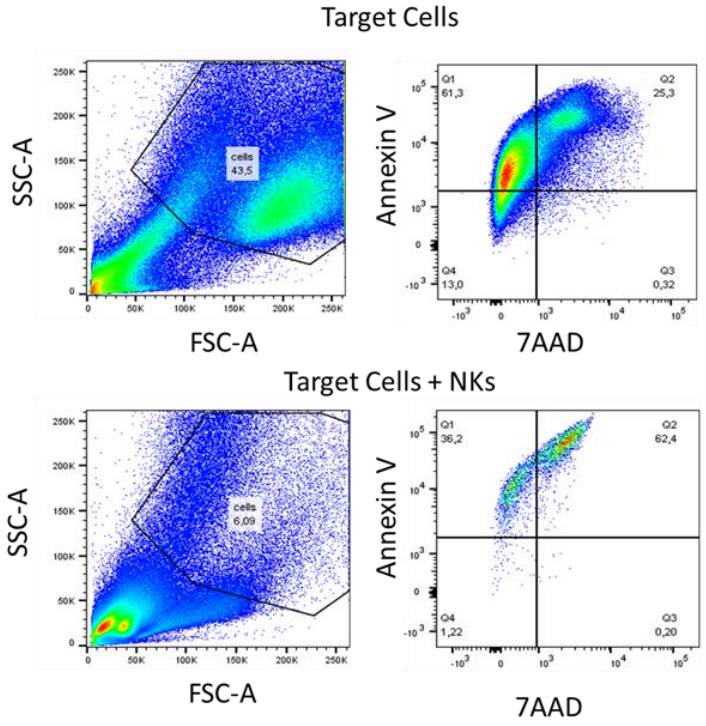

Supplemental Figure 2. Assessment of NK-induced tumor cell death by flow cytometry. RAG1 mice were hydrodynamically injected with a plasmid coding for IL-15. After three days, spleens were harvested and NK isolated by immunomagnetic negative selection. MC38hEGFROVA cells were incubated with such IL-15 *in vivo* activated NK cells for 72 hours. The result of the co-culture was analyzed by flow cytometry after staining with 7-AAD, and Annexin V. Dot plots represent the gating strategy and 7-AAD and Annexin V double staining in a representative co-culture.

The tumor-cell debris obtained after NK-cell lysis showed enhanced mean fluorescence intensity for calreticulin shining on the plasma membrane. The content of HMGB1 released into the supernatant was markedly increased as had been observed with cytotoxic T lymphocytes (Fig. 1C and D).

Induction of immunogenic cell death hallmarks by cytotoxicity is not exclusive to murine cells since it is also observed when human CD8 T lymphocytes kill human HT29 tumor colon cancer cells as a result of incubation with a bispecific antibody engaging Epithelial Cell Adhesion Molecule (EpCAM) and CD3ε (EpCAM-TCB) (Supp. Fig. 3). Cytotoxicity induced in a similar setting with NK cells showed similar features on the HT29 cancer cells (Supp. Fig. 3).

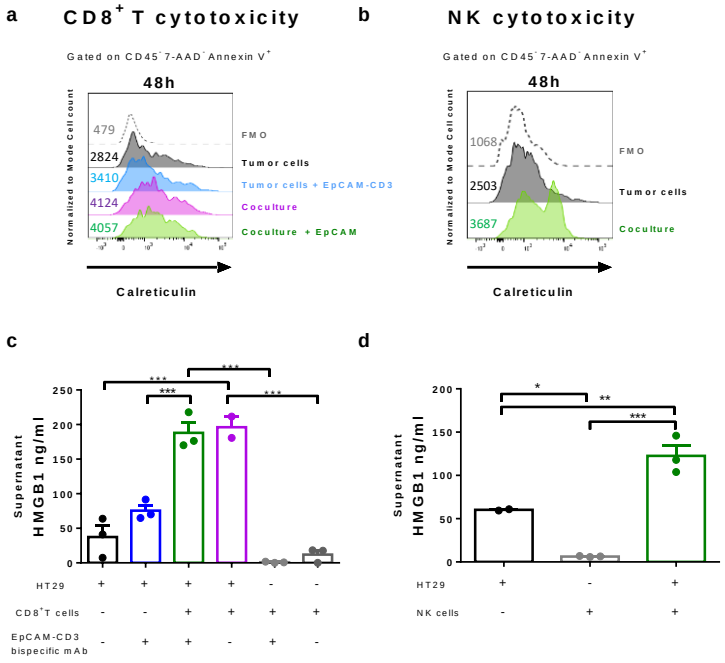

Supplemental Figure 3. Cellular cytotoxicity induces the release of danger-associated molecular patterns by dying human cancer cells in culture. A) HT29 cells were co-cultured with human T cells at a ratio 1:1 with or without EpCAM-CD3ε bispecific antibody (1µg/ml) for 48 hours and calreticulin expression on dying tumor cells ($CD45^-7\text{-}AAD^-Annexin\ V^+$) was analyzed by flow cytometry. Numbers in histograms indicate FMI. B) As in A but HT29 were killed by human $CD3^-CD56^+$ NK cells pre-activated 48 hours before with IL-2 (100 UI/ml) and IL-15 (10ng/ml). Supernatants from

the co-cultures with human T cells (C) or human NK cells (D) were analyzed for HMGB1 concentration by ELISA. n=2 for HT29+T, n=3 for other groups (C). n=2 for HT29, n=3 for other groups (D). One-way ANOVA test with Tukey's multiple comparisons tests, ***$p<0.001$. Results are representative of two experiments performed.

Tumor cell debris resulting from killing by cytotoxic T lymphocytes is immunogenic

To determine whether the dead tumor cells killed by immune cytotoxicity trigger a protective immune response in mice was the next step in our research. Vaccination consisted of cell debris of gp100-loaded MC38hEGFROVA killed by $CD8^+$ Pme1-1-lymphocytes. The tumor challenge was performed seven days later with the EG7 lymphoma cell line, which does not express the gp100 antigen but only shares the OVA protein with the colon cancer cells used for vaccination (Fig. 2A). In this setting, the administration of MC38hEGFROVA cell debris obtained after three freeze and thaw cycles did not elicit any protective immune response, and therefore EG7 tumor grew as in the non-vaccinated control group. We also introduced a positive control group with MC38hEGFROVA tumor cells killed by doxorubicin, a chemotherapeutic drug that is known to induce immunogenic cell death [17].

Interestingly, the CTL-associated debris protected all mice from a subsequent challenge with EG7, while only 37% of mice were protected by immunization with doxorubicin-derived tumor-cell debris (Fig. 2B). The tumor free-animals over time (Fig. 2C) correlated well with the circulating levels of OVA-specific $CD8^+$ T lymphocytes recognized by H-$2k^b$ tetramers (Fig. 2D). In fact, the maximum levels of specific $CD8^+$ T cells were observed in mice immunized with the CTL-killed tumor cells.

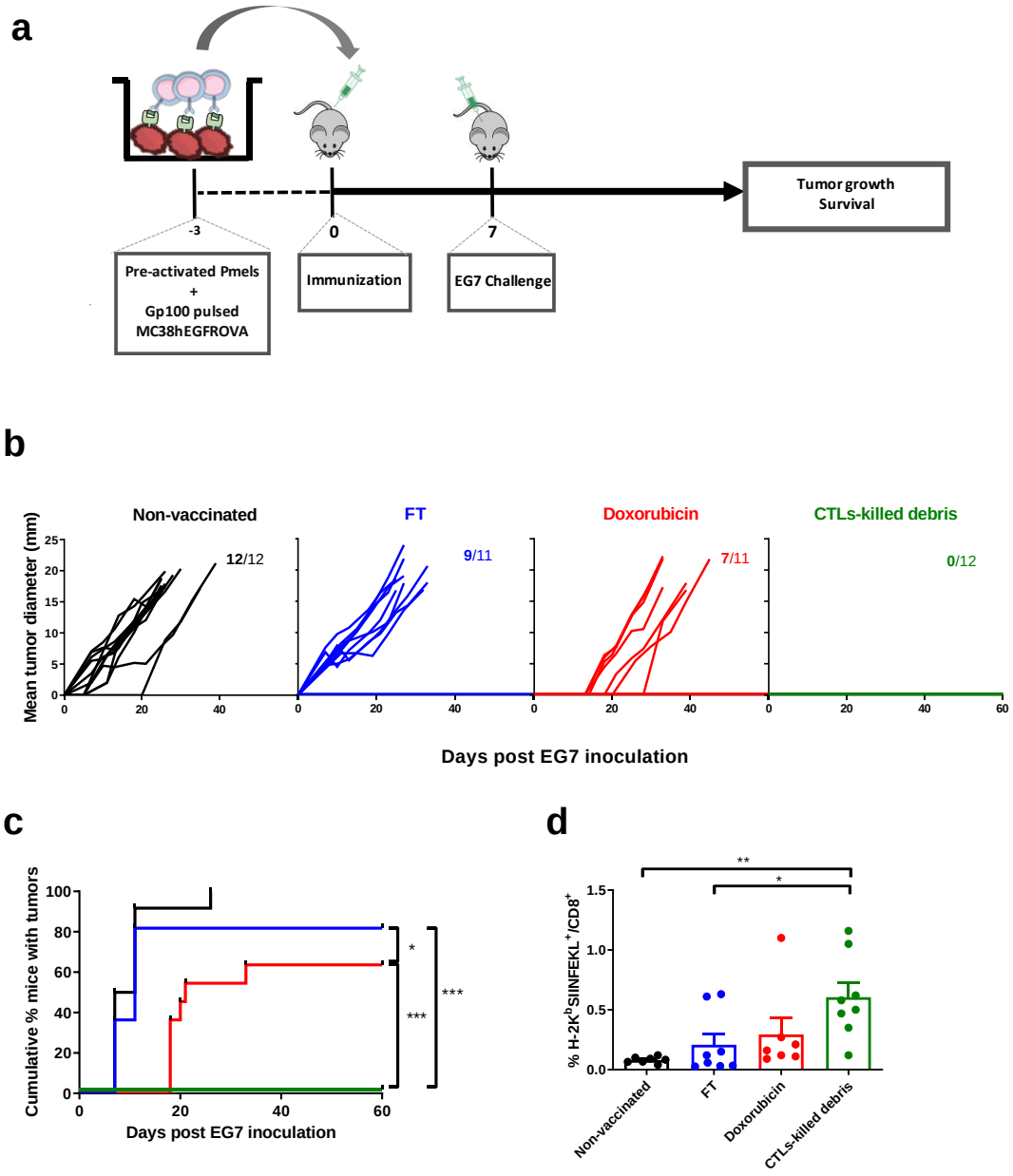

Figure 2. Tumor cells killed by cytotoxic T cells are immunogenic. A) MC38hEGFROVA cells were incubated 48 hours with IFNγ (15UI/ml) and gp100 peptide (100ng/ml). At day -3, tumor cells and activated Pme1-1 CTLs were co-cultured. At day 0, the result of the co-culture was injected subcutaneously into wild-type C57BL/6 mice. Seven days later, mice were challenged with injection of $5x10^5$ EG7 cells into the right flank, and tumor growth and survival were monitored. B) Individual EG7 tumor growth. Non-vaccinated group was mock immunized with saline. FT group was immunized with the tumor cell debris obtained from three freeze/thaw cycles. The doxorubicin positive control group was immunized with tumor cells killed in culture with 2.5 µM doxorubicin for 24 hours. C) Curves showing the percentage of tumor-free mice at different time points. Log-rank test, *p<0.05, **p<0.01, and ***p<0.001. D) At day 7, peripheral blood was collected, and OVA-specific $CD8^+$ T cells were assessed by MHC

multimer staining. One-way ANOVA test with Tukey's multiple comparisons tests, *$p<0.05$ and ***$p<0.001$. Data are pooled from three independent experiments.

To demonstrate that CTL-mediated immunogenic cell death can also take place *in vivo*, we subcutaneously co-injected MC38hEGFROVA tumor cells with pre-activated OT-I lymphocytes (Fig. 3A).

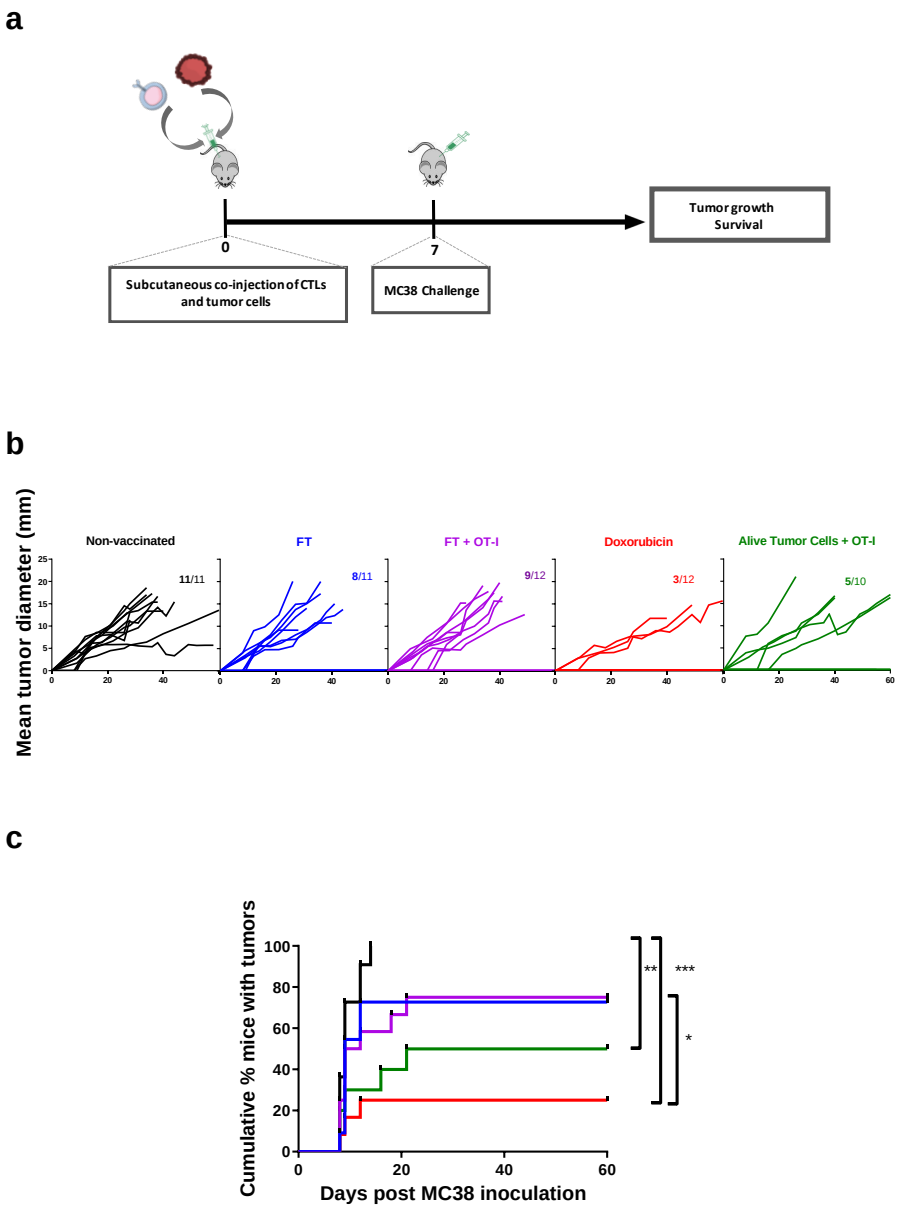

Figure 3. *In vivo* tumor cell killing by cytotoxic T cells induces epitope spreading. A) At day -4, OTI-derived splenocytes were incubated for 48 hours with SIINFEKL peptide (1 ng/ml). At day 0, 10^7 activated OTI splenocytes with MC38hEGFROVA cells at a ratio 20:1 were subcutaneously co-injected into the right flank. At day 7, mice were challenged with $5x10^5$ MC38 cells in the contralateral flank and tumor growth and survival were monitored. B) Individual MC38 tumor growth. Non-vaccinated group was mock immunized with saline. FT group was immunized with the tumor cell debris obtained after three freeze/thaw cycles. FT+OT-1 group, received the frozen/thaw tumor

cell debris with OT-1 splenocytes. The doxorubicin positive control group was immunized with tumor cells killed with 2.5 μM doxorubicin for 24 hours in culture. The fraction of mice with detectable tumor growth is shown in each graph. C) Curves showing the percentage of tumor-free mice at different time points. Log-rank test, *$p<0.05$, **$p<0.01$, and ***$p<0.001$. Data are pooled from two independent experiments.

These TCR-transgenic T lymphocytes were able to kill the MC38hEGFROVA tumor cells when coinjected in the dermis (Supp. Fig. 4).

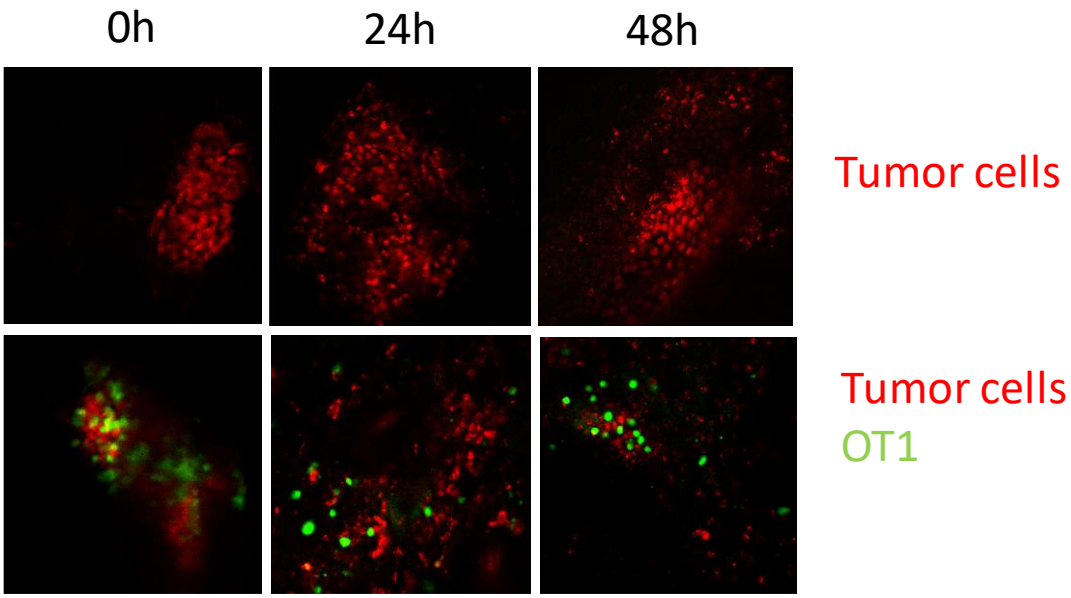

Supplemental Figure 4. Visualization of OTI-mediated killing of tumor cells *in vivo*. *In vitro* activated OT-1-EGFP-derived splenocytes were co-injected with DRAQ 5 pre-labeled MC38hEGFROVA cells at a ratio 20:1 and injected subcutaneously into the ear dermis of C57BL/6 mice. Tumor and OT-1 cells were visualized at day 0, 1, and 2 in mice by intravital imaging using an inverted confocal microscope.

In these experiments, we challenged immunized mice with MC38 in the contralateral flank since these cells are not recognized by OT-I T lymphocytes. In this setting, 50 % of the mice which received MC38hEGFROVA tumor cells + OT-1 T lymphocytes remained tumor-free at the end of the experiment, while only 25 % of the mice which received tumor cell debris as generated by three cycles of freeze and thaw with or without OT-I cells rejected the MC38 challenge. Doxorubicin-killed cells as a positive control for immunogenic cell death protected 75 % of mice in a similar experimental setting (Fig. 3B and C).

Tumor cell debris generated by natural-killer cell killing is immunogenic

Once having demonstrated that cytotoxicity mediated by T lymphocytes triggers an immunogenic form of tumor cell death both *in vitro* and *in vivo*, we next aimed at extending this observation to the cytotoxicity mediated by NK cells. Large numbers of activated mouse NK cells were obtained using hydrodynamic injections of a plasmid encoding a fusion protein of IL15, encompassing the sushi domain of the IL-15Rα and apolipoprotein A-I as a stabilizing moiety [88, 94]. *In vitro* co-culture of MC38hEGFROVA tumor cells with activated NK cells for 72 hours leads to extensive tumor cell lysis (Fig. 4A). Upon subcutaneous injection of the tumor cell debris, an effective antitumor immunity was developed in immunized mice that prevented tumor development when the animals were subsequently challenged with EG7 tumor cells in the right flank away from the site of immunization (Fig. 4B and C). The onset of antitumor immunity was also reflected by the increase in tumor-specific T cells in circulation seven days after immunization (Fig. 4D). All the parameters analyzed to detect the CD8 antitumor immune responses were more intense in the group immunized with the NK cell-killed dead tumor cells than in any of the groups treated with dead tumor cells generated either by freeze/thaw or doxorubicin (Fig. 4B and C).

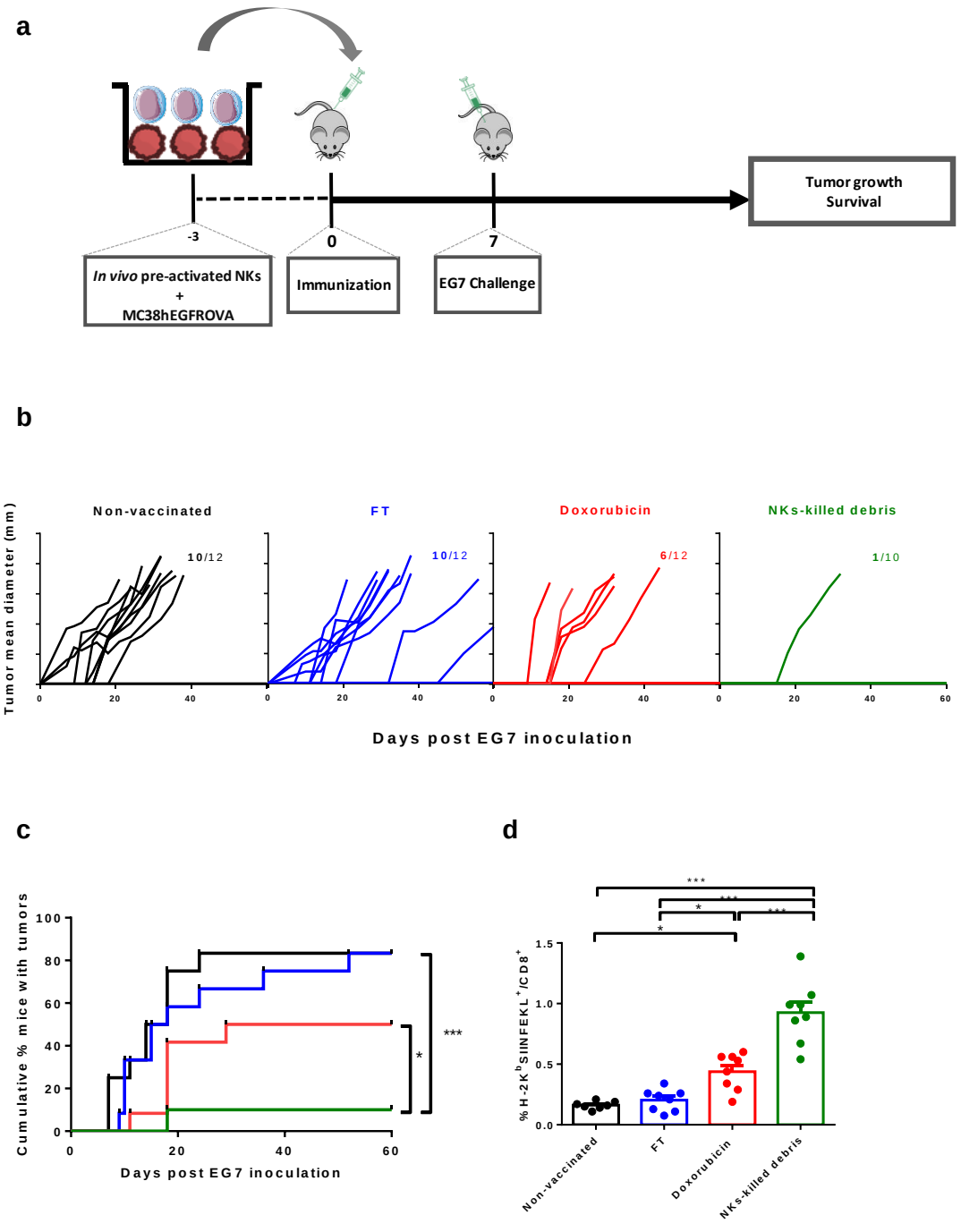

Figure 4. Tumor cells killed by NK cells are immunogenic. A) RAG1 mice were hydrodynamically injected with a plasmid coding for IL-15. After three days, spleens were harvested and NK isolated by immunomagnetic negative selection. MC38hEGFROVA cells were incubated with *in vivo* activated NK cells for 72 hours. The result of the co-culture was then injected subcutaneously into wild-type C57BL/6 mice. After seven days, mice were challenged subcutaneously with $5x10^5$ EG7 cells. B) Individual EG7 tumor growth. The non-vaccinated group was mock immunized with saline. The FT group was immunized with the tumor cell debris obtained after three freeze/thaw cycles. The doxorubicin positive control group was immunized with tumor cells killed with 2.5 μM doxorubicin for 24 hours in culture. C) Curves showing the

percentage of tumor-free mice at different time points. D) At day 7, peripheral blood was collected, and OVA-specific $CD8^+$ T cells were assessed by MHC multimer staining studied by FACS. One-way ANOVA test with Tukey's multiple comparisons tests, *$p<0.05$ and ***$p<0.001$. Data are pooled from two independent experiments.

Immunogenicity of CTL- or NK-killed dead tumor cells depends on Batf3-dependent DCs but not on STING or IFNAR

We next sought to determine the host requirements to develop the antitumor immune response by dead tumor cells generated by cytotoxicity as performed by immune effector cells. We took advantage of mice genetically deficient in different key molecules for immunosurveillance. Type I interferons are critical cytokines for the activation of effector T lymphocytes and NK cells in the priming phase of the immune response. To address the role of type I interferons, we used knock-out mice for the IFNA receptor as well as STING knock-out mice. The STING pathway is essential for the detection of dsDNA and the release of type I interferon upon detection of DNA released by dying tumor cells. We also used BATF3 knock-out mice. This transcription factor is critically involved in the ontogeny of cDC1, dendritic cells which exert an essential activity to cross-present exogenous antigens via the MHC I pathway and in the production of the pro-inflammatory cytokine IL-12 [67]. We immunized both wild type and knockout mice with tumor cell debris generated by CTLs or by NK cells. As shown in Figure 5 A, CTL-derived debris protected wild type and IFNAR or STING deficient mice, whereas the protective effect was completely lost in mice deficient in cross-presenting specialized cDC1 dendritic cells. The same pattern was obtained when the experiments were performed immunizing mice with NK cell-killed dead tumor cells (Fig. 5 B).

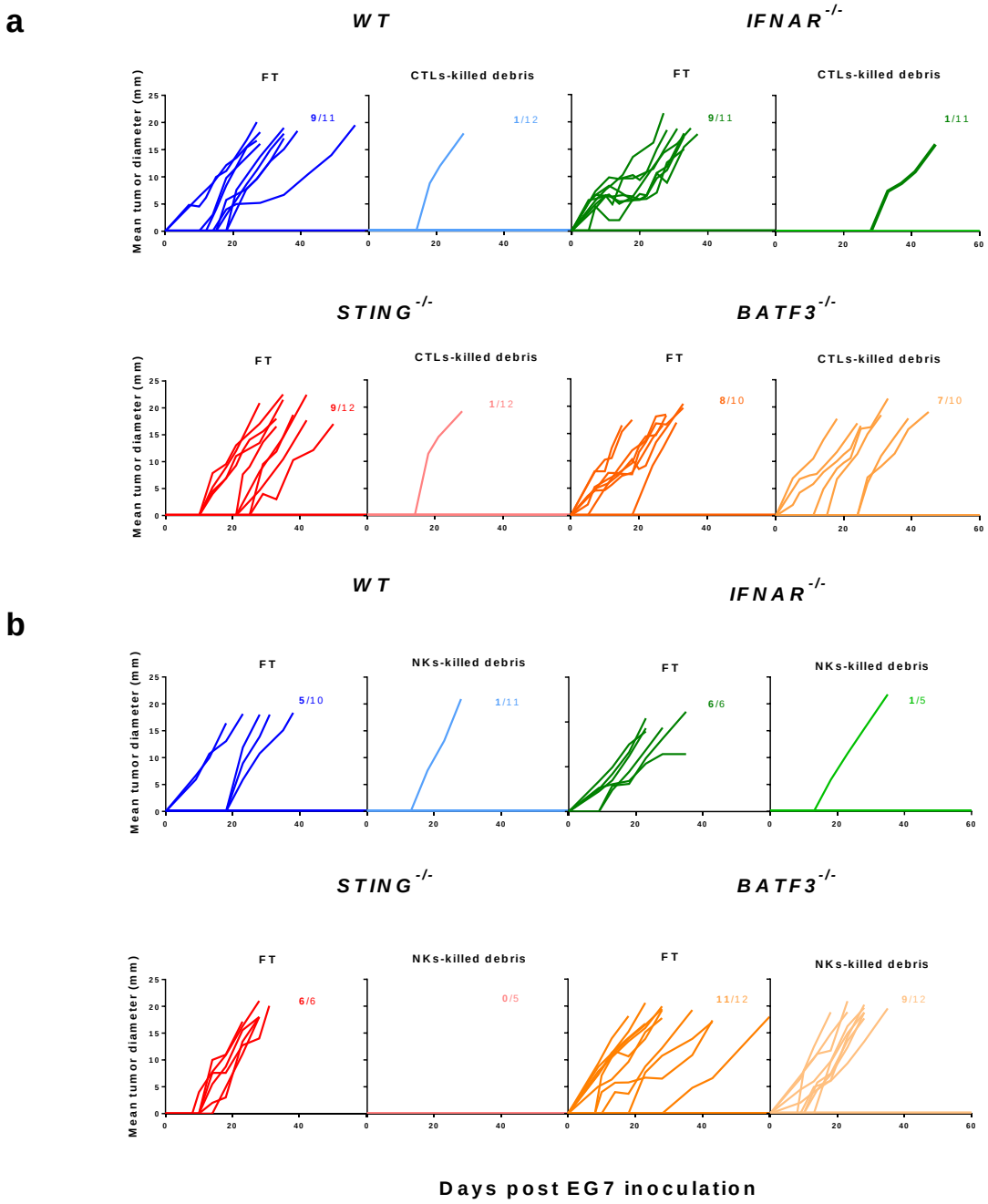

Figure 5. cDC1 absolute requirement for effective vaccination with CTL- and NK-derived tumor cell debris. A) Wild-type, IFNAR$^{-/-}$, STING$^{-/-}$ and BATF3$^{-/-}$ mice were immunized with MC38hEGFROVA tumor cell debris obtained after three cycles of freeze/thaw or after Pmel-1 CTL-mediated killing in culture. After seven days, mice were challenged with 5x10^5 EG7 cells subcutaneously injected into the right flank, and tumor growth was monitored. B) Experiments as in A) but using MC38hEGFROVA tumor cell debris obtained after NK cell killing. Immunized with cytotoxic debris BATF3$^{-/-}$ mice were statistically different from all the other groups with $p<0.05$ by Log-Rank tests for EG7 engraftment. Data are pooled from three (A) and two (B) independent experiments.

Further addressing the role of cDC1 cells in the process, we generated these cells in culture by differentiating bone marrow precursors under the influence of soluble FLT3-L and GM-CSF [93]. Debris of OVA-expressing cells killed by Pmel-1 CTLs or NK cells resulted in OVA cross-presentation and *in vitro* priming of OT-1 cells. Using FACS sorting to recover the $CD11c^{+}CD103^{+}$ dendritic cells from the culture of cytotoxic debris and such dendritic cells, we were able to expose them in a subsequent co-culture with OT-I lymphocytes loaded with a fluorescent dye to monitor proliferation (Fig. 6). These results are consistent with a train of events in which cDC1 cells capture the tumor-cell remains and cross-present tumor-associated antigens. Figure 6 shows the experimental setting (Fig. 6A) and the OT-I proliferation responses (Fig. 6B and C) that indicate that $CD8^{+}$ T cell or NK cell cytotoxic debris leads to cross-presentation that is not observed with cDC1 pulsed with freeze and thaw tumor cell lysates.

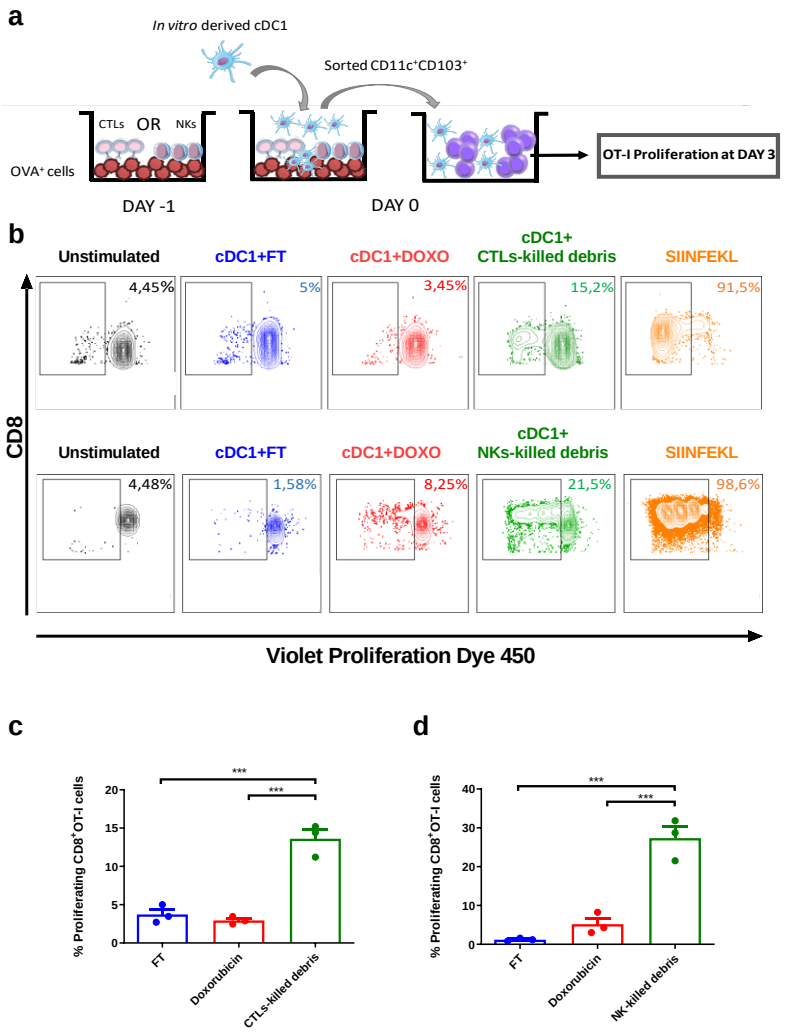

Figure 6. Antigens in dead cells from cytotoxicity are cross-presented by cDC1 cells
A) Cross-presenting CD103$^+$ DCs were differentiated in culture from bone marrow cells for 14 days in the presence of GM-CSF and soluble FLT3-L. On day -1, B16OVA (C) or MC38hEGFROVA (D) were killed with activated Pmel-1-derived splenocytes or activated NK cells, respectively. FT was derived from tumor cell debris obtained after three freeze/thaw cycles. The doxorubicin samples are tumor cells debris from cells killed with 2.5 µM doxorubicin dying 24 hours in culture. At day 0, DCs were added. After 3 hours, CD11c$^+$CD103$^+$ DCs were FACS-sorted and incubated with resting OVA-specific OTI CD8$^+$ cells previously labeled with a proliferation dye. After three days, OT-1 proliferation was assessed by flow cytometry. B) Representative contour of DC-OT-I co-cultures showing a representative case. C) Percentage of proliferating CD8$^+$ OT-I cells incubated with cDC1 pre cocultured with CTL-derived debris. D) Percentage of proliferating CD8$^+$ OT-I cells incubated with cDC1 pre cocultured with NK-derived debris Data are mean ± SEM. n=3 for each group. One-way ANOVA test with Tukey's multiple comparisons tests, *p<0.05 and ***p<0.001. Results from a single experiment for T cells and independent experiment for NK cells are available.

DISCUSSION

We present evidence strongly arguing that cytotoxicity, as mediated by CTLs and NKs cells on malignant cells, is immunogenic. This is coherent with the proposed model of the tumor immunity cycle [2] and represents a self-amplifying mechanism to gain *momentum* in tumor rejection upon successful immunotherapy. Our results would explain the phenomena of epitope spreading seen in vaccination experiments in mice [95, 96] and clinical trials of vaccination using defined antigens [97, 98].

From the point of immune regulation, these observations are relevant since once started, an effector immune response towards a given antigen will continue until cells expressing the antigen are cleared. It remains to be seen if these mechanisms are only relevant in the context of transformed tumor cells or would also apply to non-malignant counterparts. For instance, it could be important in the field of β-cell dysfunction in diabetes mellitus or acute rejection of transplants [99, 100].

In our experiments, we have followed the logic that allowed us to establish that certain chemotherapeutic drugs or radiotherapy are immunogenic because they induce immunogenic cell death [17, 101].

To explain our results, we invoke the interplay of dendritic cells and cross-presentation of tumor antigens [57, 81]. In essence, both antigen release and DAMPs are required to accomplish immunization. The exact nature of antigen processing and redirection to the MHC-I antigen presentation pathway remains to be determined and is a matter of speculation [67, 102]. The main DAMPs associated with cytotoxicity are to be defined, but HMGB1 and calreticulin exposure are likely to contribute to immunogenicity.

Indeed, our experiments pinpoint a necessary role for BATF-3 dependent cDC1 cells that in this case do not need the contribution of type I IFN receptor on endogenous cells or STING sensing as reported in other related experimental settings [103]. Moreover, our results go on to demonstrate that cDC1 can cross-present antigens from tumor cell debris derived from CTL and NK cytotoxicity.

Our findings may have fundamental implications for the development of immunotherapies from adoptive T-cell transfer to checkpoint inhibitors. For instance, it has been reported that cDC1 cross-priming is relevant for adoptive T-cell therapy [104] and the efficacy of checkpoint inhibitors [60, 61].

In our view, the main consequence of the link between cytotoxicity and immunogenic cell death of malignant cells is that it offers a mechanism of amplification and self-perpetuation of the immune response against cancer neoantigens. Indeed, certain tumor antigens might remain ignored by the immune system until a cytotoxic response is set in motion [105, 106]. Once CTL responses are unleashed, our results imply that strategies aimed at fostering cross-priming are due to consolidate and amplify clinical responses to immunotherapy. Furthermore, these findings predict that established tumors have likely evolved escape mechanisms that allow them to evade cross-priming of their antigens when under attack by CTLs or NK cells. Identification of such evasive mechanisms offers interesting opportunities in cancer immunotherapy.

Competing interests

I.M. reports advisory roles with Roche-Genentech, Bristol-Myers Squibb, CYTOMX, Incyte, MedImmune, Tusk, F-Star, Genmab, Molecular Partners, Alligator, Bioncotech, MSD, Merck Serono, Boehringer Ingelheim, Astra Zeneca, Numab, Catalym, and Bayer, and research funding from Roche, BMS, Alligator, and Bioncotech. P.B. reports advisory roles with Tusk and Moderna, research funding from Sanofi, and Bavarian Nordic and speaker honoraria from BMS, MSD, Novartis and AstraZeneca. The rest of the authors have no conflict of interest to declare.

Funding:

This study was supported by Spanish Ministry of Economy and Competitiveness (MINECO SAF2014-52361-R and SAF 2017-83267-C2-1R); a Worldwide Cancer Research Grant (15-1146); the Asociación Española Contra el Cancer (AECC) Foundation under grant GCB15152947MELE; and the European Union's Horizon 2020 Program (grant agreement no. 635122 PROCROP) to I.M; and Instituto de Salud Carlos III (PI16/00668) cofinanced by Fondos Feder and Joint Translational Call for Proposals 2015 (JTC 2015) TRANSCAN-2 (code: TRS-2016-00000371) to P.B. A.T. has received financial support through la Caixa Banking Foundation (LCF/BQ/LR18/11640014). M.A. has received a Marie Skłodowska-Curie fellowship (CINK 746985).

Chapter 2

“PROPHYLACTIC TNF BLOCKADE UNCOUPLES EFFICACY AND TOXICITY IN DUAL CTLA-4 AND PD-1 IMMUNOTHERAPY”

PROPHYLACTIC TNF BLOCKADE UNCOUPLES EFFICACY AND TOXICITY IN DUAL CTLA-4 AND PD-1 IMMUNOTHERAPY

Authors: Elisabeth Perez-Ruiz[1,2,3,4,5], Luna Minute[1,2], Itziar Otano[1,2], Maite Alvarez[1,2], Maria Carmen Ochoa[1,2,6], Virginia Belsue[1,2], Carlos de Andrea[2,7], Maria Esperanza Rodriguez-Ruiz[1,3], Jose Luis Perez-Gracia[2,3,6], Ivan Marquez-Rodas[6,8], Casilda Llacer[9], Martina Alvarez[5,10,11], Vanesa De Luque[5,10], Carmen Molina[1,2], Alvaro Teijeira[1,2,6], Pedro Berraondo[1,2,6], Ignacio Melero[1,2,3,6,12].

Affiliations:[1]Program of Immunology and Immunotherapy, Cima Universidad de Navarra, Pamplona, Spain.[2]Navarra Institute for Health Research (IDISNA), Pamplona, Spain.[3]Department of Oncology, Clínica Universidad de Navarra, Pamplona, Spain.[4]Department of Oncology, Hospital Costa del Sol, Marbella, Spain.[5]Instituto de Investigación Biomédica de Málaga (IBIMA), Hospitales Universitarios Regional y Virgen de la Victoria, Málaga, Spain.[6]Centro de Investigación Biomédica en Red de Cáncer (CIBERONC), Spain.[7]Department of Pathology, Clínica Universidad de Navarra, Pamplona, Spain.[8]Department of Oncology, Hospital General Universitario Gregorio Marañon, Madrid, Spain.[9]Department of Oncology, Hospital Universitario Virgen de la Victoria, Malaga, Spain.[10]Laboratorio de Biología Molecular del Cáncer, Centro de Investigaciones Médico-Sanitarias (CIMES), Universidad de Málaga, Málaga, Spain.[11]Department of Pathology, Faculty of Medicine, Universidad de Málaga, Málaga, Spain[12]Department of Immunology and Immunotherapy, Clínica Universidad de Navarra, Pamplona, Spain

Keywords: CTLA-4, PD-1, immunotherapy, cancer, TNF-α, toxicity, colitis.

ABSTRACT

Combined PD-1 and CTLA-4 targeted immunotherapy with Nivolumab and Ipilimumab achieves remarkable efficacy against melanoma, renal cell carcinoma, and non-small cell lung cancer[107-109]. However, this comes at the cost of frequent, serious and dose-limiting immune-related adverse events, that required dose-reductions of Ipilimumab[110]. In mice co-treated with surrogate anti-PD-1 and anti-CTLA-4 monoclonal antibodies, there is exacerbation of autoimmune colitis concomitant with remarkable efficacy against transplantable cancer models. Pretreatment with TNF-α inhibitors with clinically available agents ameliorates colitis and unexpectedly improves antitumor efficacy. Interestingly, the TNF-α inflammatory axis in the intestine is overactivated in patients suffering colitis following Ipilimumab plus Nivolumab treatment. Prophylactic human TNF-α blockade improves mouse xenograft versus host colitis and hepatitis as exacerbated by Ipilimumab plus Nivolumab co-treatment, while preserving immunotherapeutic control of xenografted tumors. These results put forward clinically feasible strategies to dissociate efficacy and toxicity in the use of combined immune checkpoint blockade for cancer immunotherapy.

MATERIALS AND METHODS

Mice and cell lines

6 weeks old, female C57BL/6 mice were obtained from The Jackson Laboratory (Bar Harbor, ME) and maintained in the animal facility of Cima Universidad de Navarra. Rag2$^{-/-}$IL2Rγ^{null}, OT-I and Pmel-1 mice were bred and maintained in the animal facility of Cima Universidad de Navarra. Experimental protocols were approved by the Ethics Committee of the Universidad de Navarra and the Institute of Public Health of Navarra according to European Council Guidelines (protocol numbers: 060-17 and 024-17). Sample size estimations were performed using the G Power software. Mice were randomized at the beginning of each experiment and experiments were not blinded. Mice were sacrificed when the tumor reached 20mm and in none of the experiments were these limits exceeded. We have complied with all ethical regulations. MC38 cells were a kind gift from Dr. Karl E. Hellström (University of Washington, Seattle, WA) in September 1998. B16-OVA cells were provided by Dr. Lieping Chen (Yale University, New Haven, CT) in November 2001. These cell lines were authenticated by Idexx Radil (Case 6592-2012) in February 2012. HT29 were obtained from ATCC. MC38, B16OVA, and HT29 cell lines were maintained at 37ºC in 5% CO_2 and were grown in RPMI medium (RPMI 1640) with Glutamax (Gibco, Invitrogen, Carlsbad, CA) containing 10% heat-inactivated FBS (Gibco, Invitrogen), 100 IU/mL penicillin and 100 g/mL streptomycin (Biowhittaker, Walkersville, MD). After 7-9 days in culture, cells were tested for mycoplasma contamination and 500.000 cells/mice were injected subcutaneously. Tumor growth was monitored twice a week with an electronic caliper.

Treatments

Mice received 100 µg of anti-CTLA-4 antibody (InVivoMAb BioXCell, West Lebanon, USA, anti-mouse CTLA-4, Clone 9D9) plus 100 µg of anti-PD-1 antibody (InVivoMab BioXCell, anti-mouse PD-1, Clone RMP1-14) per injection intraperitoneally. Colitis treatment consisted of the intraperitoneal administration of 125 µg/mice per injection of anti-mouse TNF-α antibody (InVivoMAb BioXCell, Clone XT3.11), as previously described[111] or 40 µg/mice per injection of Etanercept (Enbrel®). Anti-mouse IL-6 antibody (InVivoMAb BioXCell, Clone MPF5-20F3) was administered intraperitoneally (250 µg per dose).

Dextran sulfate sodium salt (DSS)-induced colitis

Mice were orally administered 3% DSS (36–50 kDa, MP Biomedicals, Solon, OH) in drinking water during three days to induce acute colitis. The experiments were performed in this setting because the protocol reported by Mahler et al. which included 3% DSS in water over seven days proved to be very toxic and produced high mortality in our model[112].

Colitis assessment

Different parameters were used for colitis assessment. Mice weight was monitored daily. Colon ultrasound scans were performed at day 0 and 7 using a Vevo 770 ultrasound system (Visualsonics, Toronto, Canada) equipped with a real-time micro-visualization scan head probe (RMV-710 B) working at a frame rate ranging from 110 to 120 frames per sec (fps). The nosepiece-transducer used had a central frequency of 25 MHz, a focal

length of 15 mm and 70 mm of nominal spatial resolution. It was performed by a trained technician and bowel wall thickness was determined. For histological studies, paraffin-embedded colon sections (4 μm) from each animal were stained with hematoxylin and eosin. Histological changes were graded as previously described[113]. Briefly, histological scores were determined blindly based on the analysis of the inflammatory cell infiltrate and intestinal architecture changes.

Inflammatory cell infiltrate score: 0 = regular infiltrate; 1 = Infiltration of the Lamina Propia; 2 = Cryptitis; 3 = Crypt abscesses/surface erosion/ulceration.

Intestinal architecture score: 0 = regular architecture; 1 = Irregular crypts/Irregular villous surface; 2 = Crypt loss; 3 = Ulceration/Granulation tissue.

Murine lymphocyte survival study

For *in vitro* experiments $1.5x10^6$ splenocytes from 6-10 week-old male or female OT-I or Pmel-1 transgenic mice were isolated and activated with 25 ng/ml of SIINFEKL (Invivogen, San Diego, CA) or 500 ng/ml of hgp100 (GenScript, Scotch Plains, NJ) peptides respectively. Splenocytes were also treated with 6.6 μg/ml of anti-CTLA-4 plus 6.6 μg/ml of anti-PD-1, 2.6 μg/ml of Etanercept or 8.3 μg/ml of anti-TNF-α. After 72 hours survival analysis was performed by flow cytometry (BD FACSCanto™ II system; anti-CD8 BV510 clone 53-6.7 Biolegend (San Diego, CA), anti-CD3 PeCy7 clone 17A2 Biolegend, Zombie NIR Biolegend).

For *in vivo* experiments, MC38 tumors were implanted sc and treated as described before. Seven days after treatment initiation, tumors were harvested, and survival of antigen-specific $CD8^+$ cells was analyzed by flow cytometry in tumor and draining lymph nodes. (BD FACSCanto™ II system; anti-CD8 BV510 clone 53-6.7 Biolegend, anti-CD3 PeCy7

clone 17A2 Biolegend, Zombie Nir, H-2K^{b} KSPWFTTL R-Pe Labelled Pro5 MHC Pentamer ProImmune (Oxford, UK)).

Human lymphocyte survival study

PBMCs from 21 healthy caucasian donors (21-42 years, male and female) were enriched using Ficoll-Paque Plus (GE Healthcare, Menlo Park, CA) and isolated by density gradient centrifugation. All samples were obtained after consent from the healthy donors and Institutional Review Board approval from Clínica Universidad de Navarra and we have complied with all ethical regulations. PBMCs were stimulated with 0.5 μg/ml plate-bound anti-CD3 (OKT-3; eBioscience) and 1 μg/ml anti-CD28 (CD28.2; eBioscience) in the presence or absence of 10 μg/ml of anti-hTNF-α (Infliximab) or 4 μg/ml of Etanercept. All cultures were carried out in the presence of 20 IU/ml recombinant human IL-2 (Proleukin, Novartis) in RPMI-10% FBS at 37 °C. Seven days later, cells were re-plated into fresh anti-CD3/CD28 coated plates and cultured overnight in the presence of all stimuli. Cells were analyzed by multicolor flow cytometry (BD FACSCanto™ II system; Zombie NIR Biolegend, anti-CD3 PeCy7 clone UCHT1 BD, anti-CD8 BV510 clone BC96 Biolegend, CD4-APC clone OKT4 Biolegend, AnnexinV-FITC Biolegend). All analysis was performed using FlowJo 10.4.2 software (Tree Star, San Carlos, CA).

NanoString and nCounter® technology

For TNF-α signature analysis, we selected four mucosa biopsies from patients without bowel disease, four from patients presenting ulcerative colitis not associated with immunotherapy and four from patients who have immunotherapy-induced colitis. Two cases of grade 4 colitis refractory to corticosteroids after treatment with Ipilimumab (male

and female) and two after combined Ipilimumab plus Nivolumab treatment. Three patients out of four from the immunotherapy-induced colitis group were refractory to corticosteroids. Three of them were male and ages ranged from 20 to 69 year-old. Patients without bowel disease had colorectal adenocarcinoma, ages were between 61 and 86 year-old, and two of them were female. Sample anonymization was performed by the corresponding biobanks. All biopsies were obtained after consent from the patients, and Institutional Review Board approval from Clínica Universidad de Navarra, Hospital General Universitario Gregorio Marañon and Hospital Universitario Virgen de la Victoria and we have complied with all ethical regulations. A pathologist selected the FFPE tumor block with the greatest area of viable normal mucosa of colon or ulcerative colitis and estimated tumor cellularity (> 10%) and tumor surface area within the circled area of the H&E-stained slide (> 4 mm^2). FFPE samples were sent to University of Malaga (CIMES) for macrodissection of material and RNA extraction using a RNA isolation kit and procedures provided by NanoString Technologies. The optical density of total RNA was measured at 260 and 280 nm to determine yield and purity. RNA samples were used if the measured concentration was ⩾12.5ng/μl and the A260/280 ratio was 1.7–2.5. Gene-expression profiling was performed on a nCounter Analysis System using the PanCancer Immune Profiling Panel probe set (770 genes: 730 cancer-related human genes + 40 internal reference controls). The hybridization reaction was performed using a nominal RNA input of 250 ng. Hybridization time was 15–21 h using a bench-top thermocycler set to 65°C with a heated lid set to 70°C. The manufacturer's specifications were followed for the nCounter Prep Station, which prepares the hybridized products for imaging. The nCounter Digital Analyzer reports the digital counts representing the number of molecules labeled with a fluorescent barcode for each probe-targeted transcript. Data

were analyzed using the nSolver software (Nanostring Technologies, Seattle, WA) and Ingenuity Pathway Analysis (Ingenuity Systems, Redwood City, CA).

Xenograft-induced colitis experiment

At day 0, 8-12 week-old female $Rag2^{-/-}IL2R\gamma^{null}$ mice were inoculated sc with $5x10^5$ HT29 cells. At day 7 post tumor-cell inoculation, 10^7 human PBMCs resuspended in 1ml of PBS were injected intraperitoneally. Human blood samples were obtained from healthy donors, and fresh PBMCs were isolated by density gradient separation (Ficoll® Paque Plus, GE Healthcare).

At day 7, 11, 14, 17 mice were injected intraperitoneally with Ipilimumab (200µg) plus Nivolumab (200µg) and Etanercept (40µg) subcutaneously. As an antibody control, we used human IgG (200µg). Ultrasound analyses of the intestine were performed at day 24, and photographs obtained. Mice were bled at day 24 for sera collection. Transaminase analyses were performed on the Roche Cobas platform. Xenografted tumors were measured every three days.

Anti-drug antibody assay

Serum samples were collected from MC38 tumor-bearing mice treated with DSS +/- anti-TNF-α or Etanercept on day 4 and 8 after the beginning of treatment and stored at -20ºC until analysis for anti-drug antibodies by an ELISA assay. Briefly, 1:5 serially diluted serum samples, starting from a 1:10 dilution, were added to 96-well plates pre-coated with 0.1 µg in 50 µL of rat anti-TNF-α or Etanercept for the individual detection of anti-drug antibodies on DSS + ICB + α-TNF- or DSS + ICB + Etanercept-treated mice

respectively. As negative controls, sera collected from mice treated only with DSS were used. As a positive control, purified mouse IgG pre-coated wells were used. To allow the binding between immobilized antibody and anti-drug antibodies, samples were incubated for 1.5h at 37ºC followed by thorough washing with PBS TWEEN® 0.05% buffer (PBST) to eliminate unbound samples. Next, a highly cross-absorbed HRP-labeled goat anti-mouse IgG (H+L) (Life Technologies) was added at a 1:8000 dilution and the samples incubated for 1.5h at 37ºC followed by a thorough wash with PBST. HRP was detected by incubation with 3,3',5,5'-Tetramethylbenzidine (TMB) substrate reagent (BD) following the manufacturer's instructions. The colorimetric reaction was measured in a spectrophotometer (λ = 450 nm). Data were represented by normalizing the absorbance data from serum samples to the absorbance data obtained from the positive control. EC50 were calculated by a sigmoidal regression model.

TNF-α Detection

To determine TNF-α protein levels in the tumor microenvironment, the tumor was first homogenized by mechanic disruption with a pestle in PBS buffer with Complete Protease Inhibitors. After centrifugation, the supernatant was collected and stored at -20ºC for further use. Circulating TNF-α was measured in serum samples. 1:10 dilutions of tumor supernatant or 1:2 dilutions of serum were used to evaluate the protein level of TNF-α using the Mouse TNF ELISA Set II kit (BD OptEIATM) following the manufacturer's instructions. The colorimetric reaction was measured in a spectrophotometer (λ = 450 nm).

Antibody list used for T cell exhaustion-related markers

Anti-mouse Eomesodermin (clone Dan11mag) eFluor 660, anti-mouse Tim3 (clone B8.2C12) PE/Dazzle 594, anti-human/mouse Tbet (clone eBio4B10) PECy7, anti-mouse CD45 (clone 30-F11) BV510, anti-mouse TCRβ (clone H57-597) BV610, anti-mouse CD19 (clone 6D5) BV660, anti-mouse CD8 (clone 53-6.7) BUV395, anti-mouse CD4 (clone GK1.5) BV496, anti-mouse Foxp3 (clone MF-14) BV421, anti-mouse Ki67 (clone 188A) Alexa Fluor 700, anti-mouse PD1 (clone 29F.1A12) anti-mouse CTLA4 (clone 1B8) FITC, anti-mouse Lag3 (clone C9B7W) PerCP-eFluor 510, anti-mouse 2B4 (clone m2B4-B6-4558.1) FITC, anti-mouse BTLA (clone 6F7) PerCP-eFluor 510, anti-mouse CD160 (clone CNX46-3) BV421, gp70 pentamer-PE, gp100 (KVPRNQDWL) pentamer-APC, and OVA (SIINFEKL) tetramer-PE. Stained cell suspensions were analyzed by multicolor flow cytometry (Cytoflex, Beckman Coulter).

Statistical analysis

Prism software (GraphPad Software, Inc.) was employed for statistical analysis. We used the log-rank test to determine the significance of differences in survival curves. Mean differences were compared with t-tests for two group comparisons or one-way ANOVA followed by multiple comparison tests for three or more group comparisons. Longitudinal data were fitted to a third order polynomial equation and compared with the Extra sum-of-squares F test. P values <0.05 were considered to be statistically significant.

RESULTS

Nivolumab in combination with Ipilimumab results in synergistic immunotherapeutic effects for patients affected by an expanding spectrum of malignancies[107-110]. Following compelling evidence in mouse models of cancer upon combined CTLA-4 plus PD-1 blockade[114-117], a phase I dose-escalation clinical trial was conducted in metastatic cutaneous melanoma patients, showing frequent, deep and durable objective clinical responses[110]. However, over 40% of patients suffer serious immune-related adverse events that have been conducive to dose reduction of Ipilimumab in the recommended combination regimens for phase-II[118]. Of note, in a cohort biweekly dosed at 3 mg/kg of Nivolumab plus 3 mg/kg of Ipilimumab that had to be halted because of dose-limiting toxicity, six out of six melanoma patients experienced dramatic clinical responses[110]. Moreover, randomized evidence in melanoma patients concludes that dosing single-agent Ipilimumab at 10 mg/kg every three weeks results in longer overall survival than 3 mg/kg regimens[119].

Immune-related adverse events upon treatment with checkpoint inhibitors are usually satisfactorily treated by suspending the therapeutic agents and initiating steroids[120]. TNF-α blockade with Infliximab is recommended for serious or steroid-refractory cases[120] with the exception of hepatitis because of the putative role of TNF-α in promoting liver regeneration[121]. In this study, we provide evidence that the prophylactic blockade of TNF-α prior to instigation of combined CTLA-4 plus PD-1 checkpoint inhibitors prevents mouse-modeled autoimmune adverse events and surprisingly even enhances the antitumor efficacy of combined treatment.

Colitis is among the most frequent and worrisome immune-mediated adverse events upon dual checkpoint inhibition[120]. Inflammatory bowel disease can be modeled in mice by

providing dextran sulfate sodium (DSS) in the drinking water[122, 123]. A series of experiments administering a combination of anti-CTLA-4 and anti-PD-1 mAbs (Fig. 1a) exacerbated the autoimmune colitis syndrome, resulting in weight loss (Figure 1B), engrossed large intestinal wall upon ultrasound examination (Fig. 1c-d) and worsening of colon inflammation as assessed by histological techniques (Fig. 1e). TNF-α blockade is a recommended treatment for ulcerative colitis[124] and Crohn's disease, and we found that prophylactic administration of anti-mTNF-α mAb or the TNF-α trap Etanercept (TNFR1-IgG)[125] clearly ameliorated DSS-induced colitis as exacerbated by the anti-PD-1 plus anti-CTLA-4 mAb combination regimen (Fig. 1 a-d).

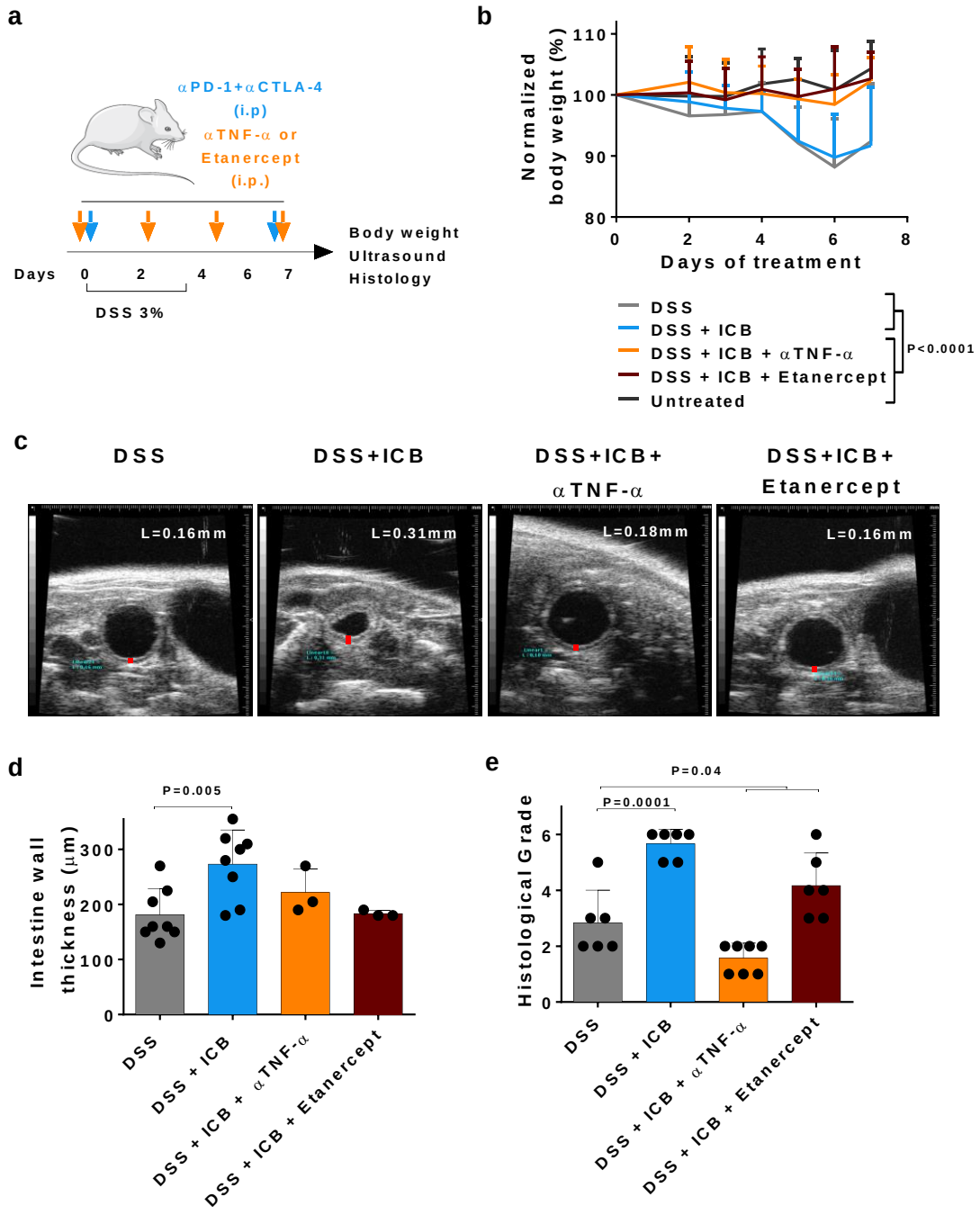

Figure 1. DSS-induced colitis as exacerbated by anti-PD-1 and anti-CTLA-4 mAb is ameliorated by prophylactic TNF-α blockade. a, Mice in which autoimmune colitis was induced by DSS administration in the drinking water were treated in different groups with anti-PD-1 + anti-CTLA-4 mAbs in combination with or without TNF-α blockade either with anti-TNF-α mAbs or Etanercept. **b**, Normalized follow-up of body weight as a surrogate indicator of colitis severity in mice (ICB stands for Immune Checkpoint Blockade). Data are mean ± s.d. of n=9 biologically independent mice. Extra sum-of-squares F test. **c**, Shows representative ultrasound assessments of intestinal wall thickness that are systematically presented in **d**. Red bars indicate the intestinal wall thickness. Data

are mean ± s.d. The numbers of biologically independent mice are: n=8 for DSS and DSS+ICB and n=3 for groups with TNF-α blockade. One-way ANOVA followed by Dunnett post-test. **e**, Represents results of a pathology score assessing the severity of colon wall inflammation in H&E stained sections evaluated by a clinical pathologist blinded to the origin of samples. Data are mean ± s.d. The numbers of biologically independent mice are n = 7 for the groups treated with anti-TNF-α and n = 6 for the other groups. One-way ANOVA followed by Dunnett post-test. Pooled data of two independent experiments.

We next studied if prophylactic TNF-α blockade would impair the antitumor activity of the anti-PD-1 plus anti-CTLA-4 mAbs combination in mice bearing established MC38 or B16 OVA-derived tumors. As shown in figure 2a-c, TNF-α inhibition with a specific mAb or Etanercept did not hamper the prominent antitumor effects of the dual checkpoint inhibition against MC38-derived tumors.

Similar observations were made on B16-OVA-derived melanomas (Extended Data Fig.1).

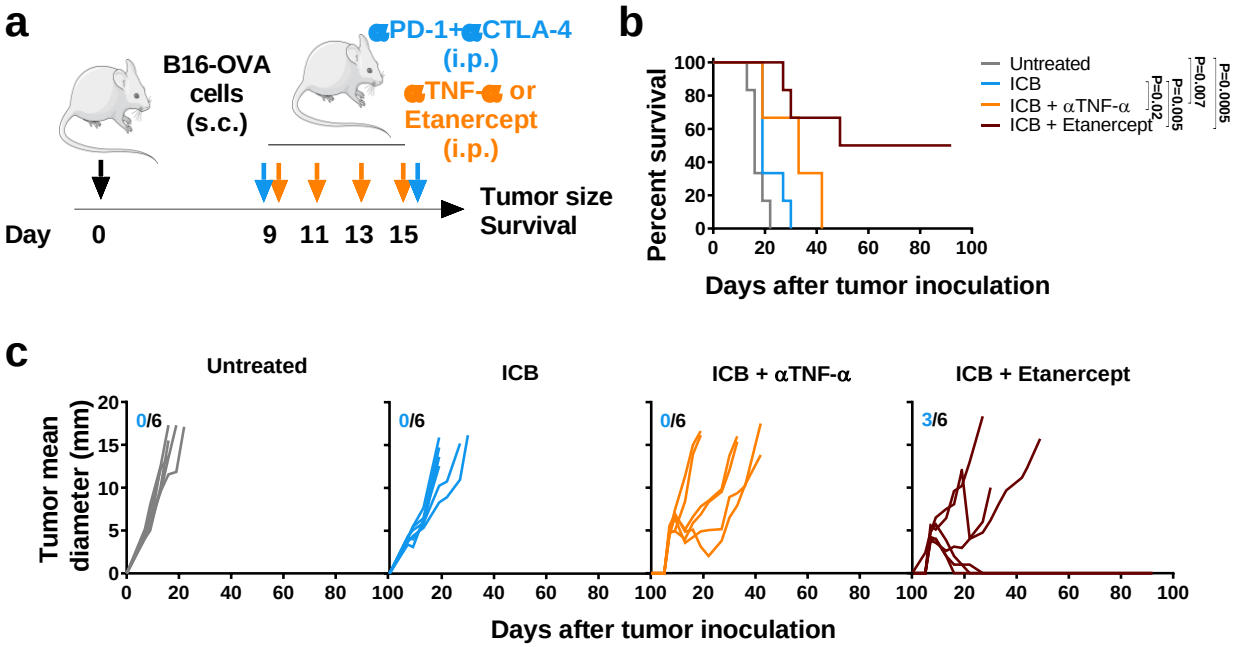

Extended Data Figure 1. Antitumor activity of double immune checkpoint blockade on B16-OVA derived tumors. Experiments as in Fig. 2a but performed on mice bearing B16-OVA-derived tumors treated in different groups as schematically represented in a. **b**, shows the overall survival of treatment groups. n is indicated in panel c; two-sided log-rank test. **c**, Individual follow-up of tumor size depicting the fraction of mice completely rejecting their tumors. Representative experiment of two independent experiments.

These data indicated that TNF-α functions are dispensable and, to some extent, harmful to the antitumor activities of the combined immunotherapy regimens. In parallel experiments, preventive IL-6 blockade was also attempted due to previous reports on IL-6 neutralization for cancer treatment[126, 127]. However in our case, antitumor efficacy was partially reduced in the MC38 and B16-OVA models (Extended Data Fig. 2).

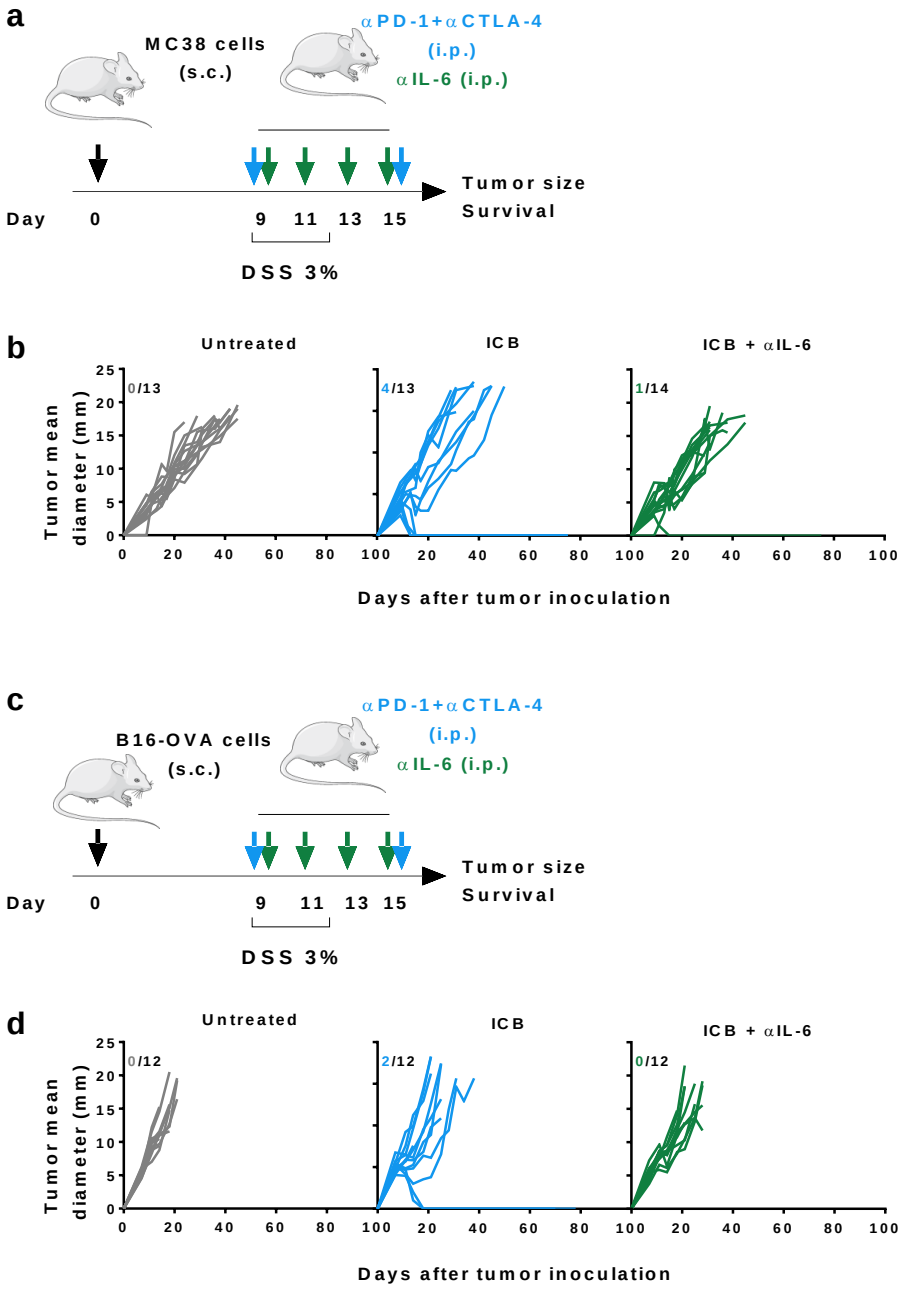

Extended Data Figure 2. Prophylactic IL-6 blockade hinders the antitumor activity of the anti-PD-1 + anti-CTLA-4 mAb immunotherapy regimen. a, Schematic representation of treatments applied to mice subcutaneously engrafted with MC38 colon carcinoma cells whose results are shown in panel b. **b**, Individual follow-up of tumor mean diameters indicating the fraction of mice completely rejecting established tumors. **c**, Schematic representation of treatments applied to mice subcutaneously engrafted with B16-OVA melanoma cells whose results are presented in panel d. **d**, Individual tumor size follow-up depicting fractions of complete rejections. Pooled data of two independent experiments

Unexpectedly, with some experimental variability, TNF-α neutralizing agents resulted in a higher fraction of mice completely rejecting their tumor grafts (Fig. 2).

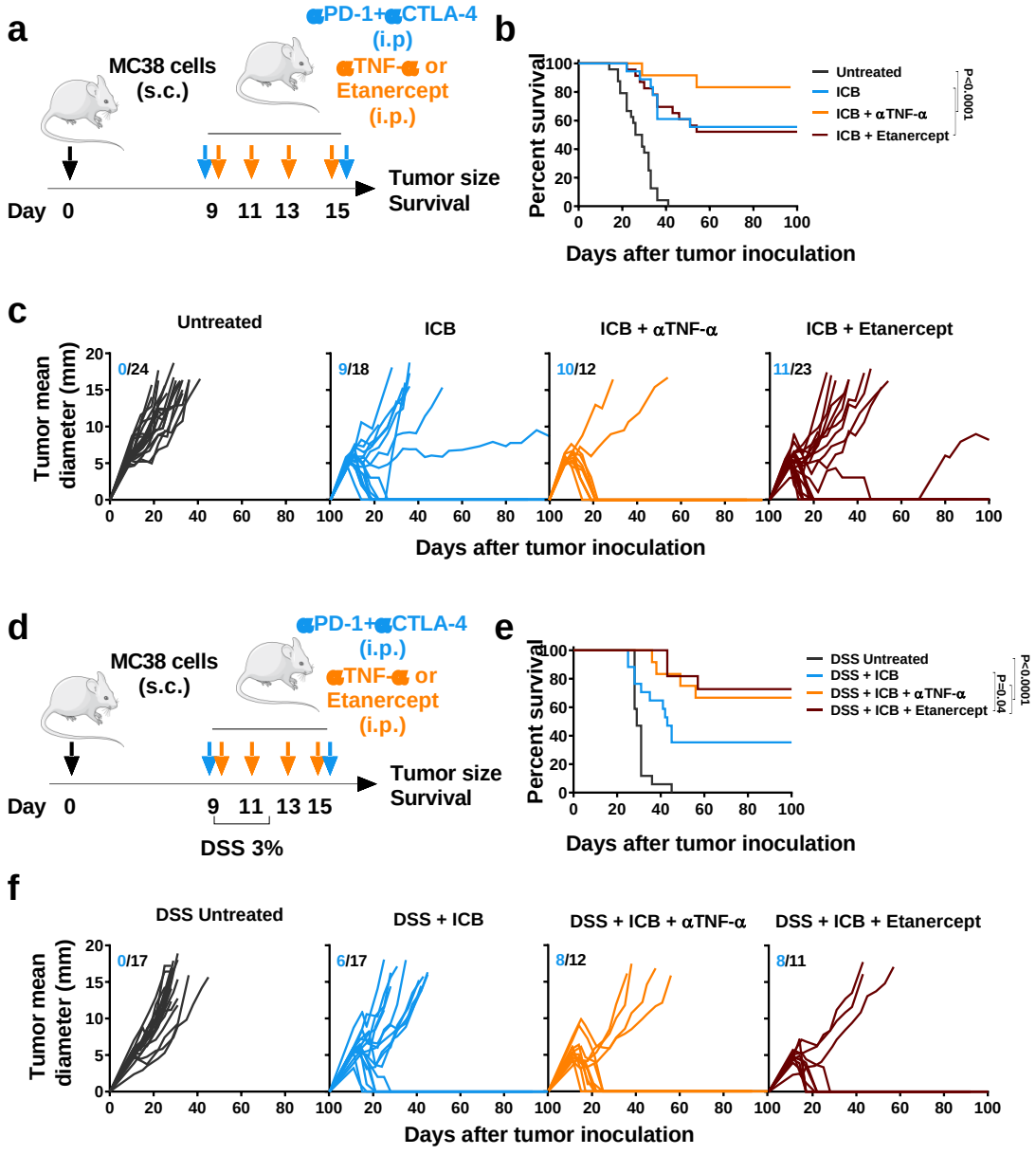

Figure 2. Prophylactic TNF-α blockade doses do not hinder and even enhance the antitumor activity of the anti-PD-1 + anti-CTLA-4 mAb immunotherapy regimen. **a**, Schematic representation of treatments applied to mice subcutaneously engrafted with MC38 colon carcinoma cells whose results are presented in panels **b** and **c**. **b**, Overall

survival of the indicated treatment groups. The numbers of biologically independent mice are indicated in panel c; Two-sided log-rank test. **c**, Individual follow-up of mean tumor diameters indicating the fraction of mice completely rejecting established tumors. **d**, Schematic representation of experiments performed as in **a** but with colitis induced from day +9 by providing DSS in the drinking water. **e**, Shows overall survival of the mice. Biologically independent mice are indicated in panel f; Two-sided log-rank test. **f**, Individual tumor size follow-up depicting fractions of complete rejections. Pooled data of three independent experiments.

These data are reminiscent of a recent report in which tumor-bearing mice genetically deficient in TNF-α or under TNF-α blockade responded slightly better to anti-PD-1 single-agent treatment[128].

We sought to determine if the enhancement of antitumor effects would also occur in MC38 tumor-bearing mice in which DSS colitis had been concomitantly induced. A series of experiments that were undertaken suggested an advantage in tumor rejection and survival for mice which in addition to double checkpoint blockade also received Etanercept or anti-TNF-α (Fig. 2d-f). Of note, the neutralizing antibody was more consistently efficacious than Etanercept. This can be related to the fact that in response to Etanercept immune competent mice develop anti-drug antibodies more efficiently (Extended Data Fig. 3).

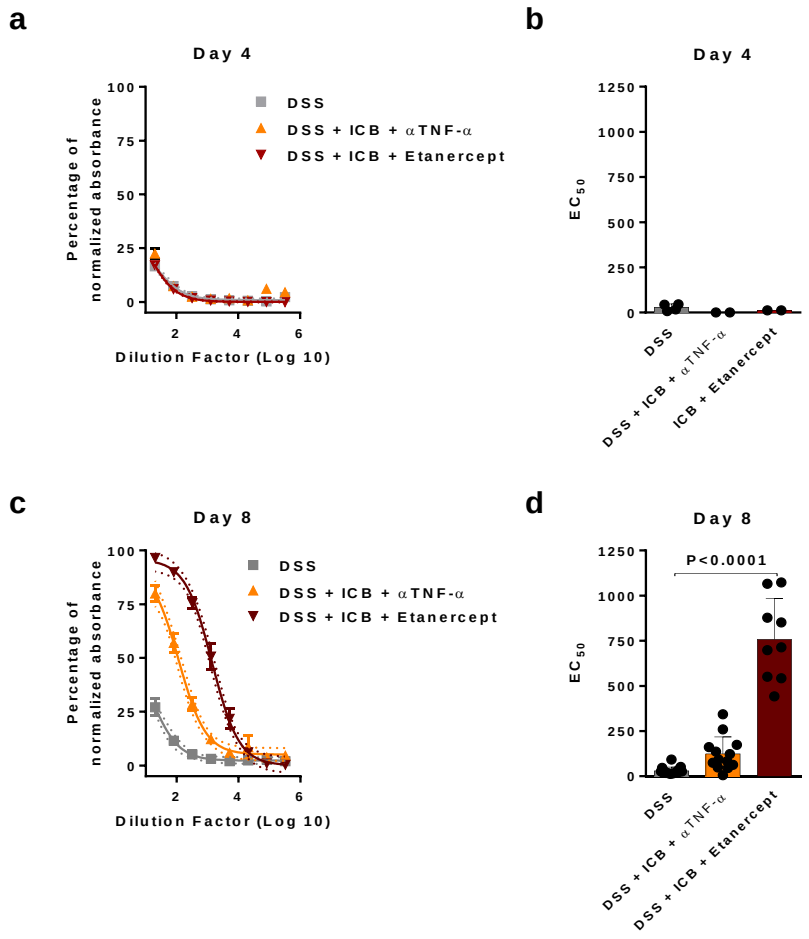

Extended Data Figure 3. Etanercept administration elicits anti-drug antibodies in mice. An anti-drug antibody detection assay was performed on serum collected from MC38 tumor-bearing mice 4 or 8 days after the beginning of TNF-α blockade treatment as in Fig. 2d. **a** and **c**, Percentage of normalized absorbance reflecting the levels of antibody against rat anti-TNF-α or anti-Etanercept by ELISA on days 4 (**a**) and 8 (**c**). **b** and **d**, Representation of the half maximal effective serum concentrations (EC_{50}) are shown for days 4 (b) and 8 (d). Data are mean ± s.d.; The numbers of biologically independent mice are: n=15 (DSS), n=13 (DSS + ICB + α-TNF) and n=9 (DSS + ICB + Etanercept) from three independent experiments. One-way ANOVA followed by Dunnett post-test. A sigmoidal dose-response equation was used to determine EC_{50}. The continuous line represents the nonlinear regression curve fit, and the dotted line represents the s.d. Pooled data of three independent experiments.

In addition, anti-CTLA-4 + anti-PD-1 treatment increased TNF-α concentrations in the tumor microenvironment without detectable circulating levels (Extended Data Fig. 4) and perhaps tissue penetration of the TNF-α neutralizing agent is desirable

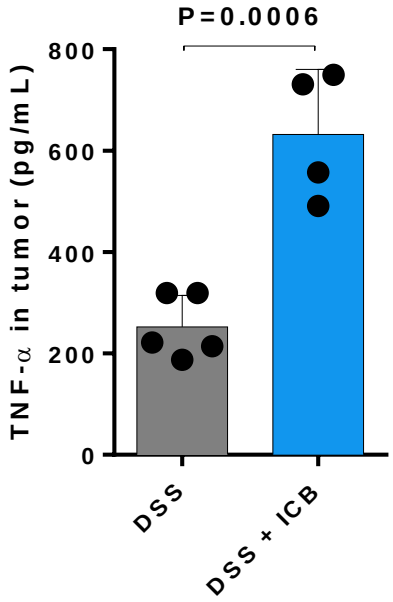

Extended Data Figure 4. Increased concentrations of TNF-α in the tumor microenvironment upon ICB therapy. Tumor homogenates were prepared 24h after finishing the treatment regimen described in Fig. 2d. Levels of TNF-α in the tumor are shown. Data are mean ± s.d.; n=4 biologically independent mice. Two-sided t-test. TNF-α was undetectable in serum samples from the same mice. Representative experiment of two independent experiments.

Double checkpoint inhibition in mice bearing MC38 and B16-OVA tumors gave rise to an increase in the infiltrate of $CD8^+$ T cells in the tumors that was further enhanced by anti-TNF-α or Etanercept (Extended Data Fig. 5a).

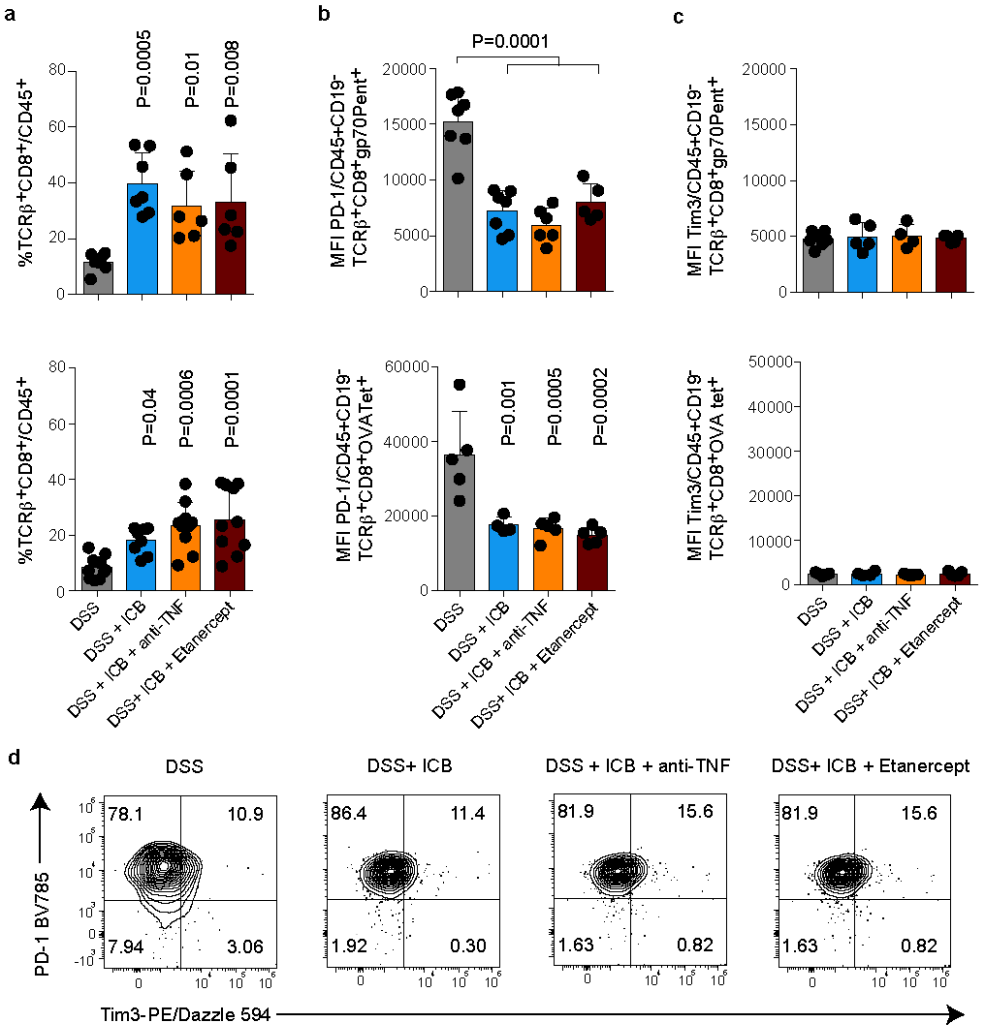

Extended Data Figure 5. Downregulation of PD1 expression on tumor-infiltrating antigen-specific $CD8^+$ T cells following the anti-PD-1 + anti-CTLA-4 mAb immunotherapy regimen. Tumors from MC38 and B16-OVA mouse models were collected 24h after finishing the treatment according to the dose regimens described in Fig. 2d and cell suspensions were analyzed by flow cytometry. **a**, Percentages of total

$TCR\beta^+CD8^+$ T cells among viable $CD45^+$ cells are shown for MC38 (upper panel) and B16-OVA (lower panel). **b**, Median fluorescence intensities (MFI) of surface PD1 are shown for $PD1^+$ cells gated on viable $CD45^+CD19^-TCR\beta^+CD8^+$ gp70 pentamer$^+$ (upper panel) or OVA tetramer$^+$ cells (lower panel). **c**, MFI of surface Tim3 is shown for $Tim3^+$ cells previously gated on viable $CD45^+CD19^-TCR\beta^+CD8^+$ gp70 pentamer$^+$ (upper panel) or OVA tetramer$^+$ cells (lower panel). Data are mean ± s.d. The numbers of biologically independent mice are: Upper panels (MC38) n=7 for DSS and DSS+ICB and n=6 for groups with TNF-α blockade. Lower panels (B16-OVA) n=6 for DSS+ICB+αTNF-α and n=10 for the other groups. One-way ANOVA followed by Dunnett test, each condition compared with the DSS group as a control. **d**, Representative contour-plots of PD1 and Tim3 in experimental groups described in b are shown for viable $CD45^+CD19^-$ $TCR\beta^+CD8^+$ gp70 pentamer$^+$ cells. Fluorescence minus one stainings were used as negative controls. Representative data of two independent experiments.

Importantly, this increase was also substantiated for tumor antigen-specific $CD8^+$ T cells as detected by gp70 H-$2K^b$- pentamer immunostainings in the tumor microenvironment and tumor-draining lymph nodes (Fig. 3a and b).

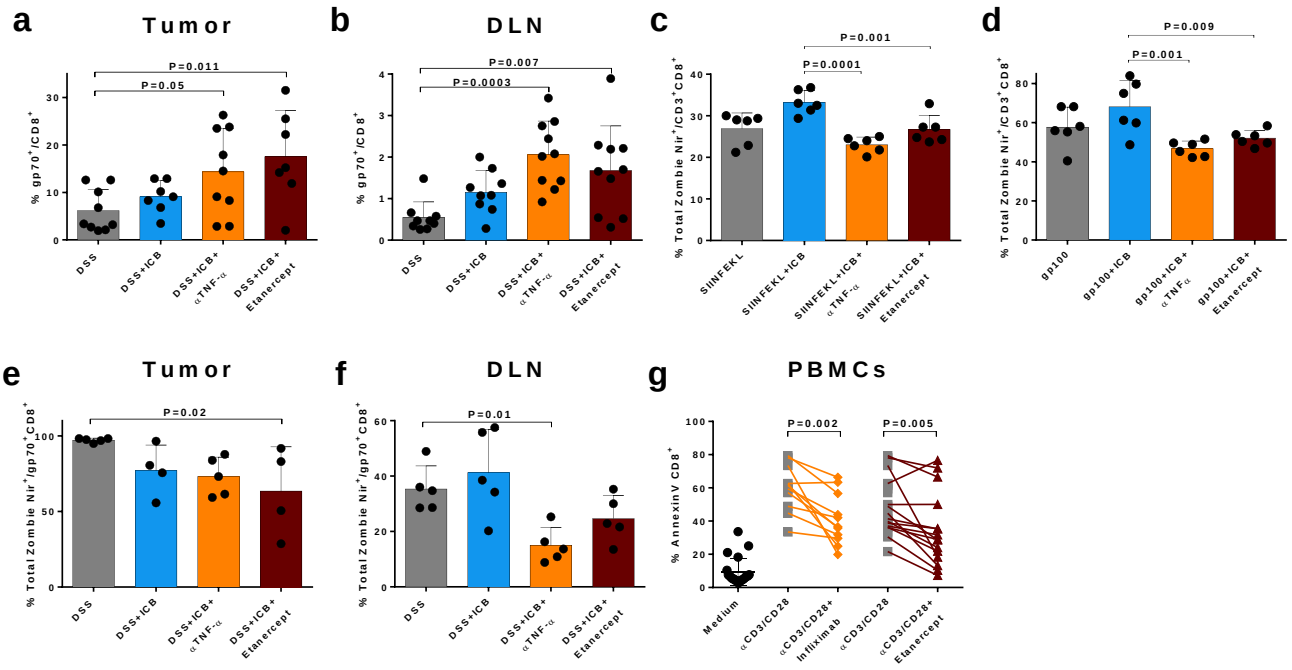

Figure 3. TNF-α blockade increases infiltration of tumor-specific T cells in MC38-derived tumors and decreases activation-induced cell death in $CD8^+$ T cells from mice and humans. Mice bearing MC38 tumors were treated as in Fig. 2**d** and sacrificed on day 16 to retrieve their tumors. **a**, Represents the content of tumor-specific $CD8^+$ T cells as detected with a gp70 H-$2K^b$ pentamer in the tumor microenvironment. Data are mean ± s.d. The numbers of biologically independent mice are n=9 for DSS and DSS+ICB+αTNF-α and n=7 for DSS+ICB and DSS+ICB+Etanercept. One-way ANOVA followed by Dunnett post-test. (**b**) Tumor-specific $CD8^+$ T cells as detected with a gp70 H-$2K^b$ pentamer in the tumor-draining lymph nodes. Data are mean ± s.d. The numbers of biologically independent mice are n=9 for DSS and DSS+ICB and n=10 for groups with TNF-α blockade. One-way ANOVA followed by Dunnett post-test. **c**, OT-1 $CD8^+$ T cells isolated from the spleen of TCR-transgenic mice were activated with cognate SIINFEKL peptide at 25 ng/ml. Anti-PD-1 and anti-CTLA-4 mAbs at 6.6 µg/ml were added to the ICB-treated cultures. Simultaneously anti-TNF-α (8.3 µg/ml) or Etanercept (2.6 µg/ml) were added to the indicated conditions. Cell death was monitored by Zombie Nir staining of T cells assessing the percentage of dead lymphocytes 72h after adding stimuli. Data are mean ± s.d. n=6 biologically independent samples. One-way

ANOVA followed by Dunnett post-test. **d**, Experiments as in c were performed with Pmel-1 T cells activated with 500 ng/ml of cognate gp100 peptide. Data are mean ± s.d. n=6 biologically independent samples. One-way ANOVA followed by Dunnett post-test. Pooled data of two independent experiments in a, b, c and d. **e** and **f**, Mice bearing MC38 tumors were treated as in a and the fraction of viable gp70-reactive CD8 T cells was assessed by viability-dye exclusion in gated $CD8^+$ T cells from cell suspensions derived from either (**e**) tumor-infiltrating lymphocytes, or (**f**) tumor-draining lymph nodes. Data are mean ± s.d. The numbers of biologically independent mice are n=5 for all groups except n=4 for DSS+ICB and DSS+ICB+Etanercept. One-way ANOVA followed by Dunnett post-test. Representative experiment out of three independent experiments in e and f. **g**, PBMCs from healthy donors were activated with plate-bound anti-CD3/CD28 antibodies for 7 days in the presence or absence of Infliximab (anti-hTNF-α, 10 μg/ml) or Etanercept (4 μg/ml). Cell death was monitored by % Annexin V staining of $CD8^+$ T cells. Data are mean ± s.d. The numbers of biologically independent healthy donors are n=15 for anti-CD3/CD28 + Etanercept and n=11 for anti-CD3/CD28 + Infliximab. Two-sided paired t-test. Pooled data of nine experiments.

We explored if these beneficial antitumor effects of prophylactic TNF-α blockade could be related to reversion of an exhaustion phenotype of CD8 T cells. In this regard, MC38 tumor-infiltrating $CD8^+$ T cells under double checkpoint blockade and TNFα inhibition with mAb had a lower surface expression of PD-1 (Extended Data 5b and d) as assessed by a non-competing anti-PD-1 mAb[129]. In contrast, surface expression of TIM-3 was not modified by double checkpoint blockade (Extended data Fig. 5c).

The focus of these experiments on surface TIM-3 expression on tumor-specific tumor-infiltrating CD8 T cells came from the reported decrease in TIM-3 expression by TNF-α blockade upon anti-PD-1 single-agent treatment that was invoked to explain enhanced efficacy[128]. Moreover, we tested a wide panel of molecules associated with T-cell exhaustion without noticeable changes attributable to TNF-α blockade aside from the mentioned reduction of PD-1 (Extended Data Fig. 6). Reduction of surface PD-1 did not result from internalization[129] and probably involves selective expansion of $PD\text{-}1^{low/neg}$ CD8 T cells upon treatment as recently reported[130, 131].

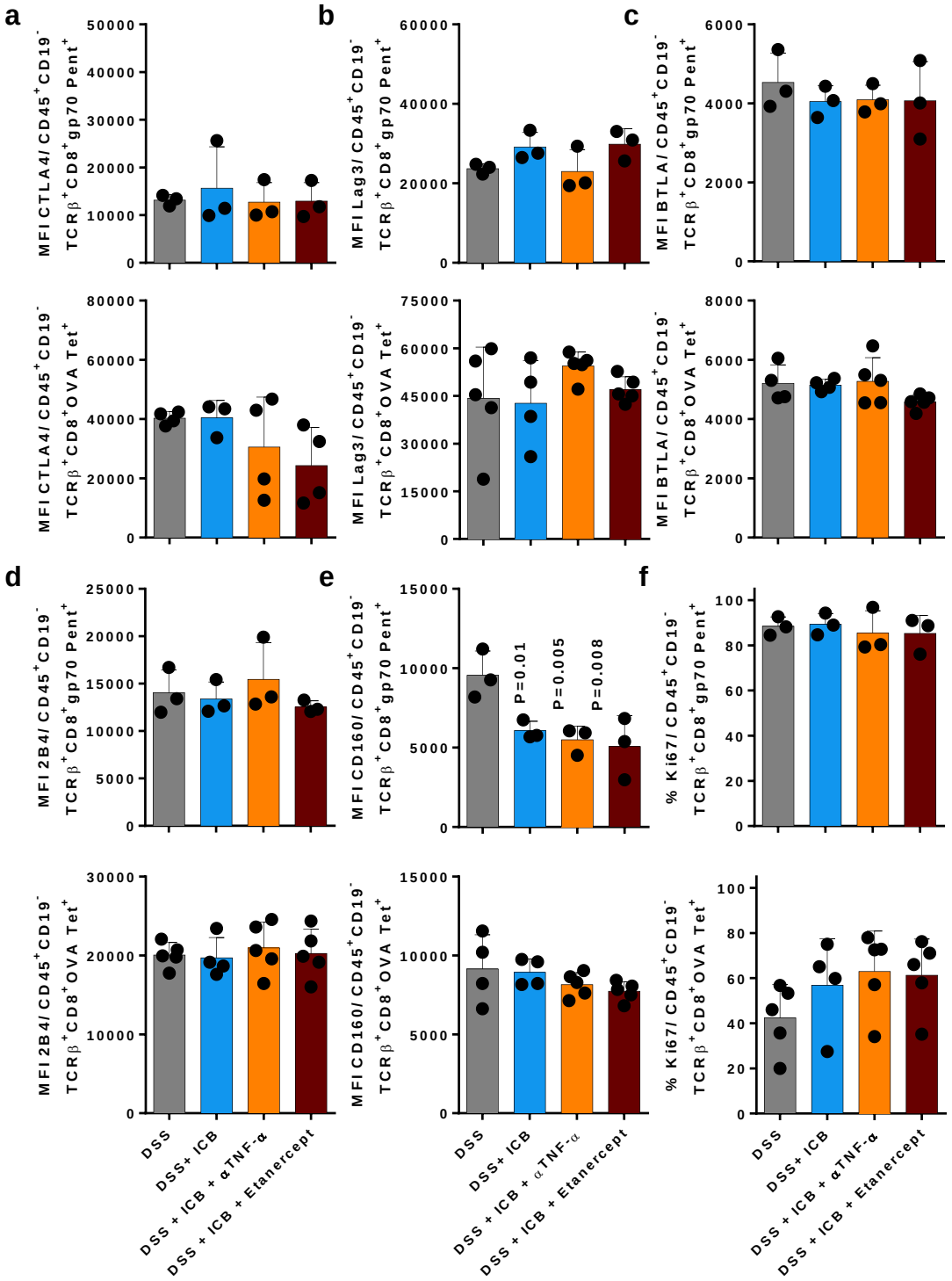

Extended Data Figure 6. Expression of T cell exhaustion related markers on T cells following ICB treatment with or without TNF-α blockade. Tumor-specific T CD8 cells recognizing gp70 (upper panels) or OVA (lower panels) in tumor cell suspensions derived one day after completion of treatments as color-coded indicated were analyzed by multicolor flow cytometry. Expression of surface CTLA-4 (a), LAG3 (b), BTLA (c), 2B4 (d), CD160 (e) and intracellular Ki67 (f) are shown. Data are MFI (mean ± s.d.) for

surface markers and % of positive cells for Ki67 (mean ± s.d.). The numbers of biologically independent mice are Upper panels (MC38) n=3. Lower panels (B16-OVA) n=4 for the DSS+ICB group and n=5 for the other groups. One-way ANOVA followed by Dunnett test, each condition compared with the DSS group as a control. Representative data of two independent experiments.

Another mechanistic possibility for the enhanced antitumor effects is the attenuation of activation-induced cell death (AICD) in T lymphocytes[132]. Indeed, murine T cells deficient in TNFR1 ($p55^{-/-}$) reportedly experience considerably more pronounced levels of AICD[133]. In keeping with this finding, we observed that TNF-α blockade with anti-TNFα or Etanercept decreases apoptosis in TCR-transgenic mouse $CD8^+$ OT-I and Pmel-1 cells activated in culture with their respective cognate peptides in the presence of anti-PD-1 and anti-CTLA-4 mAbs (Figs. 3c and d). Furthermore, in mice bearing MC38 tumors and suffering from DSS colitis that were treated with double checkpoint blockade, systemic TNF-α neutralization resulted in increased viability of tumor-reactive CD8 T cells in the tumor microenvironment (Fig. 3e) and even more prominently so in tumor-draining lymph nodes (Fig. 3f). Importantly, human CD8 T lymphocytes from a series of healthy volunteers activated with anti-CD3/anti-CD28 mAbs experienced less AICD when cultured in the presence of the anti-TNFα mAb Infliximab or Etanercept (Fig. 3g and Extended Data Fig. 7).

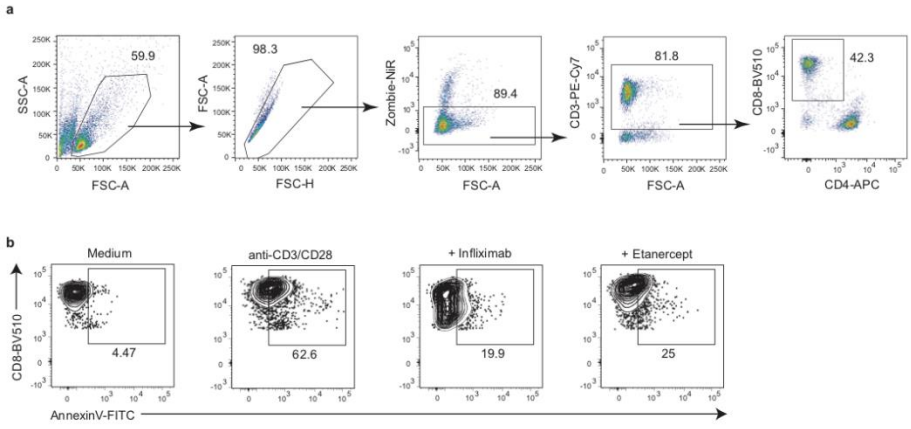

Extended Data Figure 7. Gating strategy and representative contour plots of AICD protection by TNF-α blockade in human PBMCs. a, Gating strategy for flow cytometry analysis. **b**, Representative contour plots showing annexin V positive cells among $CD8^+$ T lymphocytes after stimulation with anti-CD3/CD28 with or without TNF-α blockade with Infliximab or Etanercept of experimental groups described in Fig. 3g.

To address the clinical applicability of these mouse data, we explored if the TNF-α pathway is turned on in human cancer patients developing colitis upon Nivolumab plus Ipilimumab treatment. Figure 4a and b show NanoString-assessed mRNA expression of immune-related gene analyses in tissue sections from colon biopsies of healthy mucosa from patients with double-checkpoint induced colitis or diagnosed with *bona fide* ulcerative colitis. TNF-α mRNA was augmented in all four cases although it did not reach the levels of naturally occurring inflammatory bowel disease (Fig. 4a). Gene expression analyses were also consistent with transcripts reflecting local activation of the TNF-α gene signature (Fig. 4b). Since TNF-α is a cytokine that can be efficaciously targeted in ulcerative colitis, it makes sense to prevent or attenuate colitis induced by Nivolumab plus Ipilimumab treatment given the fact that TNF-α is also upregulated *in situ* in the intestinal lesions.

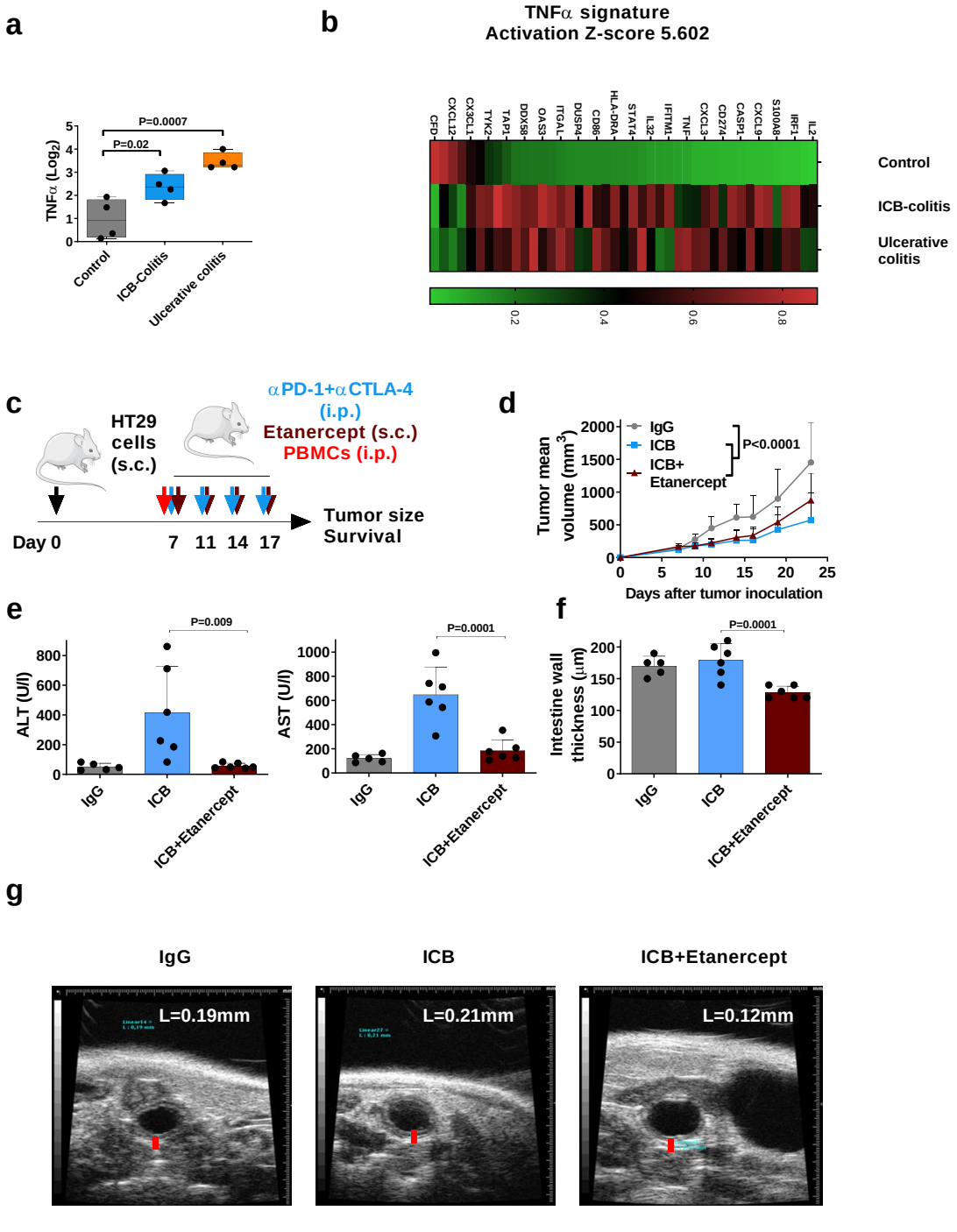
a
b
TNFα signature
Activation Z-score 5.602
P=0.0007
P=0.02
TNFα (Log2)
Control
ICB-Colitis
Ulcerative colitis
CFD
CXCL12
CX3CL1
TYK2
TAP1
DDX58
OAS3
ITGAL
DUSP4
CD86
HLA-DRA
STAT4
IL32
IFITM1
TNF
CXCL3
CD274
CASP1
CXCL9
S100A8
IRF1
IL2
Control
ICB-colitis
Ulcerative colitis
0.2
0.4
0.6
0.8
c
αPD-1+αCTLA-4 (i.p.)
Etanercept (s.c.)
PBMCs (i.p.)
HT29 cells (s.c.)
Day 0
7 11 14 17
Tumor size
Survival
d
IgG
ICB
ICB+ Etanercept
P<0.0001
Tumor mean volume (mm3)
Days after tumor inoculation
e
P=0.009
P=0.0001
ALT (U/l)
AST (U/l)
IgG
ICB
ICB+Etanercept
f
P=0.0001
Intestine wall thickness (μm)
IgG
ICB
ICB+Etanercept
g
IgG
ICB
ICB+Etanercept
L=0.19mm
L=0.21mm
L=0.12mm

Figure 4. TNF-α axis is involved in immune-mediated colitis as a side effect of combined Nivolumab+Ipilimumab in patients and in humanized mouse models of immune-mediated adverse events upon ICB anti-tumor treatment. Gene-expression profiling using a nCounter Analysis System using the PanCancer Immune Profiling Panel probe set was performed in different human colon mucosa tissue taken by colonoscopy: four healthy mucosae of large intestine (Control), four cases of colitis induced by Nivolumab+Ipilimumab immunotherapy (ICB-colitis) and four cases of ulcerative colitis (Ulcerative colitis). **a**, TNF-α gene expression. Centre line, median; box limits, minimum and maximum. n=4 biologically independent patient samples. One-way ANOVA followed by Dunnett post-test. **b**, Gene signature that denotes TNF-α activation in ICB-Colitis and Ulcerative colitis versus Control group. Data from a single experiment in a and b. **c**, Schematic representation of treatments applied to immunodeficient $Rag2^{-/-}$ $IL2R\gamma^{null}$ mice subcutaneously engrafted with HT29 colon carcinoma cells and human PBMCs after seven days. Mice were treated at days 7, 11, 14, 17 intraperitoneally with Ipilimumab plus Nivolumab with or without Etanercept (40µg) given subcutaneously. As an antibody control, we used human polyclonal IgG. **d**, Tumor mean volumes. Data are mean ± s.d. The numbers of biologically independent mice are n=5 for IgG and n=6 for treated groups. Extra sum-of-squares F test. **e**, Alanine transaminase (ALT) and aspartate transaminase (AST) serum levels at day 24. Data are mean ± s.d. of n = 5 for IgG and n = 6 for treated groups. One-way ANOVA followed by Dunnett post-test. **f**, Ultrasound assessments of intestinal wall thickness at day 24. Data are mean ± s.d. The numbers of biologically independent mice are n=5 for IgG and n=6 for treated groups. One-way ANOVA followed by Dunnett post-test. **g**, Representative ultrasound examination images of the different treatment groups described in f. Red bars indicate intestinal wall thickness. Data from a single experiment.

To further explore applicability, we used a model of xenograft versus host disease in which human PBMCs are infused into Rag$^{-/-}$IL-2Rγ$^{-/-}$ mice. This condition causes inflammation of several target organs including the colon[134]. In such a model, treatment with Ipilimumab plus Nivolumab exacerbated the disease and resulted in body weight differences (Extended Data Fig. 8a). In this setting of multiorgan autoimmunity exacerbated by double checkpoint blockade, Etanercept but not control human IgG ameliorated large intestine inflammation as assessed by ultrasound exams of intestinal wall thickness (Extended Data Fig. 8b and c). In this humanized mouse model, we subcutaneously xenografted HT29 colon cancer cells (Fig. 4c) and observed that tumor progression was controlled to some extent by Nivolumab + Ipilimumab treatment. In these conditions, concomitant Etanercept treatment did not spoil these therapeutic effects (Fig. 4d). In contrast, xenograft versus host hepatitis and colitis were markedly ameliorated (Fig. 4 e to g).

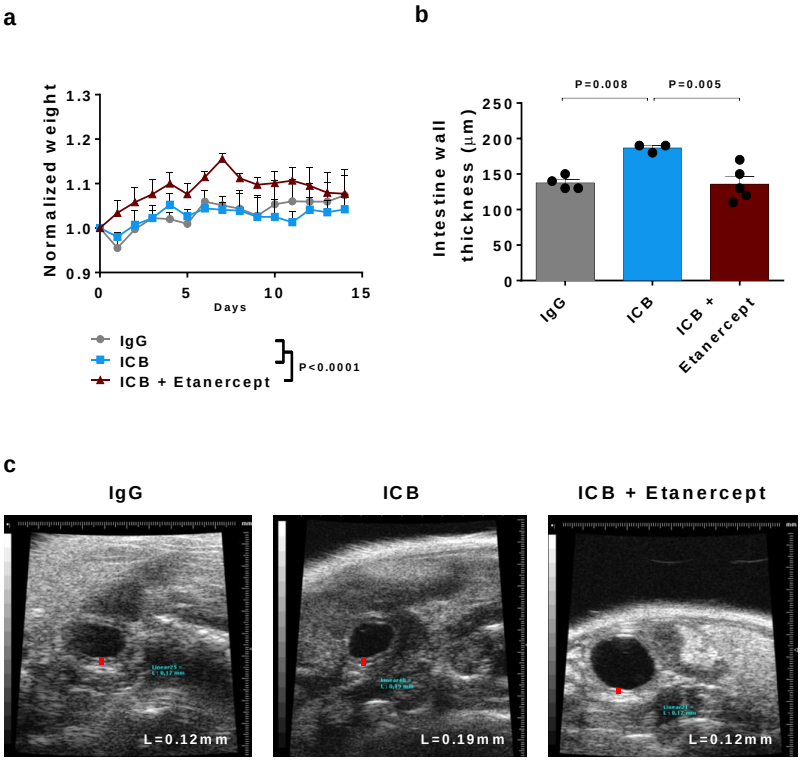

Extended Data Figure 8. TNF-α axis is involved in immune-mediated colitis exacerbated by ICB in immune-deficient mice reconstituted with human PBMCs. Fresh human PBMCs were injected intraperitoneally at day 0 into immunodeficient $Rag2^{-/-}IL2R\gamma^{null}$ mice. At day 0, 4, 7, 10, mice were injected intraperitoneally with Ipilimumab (200 µg) plus Nivolumab (200 µg) with or without Etanercept (40µg) given subcutaneously. As an antibody control, we used human polyclonal IgG. **a**, Normalized follow-up of body weight. Data are mean ± s.d.; The numbers of biologically independent mice are n=4, except n=5 for PBMCs+ICB+Etanercept. Extra sum-of-squares F test. **b**, Ultrasound assessments of intestinal wall thickness. Data are mean ± s.d. The numbers of biologically independent mice are: n=4 for PBMCs+IgG, n=3 for PBMCs+ICB and n=5 for PBMCs+Etanercept. One-way ANOVA followed by Dunnett post-test. **c**, Representative ultrasound images estimating colon wall thickness in the different experimental groups described in b. Red bars indicate intestinal wall width. Data from a single experiment.

TNF-α blockade is not new in the cancer immunotherapy arena. Pioneering work by F. Balkwill *et al*.[135] resulted in clinical trials testing infliximab for ovarian[136] and renal[137] cancer involving etanercept and infliximab. Clinical activity was modest and not sufficiently supportive to warrant further clinical research but the fact that the patients underwent treatment without any reported evidence of disease hyper-progression constitutes very reassuring evidence of the excellent safety of TNF-α inhibition in advanced cancer patients.

Taken together our results and previous experience argue in favor of conducting a sufficiently powered clinical phase II clinical trial testing the safety (% grade>2 irAEs) and objective activity (ORR) in patients undergoing Ipilimumab plus Nivolumab treatment in whom an approved anti-TNF-α agent would be given prophylactically or concomitantly with the immunotherapy regimen. Indeed, there is an ongoing phase I investigator-initiated trial testing safety of this combined approach (clinicaltrails.gov NCT03293784) that should be followed by a larger clinical trial. Our results argue in favor of better safety, at least in the gut and in the liver, and equal or perhaps enhanced efficacy. If this hypothesis is correct, prophylactic TNF-α blockade may allow Ipilimumab doses to be safely increased in the combined immune checkpoint blockade regimens which thereby are predicted to exert more robust antitumor efficacy.

Competing interests

I.M. reports advisory roles with Roche-Genentech, Bristol-Myers Squibb, CYTOMX, Incyte, MedImmune, Tusk, F-Star, Genmab, Molecular Partners, Alligator, Bioncotech, Bayer and research funding from Roche, BMS, Alligator, and Bioncotech. P.B. reports advisory roles with Tusk and Moderna, research funding from Sanofi, Moderna and Bavarian Nordic and speaker honoraria from BMS, MSD, Novartis and AstraZeneca. IM-R reports advisory roles with Roche-Genentech, Bristol-Myers Squibb, Incyte, Merck, Amgen, Pierre Fabre, Novartis, and Bioncotech. J.L.P.G. reports advisory roles with Roche, MSD and BMS, travel support from Roche, BMS, and MSD and research funding from Roche, BMS, MSD, Ipsen, Eisai, Incyte and Janssen. The rest of the authors have no conflict of interest to declare.

Funding

This work was supported by the International Immuno-Oncology Network (II-ON) from Bristol-Myers Squibb; a Worldwide Cancer Research Grant (15-1146); the Asociación Española Contra el Cancer (AECC) Foundation under grant GCB15152947MELE; the Instituto Carlos III (under grants PI14/01686, PI13/00207 and PI16/00668) co-financed with FEDER funds; and the European Union's Horizon 2020 Program (grant agreement no. 635122 PROCROP). P.B. is supported by a Miguel Servet II (CPII15/00004) contract from Instituto de Salud Carlos III; E.P.-R is supported by the Carmen Lavigne training program of the Asociación Española contra el Cancer and by Consejeria de Salud de la Junta de Andalucía; and A.T. has received financial support through la Caixa Banking Foundation (LCF/BQ/LR18/11640014).

GENERAL DISCUSSION

Immunotherapy has revolutionized the medical practice in clinical oncology, allowing a gain in overall survival of treated patients. The mode of action is the result of improving the patient's own immune system-mediated anti-tumor activity and in general these approaches present fewer and more tolerable side effects as compared to other therapies. Best results have been obtained by anti-PD-1 monoclonal antibodies that have been approved between 2014 and 2015 for the treatment of metastatic melanoma. Since then, anti-PD-1 antibodies are approved for thirteen more types of malignancies. Moreover, anti-PD-L1 therapies are approved for six types of cancer[142].

The success of therapies targeting the anti-PD-1/PD-L1 axis relies on different mechanisms. As it has been widely described, PD-1 ligation by its cognate ligand PD-L1 induces T-cell dysfunction causing cell cycle arrest, T-cell migration suppression, and reduction of cytotoxic effector capabilities. As discussed before, this immune checkpoint is necessary for the prevention of autoimmune reactions following chronic activation of T-cells. It has been demonstrated with preclinical models that the block of the axis PD-1/PD-L1 increases the duration of the interactions between dendritic cells and T-cells, T-cell activation, numbers of antigen-specific T-cells and consequent inhibition of tumor growth. Of significant interest are data demonstrating the role of anti-PD-1/PD-L1 in reinvigorating exhausted T-cells in melanoma patients under immune checkpoint treatment [1, 130, 131, 138, 139].

Despite the important actions of anti-PD-1/PD-L1 therapies on $CD8^+$ T cells, also $CD4^+$ cells are targeted by these monoclonal antibodies. In fact, several pieces of evidence show that immunotherapy augments cytokine production from these cells that in turn act on the response of effector $CD8^+$ cells, promotes memory formation or migration of T cells in a $CD4^+$-secreted IFNγ and chemokines dependent manner. $CD4^+$ memory T cells also

expand under PD-1 treatment and particular $CD4^+CD57^+$ population of senescent cells has been demonstrated to decrease in responders patients [1].

Despite the excellent results obtained by antibodies targeting the PD-1/PD-L1 axis, the majority of patients fails to experience a durable response. For this purpose, several combinations have been approved by FDA based on an improvement of the percentage of patients that benefit from this therapy. To date, FDA approved the combination of anti-PD-1 agents with only Ipilimumab, conventional chemotherapy, Abraxane or Axitinib.

New combination strategies are necessary to raise the rate of patients that respond to PD-1/PD-L1 agents. Although in 2018, 1700 trials of combinations with more than 240 targets were tested, more need to be done [142].

Of extreme interest would be exploiting the phenomenon of cell death for combined immunotherapy strategies. As previously described, cell death, differently from what has been thought for decades, is an active rather than a passive event. In this regard, the immune system acts as a sensor interacting with the environmental cues and responding to them to re-establish homeostasis[140]. Macroscopically, the sensors used by the immune systems are the epithelial and the mucosal barriers and in general the innate branch of the system. Microscopically, we can define as sensors the innate immune receptors, such as Toll-like receptors, that detect exogenous PAMPs and endogenous DAMPs. A successful combined immunotherapy treatment needs to act on the three signals necessary to initiate an adequate response. Must be improved the antigen-presentation by DCs (signal 1), the DCs-mediated T cell-costimulation (signal 2) and the release of polarizing cytokines (signal 3).

The three-signal model of T-cell activation may be integrated with the phenomenon of cell death and better represented by a more exhaustive framework proposed by Matthew

L. Albert and colleagues. They propose an elegant model with two additional signals. The engagement of pattern recognition receptors by PAMPs and DAMPs, leading to dendritic cells maturation and migration has been suggested to account for signal 0. Being dying cells a dominant source of PAMPs, DAMPs, and antigens, they propose the intrinsic cell mechanisms of cell death as signal 0. Therefore, dying cells release upon a source of cell stress constitutive DAMPs (i.e., calreticulin or HMGB1) or inducible DAMPs generated by the activation of specific pathways (i.e., IL1-β or Interferon Type I)[141]. Due to this peculiar immunological feature cell death could be the key for boosting the immune response against cancer. The exploitation of the characteristics of immunogenic cell death is already used when immunotherapy is combined with chemotherapy or radiotherapy. DAMPs and "eat me" signals released during cancer cell death under traditional oncological therapies lead to the loss of equilibrium between different cell subsets, attracting more dendritic cells and immune subsets related to a type-1-like response[4]. Whether a natural anti-cancer immunological response working in similar conditions to those present during the "elimination phase" of cancer progression, is able to shape the immune response generating endogenously DAMPs was still unclear and unexplored.

According to our results the immune response might gain momentum fostered by effector cytotoxicity and crosspriming of tumor antigens from killed target tumor cells.

To dissect mechanisms underlying cellular cytotoxicity and its potential as a mediator of immunogenic cell death, we established a vaccination model, and we analyzed the efficacy of antigenic specific $CD8^+$ T-cells in controlling tumor challenge. Our data demonstrate that cellular cytotoxicity is a form of immunogenic cell death that shapes the tumor microenvironment to present inflammatory properties. Analyzing our data we speculate that therapies able to reinvigorate or stimulate a cytotoxic response, such as checkpoint blockade therapy, generate a tumor microenvironment enriched by those

signals necessary to tilt the equilibrium and attract a type-1-like response. In other words, a response that generate the signal 0 and self-sustains the cancer immunity cycle with a positive feedback loop. More investigation is necessary to confirm if this kind of response occurs in patients with palpable tumors. Our model extremely forced cytotoxicity to a level not present in real conditions also because of the immunosuppressive properties of tumor cells or immune cells in the tumor microenvironment. It is therefore desirable to try to combine immunotherapy with agents that maintain the immunogenicity of the microenvironment.

Once established that immunotherapy could boost cellular cytotoxicity and generate a favorable immunogenic microenvironment, the next key questions are:

1) Is there an activation lymphocyte threshold that needs to be reached to convert a tolerogenic cell death to immunogenic cell death during tumor-killing?
2) Is there an upper threshold that would lead to detrimental immune effects, such as lymphocyte activation-induced cell death and exhaustion?

To answer the first question, more experimental evidence is needed. In this work, we qualitatively studied cell death comparing immunogenicity of different forms of cell killing (mechanical disruption by freezing and thawing and chemotherapy-induced killing) to cellular cytotoxicity. We can clearly conclude that cytotoxicity is immunogenic, but we did not determine the minimal activation "level" necessary to induce immunogenic cell death. In other words, limited by our model, we have not characterized activation markers on defined populations of T cells or NK cells to try to establish in terms of surface receptor expression or transcription factors the minimal requirements to activate an immunogenic killing. Studies in this direction would be exciting and extremely important to clarify the field of immunogenic cellular killing. In

this regard deeper understanding of cross-presentation and cross-priming by dendritic cells will be paramount.

We partially answered the second question in this project, although it was not directly related to immunogenic cell death. Studying how the excessive boost of cytotoxicity induced by immunotherapy breaks the effectiveness of the therapy itself, we concluded that cytokines considered to be essential for tumor control actually might become a source of immune-response impairment, exerting a detrimental effect on activated T lymphocytes. The immune system, trying to re-establish the homeostasis, will activate mechanisms of compensation to prevent excessive boost. Immunologists so have to focus not only on the acute effect of potentiated immunotherapy in cancer cells but also on the long-term effects of the therapies, such as persistence of activated lymphocytes, long-lasting memory responses and immunogenicity. Therefore, combinations need to be well designed and evaluated in order to promote a level of cellular cytotoxicity that reaches the threshold which leads to immunogenic cancer cell death without inducing exhaustion or activation-induced death of effector cells.

Cell death is critical for cancer immunology and immunotherapy because controls the number of effector cytotoxic T cells and the demise of malignant cells. Our results studying apoptosis as a result of NK and CD8 cytotoxicity, clearly indicate that this process leads to immunogenic cell death which through antigen crosspriming may lead to epitope spreading in such a way that the cancer immunity cycle gains momentum. On the contrary, studying the role of TNF in activation-induced T-cell death, we came to the conclusion that this mechanism is important in terms of attenuating antitumor immunity and offers a feasible therapeutic target to improve cancer immunotherapy results both gaining in efficacy and reducing side effects.

CONCLUSIONS

CONCLUSIONS

1. Cellular cytotoxicity induces immunogenic cell death *in vitro* and *in vivo.*
2. $CD8^+$ T cells and NK cells-induced immunogenic cell death depends on cDC1 and does not depend on STING and IFN type I signaling pathway.
3. Prophylactic TNF blockade ameliorates immune checkpoint blockade-exacerbated side effects.
4. Prophylactic TNF blockade does not hinder and even enhances the antitumor activity of immune checkpoint blockade therapy.
5. Prophylactic TNF blockade decreases activation-induced cell death in $CD8^+$ T cells from mice and humans.

BIBLIOGRAPHY

1. Fritz, J.M. and M.J. Lenardo, *Development of immune checkpoint therapy for cancer.* J Exp Med, 2019. **216**(6): p. 1244-1254.
2. Chen, D.S. and I. Mellman, *Oncology meets immunology: the cancer-immunity cycle.* Immunity, 2013. **39**(1): p. 1-10.
3. Kroemer, G., L. Galluzzi, and L. Zitvogel, *Immunological effects of chemotherapy in spontaneous breast cancers.* Oncoimmunology, 2013. **2**(12): p. e27158.
4. Galluzzi, L., et al., *Immunogenic cell death in cancer and infectious disease.* Nat Rev Immunol, 2017. **17**(2): p. 97-111.
5. Zitvogel, L., et al., *Microbiome and Anticancer Immunosurveillance.* Cell, 2016. **165**(2): p. 276-87.
6. Lippitz, B.E., *Cytokine patterns in patients with cancer: a systematic review.* Lancet Oncol, 2013. **14**(6): p. e218-28.
7. Mellman, I., *Dendritic cells: master regulators of the immune response.* Cancer Immunol Res, 2013. **1**(3): p. 145-9.
8. Riella, L.V., et al., *Role of the PD-1 pathway in the immune response.* Am J Transplant, 2012. **12**(10): p. 2575-87.
9. Franciszkiewicz, K., et al., *Role of chemokines and chemokine receptors in shaping the effector phase of the antitumor immune response.* Cancer Res, 2012. **72**(24): p. 6325-32.
10. Mellman, I., G. Coukos, and G. Dranoff, *Cancer immunotherapy comes of age.* Nature, 2011. **480**(7378): p. 480-9.
11. Motz, G.T. and G. Coukos, *Deciphering and reversing tumor immune suppression.* Immunity, 2013. **39**(1): p. 61-73.
12. Matzinger, P., *The danger model: a renewed sense of self.* Science, 2002. **296**(5566): p. 301-5.
13. Medzhitov, R. and C.A. Janeway, Jr., *Decoding the patterns of self and nonself by the innate immune system.* Science, 2002. **296**(5566): p. 298-300.
14. Seong, S.Y. and P. Matzinger, *Hydrophobicity: an ancient damage-associated molecular pattern that initiates innate immune responses.* Nat Rev Immunol, 2004. **4**(6): p. 469-78.
15. Gough, M.J., et al., *Induction of cell stress through gene transfer of an engineered heat shock transcription factor enhances tumor immunogenicity.* Gene Ther, 2004. **11**(13): p. 1099-104.
16. Melcher, A., et al., *Tumor immunogenicity is determined by the mechanism of cell death via induction of heat shock protein expression.* Nat Med, 1998. **4**(5): p. 581-7.
17. Casares, N., et al., *Caspase-dependent immunogenicity of doxorubicin-induced tumor cell death.* J Exp Med, 2005. **202**(12): p. 1691-701.
18. Obeid, M., et al., *Calreticulin exposure dictates the immunogenicity of cancer cell death.* Nat Med, 2007. **13**(1): p. 54-61.
19. Apetoh, L., et al., *Toll-like receptor 4-dependent contribution of the immune system to anticancer chemotherapy and radiotherapy.* Nat Med, 2007. **13**(9): p. 1050-9.
20. Scaffidi, P., T. Misteli, and M.E. Bianchi, *Release of chromatin protein HMGB1 by necrotic cells triggers inflammation.* Nature, 2002. **418**(6894): p. 191-5.
21. Thorburn, J., et al., *Autophagy regulates selective HMGB1 release in tumor cells that are destined to die.* Cell Death Differ, 2009. **16**(1): p. 175-83.
22. Garg, A.D., et al., *A novel pathway combining calreticulin exposure and ATP secretion in immunogenic cancer cell death.* EMBO J, 2012. **31**(5): p. 1062-79.

23. Gardai, S.J., et al., *Cell-surface calreticulin initiates clearance of viable or apoptotic cells through trans-activation of LRP on the phagocyte.* Cell, 2005. **123**(2): p. 321-34.
24. Ghiringhelli, F., et al., *Activation of the NLRP3 inflammasome in dendritic cells induces IL-1beta-dependent adaptive immunity against tumors.* Nat Med, 2009. **15**(10): p. 1170-8.
25. Elliott, M.R., et al., *Nucleotides released by apoptotic cells act as a find-me signal to promote phagocytic clearance.* Nature, 2009. **461**(7261): p. 282-6.
26. Vacchelli, E., et al., *Chemotherapy-induced antitumor immunity requires formyl peptide receptor 1.* Science, 2015. **350**(6263): p. 972-8.
27. Weyd, H., et al., *Annexin A1 on the surface of early apoptotic cells suppresses CD8+ T cell immunity.* PLoS One, 2013. **8**(4): p. e62449.
28. McNab, F., et al., *Type I interferons in infectious disease.* Nat Rev Immunol, 2015. **15**(2): p. 87-103.
29. Sistigu, A., et al., *Cancer cell-autonomous contribution of type I interferon signaling to the efficacy of chemotherapy.* Nat Med, 2014. **20**(11): p. 1301-9.
30. Galluzzi, L., et al., *Molecular mechanisms of cell death: recommendations of the Nomenclature Committee on Cell Death 2018.* Cell Death Differ, 2018. **25**(3): p. 486-541.
31. Aggarwal, B.B., S.C. Gupta, and J.H. Kim, *Historical perspectives on tumor necrosis factor and its superfamily: 25 years later, a golden journey.* Blood, 2012. **119**(3): p. 651-65.
32. Gibert, B. and P. Mehlen, *Dependence Receptors and Cancer: Addiction to Trophic Ligands.* Cancer Res, 2015. **75**(24): p. 5171-5.
33. Dickens, L.S., et al., *A death effector domain chain DISC model reveals a crucial role for caspase-8 chain assembly in mediating apoptotic cell death.* Mol Cell, 2012. **47**(2): p. 291-305.
34. Brenner, D., H. Blaser, and T.W. Mak, *Regulation of tumour necrosis factor signalling: live or let die.* Nat Rev Immunol, 2015. **15**(6): p. 362-74.
35. Pihan, P., A. Carreras-Sureda, and C. Hetz, *BCL-2 family: integrating stress responses at the ER to control cell demise.* Cell Death Differ, 2017. **24**(9): p. 1478-1487.
36. Roos, W.P., A.D. Thomas, and B. Kaina, *DNA damage and the balance between survival and death in cancer biology.* Nat Rev Cancer, 2016. **16**(1): p. 20-33.
37. Brumatti, G., M. Salmanidis, and P.G. Ekert, *Crossing paths: interactions between the cell death machinery and growth factor survival signals.* Cell Mol Life Sci, 2010. **67**(10): p. 1619-30.
38. Tait, S.W. and D.R. Green, *Mitochondria and cell death: outer membrane permeabilization and beyond.* Nat Rev Mol Cell Biol, 2010. **11**(9): p. 621-32.
39. Czabotar, P.E., et al., *Control of apoptosis by the BCL-2 protein family: implications for physiology and therapy.* Nat Rev Mol Cell Biol, 2014. **15**(1): p. 49-63.
40. Li, P., et al., *Cytochrome c and dATP-dependent formation of Apaf-1/caspase-9 complex initiates an apoptotic protease cascade.* Cell, 1997. **91**(4): p. 479-89.
41. Julien, O. and J.A. Wells, *Caspases and their substrates.* Cell Death Differ, 2017. **24**(8): p. 1380-1389.
42. Tang, D., et al., *The molecular machinery of regulated cell death.* Cell Res, 2019. **29**(5): p. 347-364.
43. Marino, G., et al., *Self-consumption: the interplay of autophagy and apoptosis.* Nat Rev Mol Cell Biol, 2014. **15**(2): p. 81-94.

44. Holler, N., et al., *Fas triggers an alternative, caspase-8-independent cell death pathway using the kinase RIP as effector molecule.* Nat Immunol, 2000. **1**(6): p. 489-95.
45. He, S., et al., *Toll-like receptors activate programmed necrosis in macrophages through a receptor-interacting kinase-3-mediated pathway.* Proc Natl Acad Sci U S A, 2011. **108**(50): p. 20054-9.
46. He, S., et al., *Receptor interacting protein kinase-3 determines cellular necrotic response to TNF-alpha.* Cell, 2009. **137**(6): p. 1100-11.
47. Sun, L., et al., *Mixed lineage kinase domain-like protein mediates necrosis signaling downstream of RIP3 kinase.* Cell, 2012. **148**(1-2): p. 213-27.
48. Vandenabeele, P., et al., *Necrostatin-1 blocks both RIPK1 and IDO: consequences for the study of cell death in experimental disease models.* Cell Death Differ, 2013. **20**(2): p. 185-7.
49. Broz, P. and V.M. Dixit, *Inflammasomes: mechanism of assembly, regulation and signalling.* Nat Rev Immunol, 2016. **16**(7): p. 407-20.
50. Chen, X., et al., *Pyroptosis is driven by non-selective gasdermin-D pore and its morphology is different from MLKL channel-mediated necroptosis.* Cell Res, 2016. **26**(9): p. 1007-20.
51. Yang, W.S., et al., *Peroxidation of polyunsaturated fatty acids by lipoxygenases drives ferroptosis.* Proc Natl Acad Sci U S A, 2016. **113**(34): p. E4966-75.
52. Dixon, S.J., et al., *Ferroptosis: an iron-dependent form of nonapoptotic cell death.* Cell, 2012. **149**(5): p. 1060-72.
53. Friedmann Angeli, J.P., et al., *Inactivation of the ferroptosis regulator Gpx4 triggers acute renal failure in mice.* Nat Cell Biol, 2014. **16**(12): p. 1180-91.
54. Feng, H. and B.R. Stockwell, *Unsolved mysteries: How does lipid peroxidation cause ferroptosis?* PLoS Biol, 2018. **16**(5): p. e2006203.
55. Bialik, S., S.K. Dasari, and A. Kimchi, *Autophagy-dependent cell death - where, how and why a cell eats itself to death.* J Cell Sci, 2018. **131**(18).
56. Kepp, O., et al., *Consensus guidelines for the detection of immunogenic cell death.* Oncoimmunology, 2014. **3**(9): p. e955691.
57. Sanchez-Paulete, A.R., et al., *Antigen cross-presentation and T-cell cross-priming in cancer immunology and immunotherapy.* Ann Oncol, 2017. **28**(suppl_12): p. xii74.
58. Merad, M., et al., *The dendritic cell lineage: ontogeny and function of dendritic cells and their subsets in the steady state and the inflamed setting.* Annu Rev Immunol, 2013. **31**: p. 563-604.
59. Murphy, T.L., et al., *Transcriptional Control of Dendritic Cell Development.* Annu Rev Immunol, 2016. **34**: p. 93-119.
60. Sanchez-Paulete, A.R., et al., *Cancer Immunotherapy with Immunomodulatory Anti-CD137 and Anti-PD-1 Monoclonal Antibodies Requires BATF3-Dependent Dendritic Cells.* Cancer Discov, 2016. **6**(1): p. 71-9.
61. Salmon, H., et al., *Expansion and Activation of CD103(+) Dendritic Cell Progenitors at the Tumor Site Enhances Tumor Responses to Therapeutic PD-L1 and BRAF Inhibition.* Immunity, 2016. **44**(4): p. 924-38.
62. Robbins, S.H., et al., *Novel insights into the relationships between dendritic cell subsets in human and mouse revealed by genome-wide expression profiling.* Genome Biol, 2008. **9**(1): p. R17.
63. Ma, Y., et al., *Anticancer chemotherapy-induced intratumoral recruitment and differentiation of antigen-presenting cells.* Immunity, 2013. **38**(4): p. 729-41.

64. Zhang, J.G., et al., *The dendritic cell receptor Clec9A binds damaged cells via exposed actin filaments.* Immunity, 2012. **36**(4): p. 646-57.
65. Cao, L., et al., *Keratin mediates the recognition of apoptotic and necrotic cells through dendritic cell receptor DEC205/CD205.* Proc Natl Acad Sci U S A, 2016. **113**(47): p. 13438-13443.
66. Alloatti, A., et al., *Critical role for Sec22b-dependent antigen cross-presentation in antitumor immunity.* J Exp Med, 2017. **214**(8): p. 2231-2241.
67. Theisen, D.J., et al., *WDFY4 is required for cross-presentation in response to viral and tumor antigens.* Science, 2018. **362**(6415): p. 694-699.
68. Arakaki, R., et al., *Mechanism of activation-induced cell death of T cells and regulation of FasL expression.* Crit Rev Immunol, 2014. **34**(4): p. 301-14.
69. Green, D.R., N. Droin, and M. Pinkoski, *Activation-induced cell death in T cells.* Immunol Rev, 2003. **193**: p. 70-81.
70. Martinez-Lostao, L., A. Anel, and J. Pardo, *How Do Cytotoxic Lymphocytes Kill Cancer Cells?* Clin Cancer Res, 2015. **21**(22): p. 5047-56.
71. Trapani, J.A., et al., *Perforin-dependent nuclear entry of granzyme B precedes apoptosis, and is not a consequence of nuclear membrane dysfunction.* Cell Death Differ, 1998. **5**(6): p. 488-96.
72. Zeytun, A., et al., *Fas-Fas ligand-based interactions between tumor cells and tumor-specific cytotoxic T lymphocytes: a lethal two-way street.* Blood, 1997. **90**(5): p. 1952-9.
73. Thomas, W.D. and P. Hersey, *TNF-related apoptosis-inducing ligand (TRAIL) induces apoptosis in Fas ligand-resistant melanoma cells and mediates CD4 T cell killing of target cells.* J Immunol, 1998. **161**(5): p. 2195-200.
74. Chen, D.S. and I. Mellman, *Elements of cancer immunity and the cancer-immune set point.* Nature, 2017. **541**(7637): p. 321-330.
75. Galluzzi, L. and G. Kroemer, *Common and divergent functions of Beclin 1 and Beclin 2.* Cell Research, 2013. **23**(12): p. 1341-1342.
76. Panaretakis, T., et al., *Mechanisms of pre-apoptotic calreticulin exposure in immunogenic cell death.* EMBO J, 2009. **28**(5): p. 578-90.
77. Martins, I., et al., *Molecular mechanisms of ATP secretion during immunogenic cell death.* Cell Death Differ, 2014. **21**(1): p. 79-91.
78. Yamazaki, T., et al., *Defective immunogenic cell death of HMGB1-deficient tumors: compensatory therapy with TLR4 agonists.* Cell Death Differ, 2014. **21**(1): p. 69-78.
79. Matzinger, P., *An innate sense of danger.* Semin Immunol, 1998. **10**(5): p. 399-415.
80. Schaefer, L., *Complexity of danger: the diverse nature of damage-associated molecular patterns.* J Biol Chem, 2014. **289**(51): p. 35237-45.
81. Durai, V. and K.M. Murphy, *Functions of Murine Dendritic Cells.* Immunity, 2016. **45**(4): p. 719-736.
82. Bottcher, J.P., et al., *NK Cells Stimulate Recruitment of cDC1 into the Tumor Microenvironment Promoting Cancer Immune Control.* Cell, 2018. **172**(5): p. 1022-1037 e14.
83. Barry, K.C., et al., *A natural killer-dendritic cell axis defines checkpoint therapy-responsive tumor microenvironments.* Nat Med, 2018. **24**(8): p. 1178-1191.
84. Overwijk, W.W., et al., *Tumor regression and autoimmunity after reversal of a functionally tolerant state of self-reactive CD8+ T cells.* J Exp Med, 2003. **198**(4): p. 569-80.

85. Hildner, K., et al., *Batf3 deficiency reveals a critical role for CD8alpha+ dendritic cells in cytotoxic T cell immunity.* Science, 2008. **322**(5904): p. 1097-100.
86. Sauer, J.D., et al., *The N-ethyl-N-nitrosourea-induced Goldenticket mouse mutant reveals an essential function of Sting in the in vivo interferon response to Listeria monocytogenes and cyclic dinucleotides.* Infect Immun, 2011. **79**(2): p. 688-94.
87. Schilte, C., et al., *Type I IFN controls chikungunya virus via its action on nonhematopoietic cells.* J Exp Med, 2010. **207**(2): p. 429-42.
88. Ochoa, M.C., et al., *Antitumor immunotherapeutic and toxic properties of an HDL-conjugated chimeric IL-15 fusion protein.* Cancer Res, 2013. **73**(1): p. 139-49.
89. Spiess, C., Q. Zhai, and P.J. Carter, *Alternative molecular formats and therapeutic applications for bispecific antibodies.* Mol Immunol, 2015. **67**(2 Pt A): p. 95-106.
90. Sanchez-Paulete, A.R., et al., *Intratumoral Immunotherapy with XCL1 and sFlt3L Encoded in Recombinant Semliki Forest Virus-Derived Vectors Fosters Dendritic Cell-Mediated T-cell Cross-Priming.* Cancer Res, 2018. **78**(23): p. 6643-6654.
91. Puttur, F., et al., *Absence of Siglec-H in MCMV infection elevates interferon alpha production but does not enhance viral clearance.* PLoS Pathog, 2013. **9**(9): p. e1003648.
92. Zal, T., A. Volkmann, and B. Stockinger, *Mechanisms of tolerance induction in major histocompatibility complex class II-restricted T cells specific for a blood-borne self-antigen.* J Exp Med, 1994. **180**(6): p. 2089-99.
93. Mayer, C.T., et al., *Selective and efficient generation of functional Batf3-dependent CD103+ dendritic cells from mouse bone marrow.* Blood, 2014. **124**(20): p. 3081-91.
94. Ochoa, M.C., et al., *Daratumumab in combination with urelumab to potentiate anti-myeloma activity in lymphocyte-deficient mice reconstituted with human NK cells.* Oncoimmunology, 2019. **8**(7): p. 1599636.
95. Carbone, F.R. and M.J. Bevan, *Class I-restricted processing and presentation of exogenous cell-associated antigen in vivo.* J Exp Med, 1990. **171**(2): p. 377-87.
96. el-Shami, K., et al., *MHC class I-restricted epitope spreading in the context of tumor rejection following vaccination with a single immunodominant CTL epitope.* Eur J Immunol, 1999. **29**(10): p. 3295-301.
97. Thomas, A.M., et al., *Mesothelin-specific CD8(+) T cell responses provide evidence of in vivo cross-priming by antigen-presenting cells in vaccinated pancreatic cancer patients.* J Exp Med, 2004. **200**(3): p. 297-306.
98. Gulley, J.L., et al., *Immune impact induced by PROSTVAC (PSA-TRICOM), a therapeutic vaccine for prostate cancer.* Cancer Immunol Res, 2014. **2**(2): p. 133-41.
99. Ohashi, P.S., et al., *Ablation of "tolerance" and induction of diabetes by virus infection in viral antigen transgenic mice.* Cell, 1991. **65**(2): p. 305-17.
100. Suciu-Foca, N., P.E. Harris, and R. Cortesini, *Intramolecular and intermolecular spreading during the course of organ allograft rejection.* Immunol Rev, 1998. **164**: p. 241-6.
101. Golden, E.B. and L. Apetoh, *Radiotherapy and immunogenic cell death.* Semin Radiat Oncol, 2015. **25**(1): p. 11-7.
102. Gutierrez-Martinez, E., et al., *Cross-Presentation of Cell-Associated Antigens by MHC Class I in Dendritic Cell Subsets.* Front Immunol, 2015. **6**: p. 363.
103. Woo, S.R., et al., *STING-dependent cytosolic DNA sensing mediates innate immune recognition of immunogenic tumors.* Immunity, 2014. **41**(5): p. 830-42.

104. Spranger, S., et al., *Tumor-Residing Batf3 Dendritic Cells Are Required for Effector T Cell Trafficking and Adoptive T Cell Therapy.* Cancer Cell, 2017. **31**(5): p. 711-723 e4.
105. Melero, I., et al., *Immunological ignorance of an E7-encoded cytolytic T-lymphocyte epitope in transgenic mice expressing the E7 and E6 oncogenes of human papillomavirus type 16.* J Virol, 1997. **71**(5): p. 3998-4004.
106. Ochsenbein, A.F., et al., *Immune surveillance against a solid tumor fails because of immunological ignorance.* Proc Natl Acad Sci U S A, 1999. **96**(5): p. 2233-8.
107. Wolchok, J.D., L. Rollin, and J. Larkin, *Nivolumab and Ipilimumab in Advanced Melanoma.* N Engl J Med, 2017. **377**(25): p. 2503-2504.
108. Motzer, R.J., et al., *Nivolumab plus Ipilimumab versus Sunitinib in Advanced Renal-Cell Carcinoma.* The New England journal of medicine, 2018. **378**(14): p. 1277-1290.
109. Hellmann, M.D., et al., *Nivolumab plus Ipilimumab in Lung Cancer with a High Tumor Mutational Burden.* The New England journal of medicine, 2018. **378**(22): p. 2093-2104.
110. Wolchok, J.D., et al., *Nivolumab plus ipilimumab in advanced melanoma.* The New England journal of medicine, 2013. **369**(2): p. 122-33.
111. Xiao, Y.T., et al., *Neutralization of IL-6 and TNF-alpha ameliorates intestinal permeability in DSS-induced colitis.* Cytokine, 2016. **83**: p. 189-192.
112. Mahler, M., et al., *Differential susceptibility of inbred mouse strains to dextran sulfate sodium-induced colitis.* The American journal of physiology, 1998. **274**(3 Pt 1): p. G544-51.
113. Tang, Q., et al., *Role of far upstream element binding protein 1 in colonic epithelial disruption during dextran sulphate sodium-induced murine colitis.* International journal of clinical and experimental pathology, 2014. **7**(5): p. 2019-31.
114. Curran, M.A., et al., *PD-1 and CTLA-4 combination blockade expands infiltrating T cells and reduces regulatory T and myeloid cells within B16 melanoma tumors.* Proceedings of the National Academy of Sciences of the United States of America, 2010. **107**(9): p. 4275-80.
115. Duraiswamy, J., et al., *Dual blockade of PD-1 and CTLA-4 combined with tumor vaccine effectively restores T-cell rejection function in tumors.* Cancer research, 2013. **73**(12): p. 3591-603.
116. Wainwright, D.A., et al., *Durable therapeutic efficacy utilizing combinatorial blockade against IDO, CTLA-4, and PD-L1 in mice with brain tumors.* Clinical cancer research : an official journal of the American Association for Cancer Research, 2014. **20**(20): p. 5290-301.
117. Spranger, S., et al., *Mechanism of tumor rejection with doublets of CTLA-4, PD-1/PD-L1, or IDO blockade involves restored IL-2 production and proliferation of CD8(+) T cells directly within the tumor microenvironment.* Journal for immunotherapy of cancer, 2014. **2**: p. 3.
118. Larkin, J., et al., *Combined Nivolumab and Ipilimumab or Monotherapy in Untreated Melanoma.* The New England journal of medicine, 2015. **373**(1): p. 23-34.
119. Ascierto, P.A., et al., *Ipilimumab 10 mg/kg versus ipilimumab 3 mg/kg in patients with unresectable or metastatic melanoma: a randomised, double-blind, multicentre, phase 3 trial.* The Lancet. Oncology, 2017. **18**(5): p. 611-622.

120. Postow, M.A. and M.D. Hellmann, *Adverse Events Associated with Immune Checkpoint Blockade.* The New England journal of medicine, 2018. **378**(12): p. 1165.
121. Yamada, Y., et al., *Initiation of liver growth by tumor necrosis factor: deficient liver regeneration in mice lacking type I tumor necrosis factor receptor.* Proc Natl Acad Sci U S A, 1997. **94**(4): p. 1441-6.
122. Cooper, H.S., et al., *Clinicopathologic study of dextran sulfate sodium experimental murine colitis.* Laboratory investigation; a journal of technical methods and pathology, 1993. **69**(2): p. 238-49.
123. Eichele, D.D. and K.K. Kharbanda, *Dextran sodium sulfate colitis murine model: An indispensable tool for advancing our understanding of inflammatory bowel diseases pathogenesis.* World journal of gastroenterology, 2017. **23**(33): p. 6016-6029.
124. Blonski, W., A.M. Buchner, and G.R. Lichtenstein, *Treatment of ulcerative colitis.* Current opinion in gastroenterology, 2014. **30**(1): p. 84-96.
125. Popivanova, B.K., et al., *Blocking TNF-alpha in mice reduces colorectal carcinogenesis associated with chronic colitis.* The Journal of clinical investigation, 2008. **118**(2): p. 560-70.
126. Coward, J., et al., *Interleukin-6 as a therapeutic target in human ovarian cancer.* Clin Cancer Res, 2011. **17**(18): p. 6083-96.
127. Mace, T.A., et al., *IL-6 and PD-L1 antibody blockade combination therapy reduces tumour progression in murine models of pancreatic cancer.* Gut, 2018. **67**(2): p. 320-332.
128. Bertrand, F., et al., *TNFalpha blockade overcomes resistance to anti-PD-1 in experimental melanoma.* Nature communications, 2017. **8**(1): p. 2256.
129. Hettich, M., et al., *High-Resolution PET Imaging with Therapeutic Antibody-based PD-1/PD-L1 Checkpoint Tracers.* Theranostics, 2016. **6**(10): p. 1629-40.
130. Kurtulus, S., et al., *Checkpoint Blockade Immunotherapy Induces Dynamic Changes in PD-1(-)CD8(+) Tumor-Infiltrating T Cells.* Immunity, 2019. **50**(1): p. 181-194 e6.
131. Siddiqui, I., et al., *Intratumoral Tcf1(+)PD-1(+)CD8(+) T Cells with Stem-like Properties Promote Tumor Control in Response to Vaccination and Checkpoint Blockade Immunotherapy.* Immunity, 2019. **50**(1): p. 195-211 e10.
132. Arakaki, R., et al., *Mechanism of activation-induced cell death of T cells and regulation of FasL expression.* Critical reviews in immunology, 2014. **34**(4): p. 301-14.
133. Zheng, L., et al., *Induction of apoptosis in mature T cells by tumour necrosis factor.* Nature, 1995. **377**(6547): p. 348-51.
134. Sanmamed, M.F., et al., *Nivolumab and Urelumab Enhance Antitumor Activity of Human T Lymphocytes Engrafted in Rag2-/-IL2Rgammanull Immunodeficient Mice.* Cancer research, 2015. **75**(17): p. 3466-78.
135. Balkwill, F., *Tumour necrosis factor and cancer.* Nature reviews. Cancer, 2009. **9**(5): p. 361-71.
136. Madhusudan, S., et al., *Study of etanercept, a tumor necrosis factor-alpha inhibitor, in recurrent ovarian cancer.* Journal of clinical oncology : official journal of the American Society of Clinical Oncology, 2005. **23**(25): p. 5950-9.
137. Harrison, M.L., et al., *Tumor necrosis factor alpha as a new target for renal cell carcinoma: two sequential phase II trials of infliximab at standard and high dose.* Journal of clinical oncology : official journal of the American Society of Clinical Oncology, 2007. **25**(29): p. 4542-9.

138. Huang, A.C., et al., *A single dose of neoadjuvant PD-1 blockade predicts clinical outcomes in resectable melanoma.* Nat Med, 2019. **25**(3): p. 454-461.
139. He, R., et al., *Follicular CXCR5- expressing CD8(+) T cells curtail chronic viral infection.* Nature, 2016. **537**(7620): p. 412-428.
140. Veiga-Fernandes, H. and A.A. Freitas, *The S(c)ensory Immune System Theory.* Trends Immunol, 2017. **38**(10): p. 777-788.
141. Yatim, N., S. Cullen, and M.L. Albert, *Dying cells actively regulate adaptive immune responses.* Nat Rev Immunol, 2017. **17**(4): p. 262-275.

142. https://www.cancerresearch.org/scientists/immuno-oncology-landscape/pd-1-pd-l1-landscape